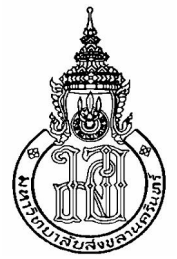

Reduction of Power Consumption in Ultrasonic Linear Motor for Linear Translation by Partially Laminated Actuators

Panumas Suybangdum

A Thesis Submitted in Partial Fulfillment of the Requirements for the Degree of
Doctor of Philosophy in Mechanical Engineering
Prince of Songkla University
2012

Thesis Title	Reduction of Power Consumption in Ultrasonic Linear Motor for Linear Translation by Partially Laminated Actuators
Author	Mr. Panumas Suybangdum
Major Program	Mechanical Engineering

Major Advisor:

……
(Assoc.Prof.Dr.Pruittikorn Smithmaitrie)

Co-advisor

…….....
(Dr. Pitak Laoratanakul)

Examining Committee:

…….....Chairperson
(Assoc.Prof.Dr. Nantakan Muensit)

…….....
(Assoc.Prof.Dr.Pruittikorn Smithmaitrie)

…….....
(Dr. Pitak Laoratanakul)

…….....
(Dr. Thanansak Theppaya)

…….....
(Asst.Prof.Dr. Sontipee Ammanee)

The Graduate School, Prince of Songkla University, has approved this thesis as partial fulfillment of the requirements for the Doctor of Philosophy Degree in Mechanical Engineering

.....
(Prof. Dr. Amornrat Phongdara)
Dean of Graduate School

ชื่อวิทยานิพนธ์	การลดการใช้พลังงานของมอเตอร์อัลตราโซนิกเชิงเส้นแบบติดตัวทำงานบางส่วน
ผู้เขียน	นายภาณุมาศ สุยบางดำ
สาขาวิชา	วิศวกรรมเครื่องกล
ปีการศึกษา	2554

บทคัดย่อ

งานวิจัยนี้ศึกษาเกี่ยวกับการลดการใช้พลังงานในมอเตอร์อัลตราโซนิกที่เคลื่อนที่แบบเส้นตรง โดยทั่วไปมอเตอร์อัลตราโซนิกมีส่วนประกอบหลักสองส่วน ได้แก่ สเตเตอร์และโรเตอร์ สเตเตอร์ทำหน้าที่ขับให้โรเตอร์เคลื่อนที่โดยอาศัยคลื่นเคลื่อนที่ที่เกิดขึ้นบนสเตเตอร์ คลื่นเคลื่อนที่เกิดจากการสั่นสะเทือนของสเตเตอร์เกิดจากการกระตุ้นด้วยแรงฮาร์โมนิกส์ โดยทั่วไปวัสดุเพียโซอิเล็กทริกถูกใช้เป็นตัวทำงานเพื่อกระตุ้นให้เกิดแรงแบบฮาร์โมนิกส์ในมอเตอร์อัลตราโซนิก มอเตอร์อัลตราโซนิกสามารถแบ่งออกได้เป็นสองประเภทใหญ่ๆ คือ มอเตอร์อัลตราโซนิกที่เคลื่อนที่แบบวงกลม และมอเตอร์อัลตราโซนิกที่เคลื่อนที่แบบเส้นตรง งานวิจัยนี้มุ่งเน้นการออกแบบมอเตอร์อัลตราโซนิกที่เคลื่อนที่แบบเส้นตรง โดยมีวัตถุประสงค์เพื่อศึกษาการลดการใช้พลังงานและประสิทธิภาพของมอเตอร์ที่เกิดจากการลดจำนวนตัวทำงานที่ติดตั้งบนสเตเตอร์ ในการศึกษานี้ได้ออกแบบมอเตอร์จำนวนสองตัวที่มีการติดตั้งตัวทำงานแตกต่างกัน ประกอบด้วย มอเตอร์ที่ติดตั้งตัวทำงานสองตัวที่ขอบทั้งสองข้างของสเตเตอร์ และมอเตอร์ที่ติดตั้งตัวทำงานเพียงตัวเดียวบนสเตเตอร์ โดยเลือกใช้วัสดุเพียโซอิเล็กทริกชนิด PZT-4 เป็นตัวทำงาน งานวิจัยนี้มีวิธีการศึกษาปัจจัยที่เกี่ยวข้องกับการลดการใช้พลังงานและหาประสิทธิภาพของมอเตอร์ ประกอบด้วย ระเบียบวิธีไฟไนต์เอลิเมนต์ สมการทางคณิตศาสตร์ และการทดลอง ระเบียบวิธีไฟไนต์เอลิเมนต์ถูกใช้ในการวิเคราะห์หาความถี่ธรรมชาติ การตอบสนองของระบบที่สภาวะคงตัว และการหาค่าความถี่ทำงานของมอเตอร์ ในขณะที่สมการทางคณิตศาสตร์ถูกใช้คำนวณหาความถี่ธรรมชาติและปริมาณพลังงานที่ใช้ในมอเตอร์ทั้งสองแบบ สำหรับการทดลองใช้เพื่อศึกษาความถี่ธรรมชาติของระบบ ความจุของวัสดุเพียโซอิเล็กทริก ปริมาณพลังงานที่ใช้ แรงกดที่เหมาะสม (pre-load) ความสัมพันธ์ระหว่างปริมาณศักย์ไฟฟ้าที่กระตุ้นกับความเร็วของมอเตอร์ ความสัมพันธ์ระหว่างปริมาณศักย์ไฟฟ้าที่กระตุ้นกับความสามารถในการขับภาระ และความสัมพันธ์ระหว่างความเร็วของมอเตอร์กับความสามารถในการขับภาระ จากนั้นจึงนำผลที่ได้มาเปรียบเทียบและวิเคราะห์ พบว่า ความถี่ธรรมชาติของระบบที่ได้จากการศึกษาทั้งสามวิธีสอดคล้องกัน ในกรณีที่ปริมาณ

ศักย์ไฟฟ้าที่กระตุ้นตัวทำงานมีค่าคงที่ ขณะที่ความถี่ทำงานที่ได้จากระเบียบวิธีไฟไนต์เอลิเมนต์กับการทดลองมีค่าใกล้เคียงกัน นอกจากนั้นจากการทดลองยังพบอีกว่า เมื่อเพิ่มแรงกดให้กับมอเตอร์จะส่งผลให้มอเตอร์มีความเร็วเพิ่มขึ้นจนถึงค่าหนึ่งและความเร็วจะมีค่าลดลงหลังจากนั้น อีกทั้งยังพบว่าความเร็วของมอเตอร์มีความสัมพันธ์กับปริมาณศักย์ไฟฟ้าที่กระตุ้นตัวทำงาน โดยเมื่อเพิ่มปริมาณศักย์ไฟฟ้าที่กระตุ้นตัวทำงานเพียโซอิเล็กทริกมอเตอร์จะมีความเร็วเพิ่มขึ้นและมอเตอร์ยังสามารถขับภาระได้เพิ่มขึ้นอีกด้วย สำหรับความสัมพันธ์ระหว่างความสามารถขับภาระกับความเร็วของมอเตอร์ ที่ปริมาณศักย์ไฟฟ้าที่กระตุ้นตัวทำงานมีค่าคงที่ พบว่า ความเร็วของมอเตอร์ลดลงเมื่อเพิ่มภาระ และยังพบอีกว่าความเร็วของมอเตอร์มีค่ามากที่สุดเมื่อไม่ขับภาระ ในทางกลับกันมอเตอร์สามารถขับภาระได้มากที่สุดเมื่อความเร็วมีค่าเท่ากับศูนย์ นอกจากนั้น มอเตอร์ที่ติดตัวทำงานสองตัวสามารถกลับทิศทางการเคลื่อนที่โดยการสลับสัญญาณไฟฟ้าที่กระตุ้น จากการศึกษายังพบอีกว่า ปริมาณพลังงานที่ใช้ในอัลตราโซนิกมอเตอร์จะขึ้นกับจำนวนตัวทำงานที่ติดตั้งบนสเตเตอร์ ความถี่ทำงาน และปริมาณศักย์ไฟฟ้าที่กระตุ้น ดังนั้นการลดจำนวนตัวทำงานที่ติดตั้งบนสเตเตอร์จึงเป็นการลดการใช้พลังงานของมอเตอร์ด้วย และพบว่าปริมาณพลังงานที่ใช้ในมอเตอร์ทั้งสองมีค่าต่ำกว่า 1 วัตต์ ซึ่งมีค่าน้อยกว่าเมื่อเปรียบเทียบกับมอเตอร์ที่ติดตั้งตัวทำงานแบบติดเต็มคาน จากการออกแบบระบบของมอเตอร์ทั้งสองรูปแบบมีโครงสร้างที่ไม่ซับซ้อนจึงง่ายต่อการสร้างและย่อขนาด ด้วยเหตุนี้มอเตอร์ดังกล่าวข้างต้นจึงมีความเหมาะสมที่จะนำไปประยุกต์ใช้กับงานที่ต้องการมอเตอร์อัลตราโซนิกที่เคลื่อนที่แบบเส้นตรงที่มีขนาดเล็กและประหยัดพลังงานอีกด้วย

Thesis Title	Reduction of Power Consumption in Ultrasonic Linear Motor for Linear Translation by Partially Laminated Actuators
Author	Mr. Panumas Suybangdum
Major Program	Mechanical Engineering
Academic Year	2011

ABSTRACT

Decreasing energy consumption of an ultrasonic linear motor is studied in this research. Ultrasonic motor system usually consists of a stator and a rotor. The stator drives the rotor by means of mechanical waves at the contact interface. The waves are generated by piezoelectric actuators which are bonded with the stator. The electrical excitation applied to the piezoelectric actuator induces deformation on the piezoelectric actuator and stator. Generally, ultrasonic motors can be classified into two major categories based on rotor movement; they are rotary and linear ultrasonic motors. In this study, the design of ultrasonic linear motor is investigated and evaluated. The main objectives of this study are to decrease the energy consumption and evaluate of the motor performance by reducing number of actuators bonded on stator. Hence, two designs of linear ultrasonic motors, dual actuator and single actuator linear ultrasonic motor, are proposed. The piezoelectric material, PZT-4, is used as actuator. Methodologies for investigation and evaluation the research are finite element, mathematical model and experiment, respectively. Three finite element analyses are used to study the motor dynamics. They are modal, harmonic and

transient analyses. Meanwhile, the mathematical models are used to calculate the natural frequency and energy consumption of the linear motors. Experimental study is used to study the motor performances which are relationships between applied voltage and velocity, driving force and velocity, applied voltage and driving force, velocity and the suitable pre-load. Furthermore, other properties such as effective capacitance of the piezoelectric actuator and natural frequency of the ultrasonic linear motors are also measured. Natural frequency of the ultrasonic linear motors is compared among all methods. It is shown well agreement. While, the operating frequency of the ultrasonic linear motors compared with the finite element and experimental results shows positive agreement. The experiment results reveal that the velocity of the linear motor increases when the pre-load increases for a certain amount of the pre-load and decreases afterward. The relationship between velocity and applied voltage shows that the motor velocity proportionally increases as the applied voltage amplitude increases. The experimental results of the relationship between driving force and the applied voltage indicates that the driving force linearly increases as applied voltage amplitude increases, and the relationship between the velocity and driving force reveals that maximum motor velocity occurred at zero driving force, while the maximum driving force is generated when the motor operates at zero speed. For the ultrasonic linear motor with dual actuators, the direction of the traveling wave can be controlled by alternating the phase difference between the two control signals. Energy consumption of the linear motors depends on the number of the actuator bonded with the stator, electrical applied voltage, operating frequency and capacitance of the piezoelectric actuator. Hence, decreasing the number of piezoelectric actuators could reduce the

energy consumption in ultrasonic linear motor. Besides, the energy consumption of the dual actuators and single actuator linear motors are less than 1 watt which is less than that of the conventional ultrasonic linear motor with fully laminated actuators. Thus, the both designs of the ultrasonic linear motors in this research open an opportunity for many applications that require a tiny translational actuator with low electrical power consumption yet easy in fabrication.

ACKNOWLADGEMENTS

This thesis cannot be completed without the direction of several people, whom I would like to thank.

I wish to express my sincere gratitude and appreciation to my advisors; Associate Professor Dr. Pruittikorn Smithmaitrie and Dr. Pitak Laoratanakul for helpful suggestions, excellent guidance, supervision, continuous encouragements throughout the entire course of this thesis.

I would like to thank examination committee members, Associate Professor Dr. Nantakan Muensit, Dr. Thanansak Theppaya and Assistant Professor Dr. Sontipee Aimmanee for their valuable time. I am thankful to Department of Mechanical Engineering, Faculty of Engineering, Prince of Songkla University and National Metal and Materials Technology Center (MTEC) for all necessary laboratory apparatus used throughout this thesis.

I am very grateful to Mr. Praneet Rodsang of Electrical Engineering Department whom repaired high voltage amplifiers that used in this work.

I am very grateful to Thailand Graduate Institute of Science and Technology (TGIST); National Science and Technology Development Agency (NSTDA) for financial support. I would like to thank all members of Smart Mechatronics Team. Their friendship, kindness and help have been valuable to me.

Finally, I would like to express my gratefulness to my father, mother, wife, teachers, and friends for their love, support, and encouragement. Without them, I could not come this far.

Panumas Suybangdum

TABLE OF CONTENT

TABLE OF CONTENT (cont.)

TABLE OF CONTENT (cont.)

TABLE OF CONTENT (cont.)

TABLE OF CONTENT (cont.)

LIST OF TABLES

LIST OF FIGURES

LIST OF FIGURES (cont.)

LIST OF FIGURES (cont.)

LIST OF FIGURES (cont.)

LIST OF FIGURES (cont.)

LIST OF FIGURES (cont.)

SYMBOLS

d_{ij}	piezoelectric charge constant
s_{ijkl}	elastic compliance
x_{ij}	stain
X_{ij}	stress
D_i	charge density
ε_0	dielectric permittivity of vacuum,
P_i	polarization of the piezoelectric element,
ε_{ij}	dielectric permittivity,
p_i	pyroelectric coefficient
T	temperature
d^t	transposed matrix of the inverse piezoelectric coefficient
U	internal energy
D	dielectric displacement
S	entropy
G	Gibbs free energy
α_{ij}	thermal expansion tensor
c	heat capacity
P	electrical power
V	applied voltage
I	current
Y	electrical admittance
Y_{11}^E	elastic modulus of piezoelectric material
E_k	electric field
h_a	actuator thickness

SYMBOLS (cont.)

b_a	actuator width
l_a	actuator length
C	effective capacitance
k_{ij}	Electromechanical coupling factor
w_1	mechanical energy output
w_2	electrical energy input
ε^T	dielectric constant at constant stress
x^E	elastic compliance at constant electric field
λ_i	dimensionless parameter
m	mass per unit length of the beam
E_b	modulus of elasticity of the beam
I_b	area moment of inertia of beam
C_N	normal equivalent stiffness
C_T	tangential equivalent stiffness
U_x^k	shear deformation
U_z^k	normal deformation
D_N	normal equivalent damping
D_T	tangential equivalent damping
ρ_c	density of the contact layer
h_c	height of the contact layer
υ	Poisson's ratio
τ_x	tangential stress in the x-direction
P_N	normal stress in the z-direction
A	amplitude of vibration
λ	wavelength

SYMBOLS (cont.)

V_w	velocity of traveling wave
a	distance between surface of stator tooth and neutral plane
V_R	rotor velocity
F_N	preload
k_f	normal equivalent stiffness
E_c	elastic modulus of the contact layer
h_c	thickness of the contact layer
b_c	width of contact region
N	number of contact wave crest
μ_k	friction coefficient
V_s	tangential velocity of the stator
P_R	power output of the rotor
η	efficiency
$p(x)$	normal contact pressure force
F_T	driving force
Y_b	Young's modulus
b	beam width
h	beam thickness
l	beam length
u_3	transverse displacement
ρ	mass density
A_c	cross-section area
A_z	transverse wave amplitude
k	wave number
v_x	velocity in the x-direction
h_t	tooth height

SYMBOLS (cont.)

b_t	tooth width
t_t	tooth thickness
l_a	actuator length
b_a	actuator width
h_a	actuator thickness

Chapter 1

Introduction

1.1 Introduction

Ultrasonic motor (USM) is a new type actuator based on the concept of driving the rotor by a mechanical vibration excited on the stator via piezoelectric effect [1]. The converse piezoelectric effect of the piezoelectric materials is adopted to obtain the vibration of stator in ultrasonic frequency. The fundamental working principle of ultrasonic motors is two-stage energy conversion. The first stage is the conversion of mechanical vibration energy by exciting the piezoelectric material which is called as electromechanical energy conversion. The second stage is the mechanical energy conversion where the mechanical vibrations are converted to linear or rotary motion by friction force generated in stator-rotor interface [2]. Ultrasonic motors can be classified into two major categories based on vibration characteristics: traveling wave motors and standing wave motors [3-4]. Ultrasonic motor system usually consists of a stator and a rotor. The stator drives the rotor by means of mechanical waves at the contact area. The waves are generated by piezoelectric actuators which are bonded with the stator. The electrical excitation applied to the piezoelectric actuator induces deformation on the piezoelectric actuator and stator [5-6].

Ultrasonic motors are attractive devices for applications such as automatic focusing device of digital camera and optical lens zooming operation in personal digital assistant (PDA) and mobile phone [7-9], image processing [10], robot,

aerospace, automatic control, military industry, medical instrument [11], chemical mixing process, pharmaceutical and food industries that demand an exact control of powder feeding [12].

In this research, the designs of ultrasonic linear motor are studied and investigated for motor performances. Generally, ultrasonic linear motors can be classified into several types. They are direct flexural waves, standing wave, hybrid transducers, sandwich vibrators [13-14], multi-mode vibrators [15-17], surface acoustic waves [18-22], impact motors [8,10-11,23], π-shape transducers and the Paderborn rowing type [3].

The ultrasonic linear motors exhibit several attractive advantages over the conventional electromagnetic motor (e.g., DC motor, induction motor, stepping motor, permanent-magnet synchronous motor, etc.) [24]. For instance, ultrasonic motors have high driving force per body weight, high precision in order of nanometer [15], high torque at low speed without a gear mechanism [4], no magnetic field working without restriction of induction, [25-26], high static friction holding-force without power supply [4,15,27], ability to work in vacuum environment [7,18], short response time, compact size, light weight and quiet operation.

There are many techniques to improve performance of a linear ultrasonic motor such as using actuators that are made of multi-layer piezoelectric ceramics instead of single layer piezoelectric ceramics [16], replacing single driving foot with double driving feet to increase torque of the motor [15], using high efficiency friction materials [10,20].

All these ultrasonic motors have been using certain numbers of active piezoelectric actuator to create mechanical vibration on the stator. A large number of

piezoelectric actuators will cause both high energy consumption and undesired system stiffness, resulting in requirement of high applied voltage for the generation of effective vibration on the stator. At the same time, the high applied voltage would raise temperature of the system during operation and would possibly cause depolarization of piezoelectric actuators [25].

At present, electronic device and components are in small-sized; the ultrasonic linear motor with the low energy consumptions is required to be a low-energy-consumption operating device. While the parameters effecting the energy consumption of the linear ultrasonic motor have not been collectively reported. Consequently, a goal of this research is to reduce the electrical energy consumption of the ultrasonic linear motor by decreasing the number of piezoelectric actuators used in the motor and to study parameters that affect the motor performance. In this research, the traveling wave type ultrasonic motor was selected because it has high propagation wave amplitude, implying high driving force when driving at the natural frequency [28].

1.2 Principle of Operation of Ultrasonic Motor

Propagation wave is generated by piezoelectric actuator patches that bonded with the stator. The electrical excitation applied on piezoelectric actuators induces deformation on piezoelectric actuator [29-32]. If the piezoelectric actuators are placed in the suitable locations on the stator and excited by appropriate signals, then the traveling wave can be created [6,31]. Elliptical motion of a point on the stator surface generated by the traveling wave drives the rotor. Thus, the traveling wave is the

source of force driving the rotor. The rotor movement either rotary or linear direction depended on the actuator patterns and stator design. Figure 1.1 shows a basic construction of an ultrasonic motor, which consists of a high frequency power supply, a vibrator and slider, respectively. The vibrator is composed of a piezoelectric driving component and elastic vibratory piece, and the slider is composed of an elastic moving piece and friction coat material [33].

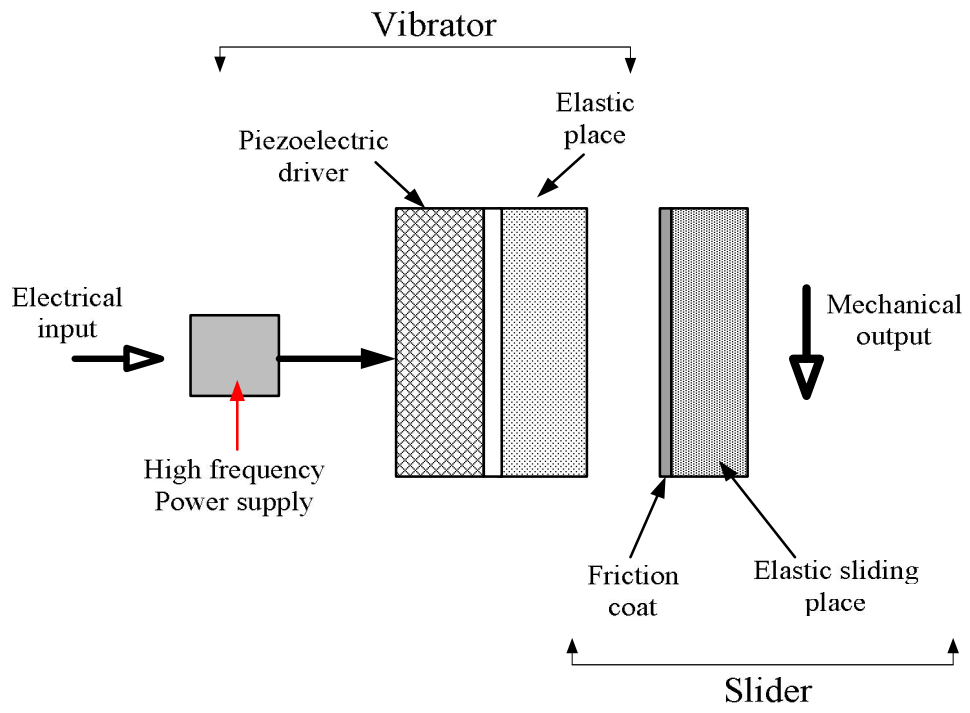

Figure 1.1 Schematic diagram of ultrasonic motor [33].

1.3 Literature Reviews

The ultrasonic motors, both rotary and linear motors, can be further grouping as follows.

1.3.1 Rotary ultrasonic motor

Constructions of rotary ultrasonic motors are illustrated in Figures 1.2, 1.3 and 1.4, respectively. The most common structures of rotary ultrasonic motor are a disk, ring and cylinder. The piezoelectric actuator and elastic stator are combined in various designs forming the composite driving structure [4,34]. For the rotary motor, the piezoelectric ceramic layer underneath the stator is excited. The rotor is pressed against the stator by a disk spring and driven by frictional force at the contact layer. The rotational direction of the rotor is opposite to the direction of the traveling wave. On the other hand, the orthogonal mode rotational motor is driven by two orthogonal modes which are simultaneously active. These modes are induced by constructing the piezoelectric actuators bonded on the stator in a pattern. The pattern (Figure 1.2b) shows the two actuator sections excited by Acos(ωt) and Asin(ωt) signals. This produces a traveling wave with a frequency of ω. Also, by changing the sign on one of the driving signals, the traveling wave would reverse its direction [35].

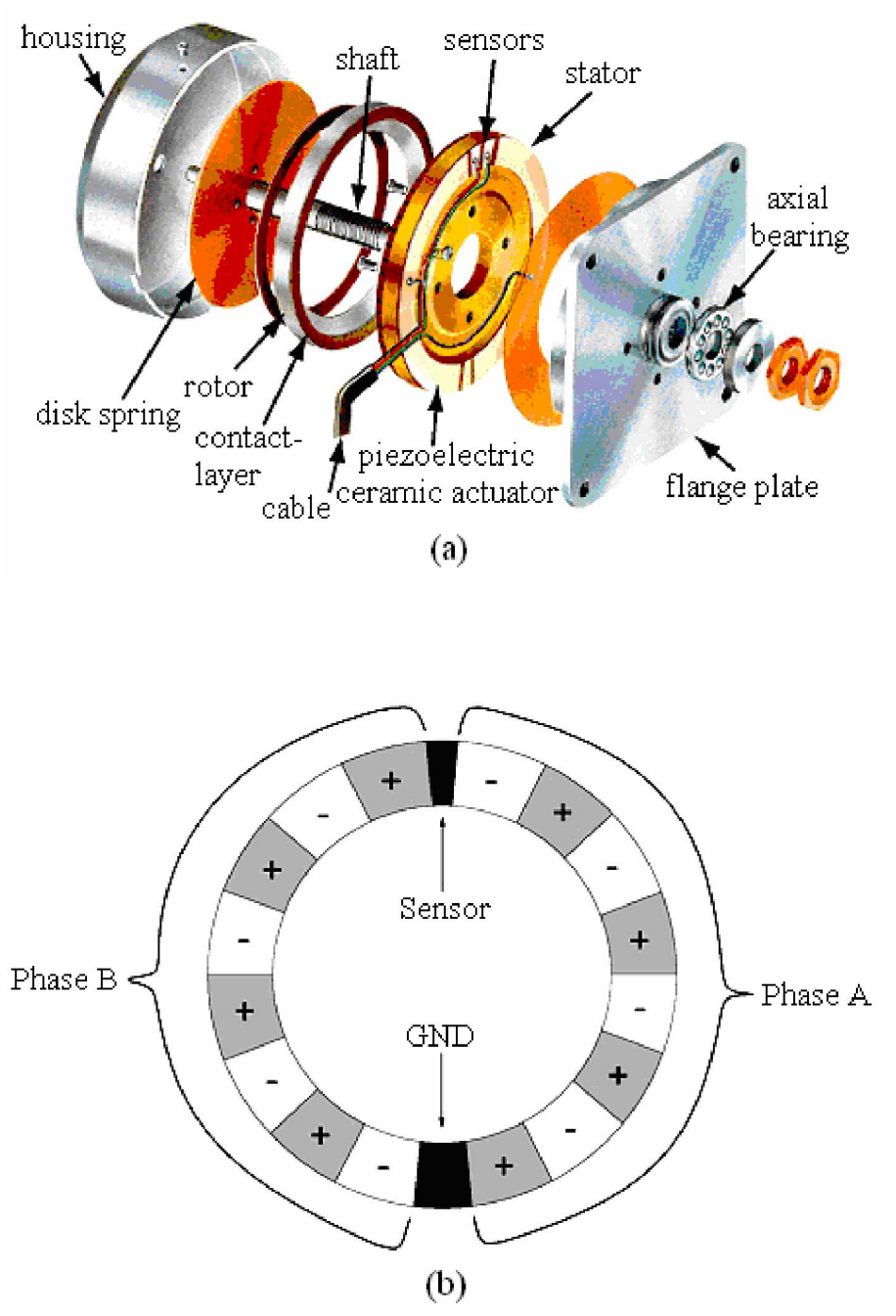

Figure 1.2 Rotary ultrasonic motor based on a ring stator structure a) schematic diagram and b) actuator pattern bonded on the stator [35]

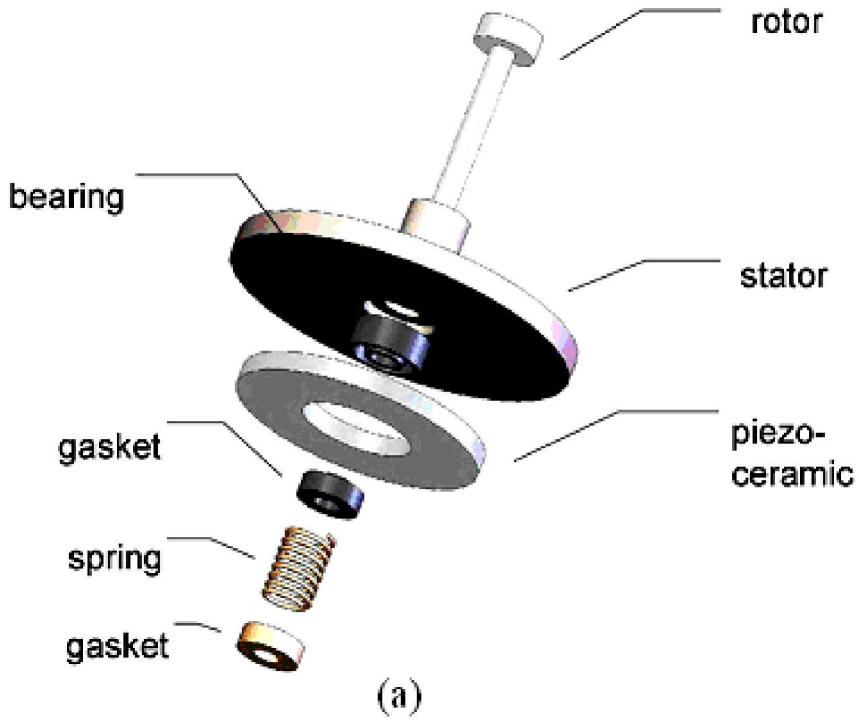

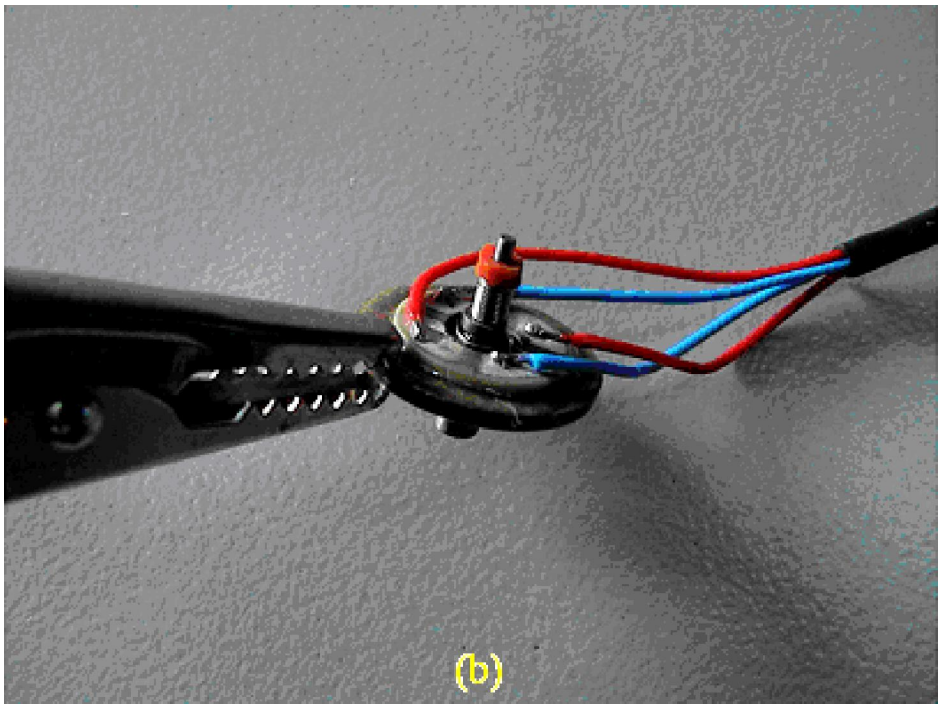

Figure 1.3 Rotary ultrasonic motor based on a disc stator structure a) structure of motor b) the prototype of the motor [36]

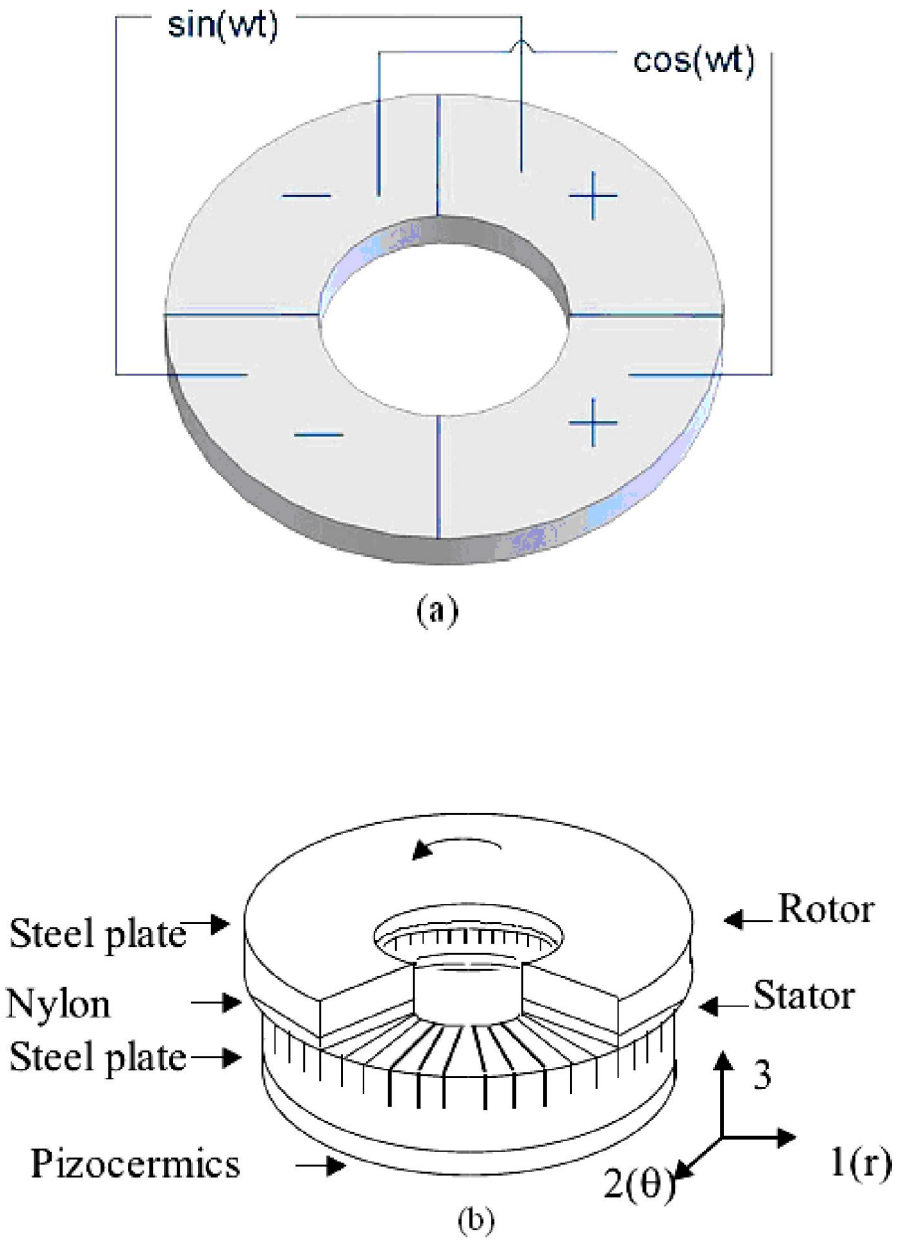

Figure 1.4 Schematic diagram of a rotary ultrasonic motor based on a ring stator structure a) construction of the motor b) Arrangement of the actuator bonded on stator [37]

Rotary ultrasonic motors are currently applied for positioning devices in auto-focus camera lenses, adjusting steering wheel in a car, precision positioning stages, positioning CD and DVD drive writing/reading heads, video recorders and card feeding for ATMs [17].

1.3.2 Linear ultrasonic motor

Another type of ultrasonic motor is a linear motor such as stepping linear motor, impact linear motor, multi-mode linear motor, traveling wave linear motor**,** standing wave linear motor and surface acoustic wave linear motor [3,38]. The details of linear motors are described in this section.

1.3.2.1 Stepping linear ultrasonic motor

The stepping ultrasonic motor relies on a single-phase excitation without feedback via a vibrator [11]. The motor is driven by a horn pressing against a rotor, the horn is excited by the piezoelectric actuator as shown in Figure 1.5. For the clockwise rotation, the horn number 1 and 3 are used. In the other hand, for the counterclockwise rotation, the horn number 2 and 4 are actived instead.

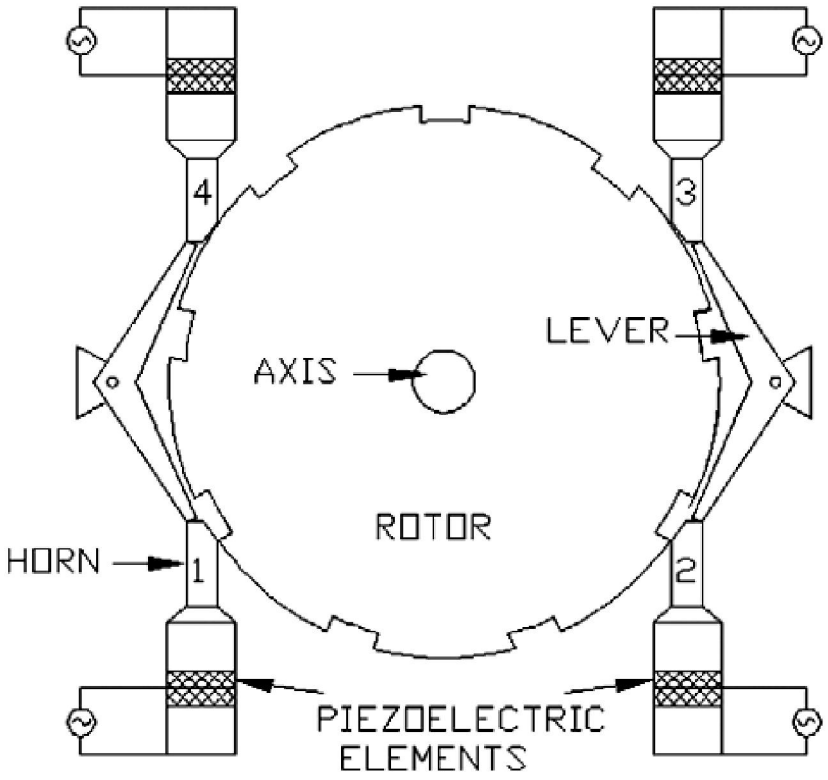

Figure 1.5 Principle of the stepping ultrasonic motor [11].

1.3.2.2 Impact ultrasonic linear motor

The impact ultrasonic linear motor has been reported by [8-10] as illustrated in Figure 1.6. The voltage is applied to a piezoelectric actuator block in the same direction as the polarization. The block extends with the voltage applied and restore back to the original state without the voltage. A rod on the motor is also moved forward by following movement of the piezoelectric actuator block. The lens holder is attached with the rod. Thus, the forward and backward motion of the rod is then translated to push the lens holder by its inertia. The impact ultrasonic linear motor

was designed for a camera lens focusing application. Their structure and picture of operation are illustrated in Figure 1.6 Figure 1.7, respectively.

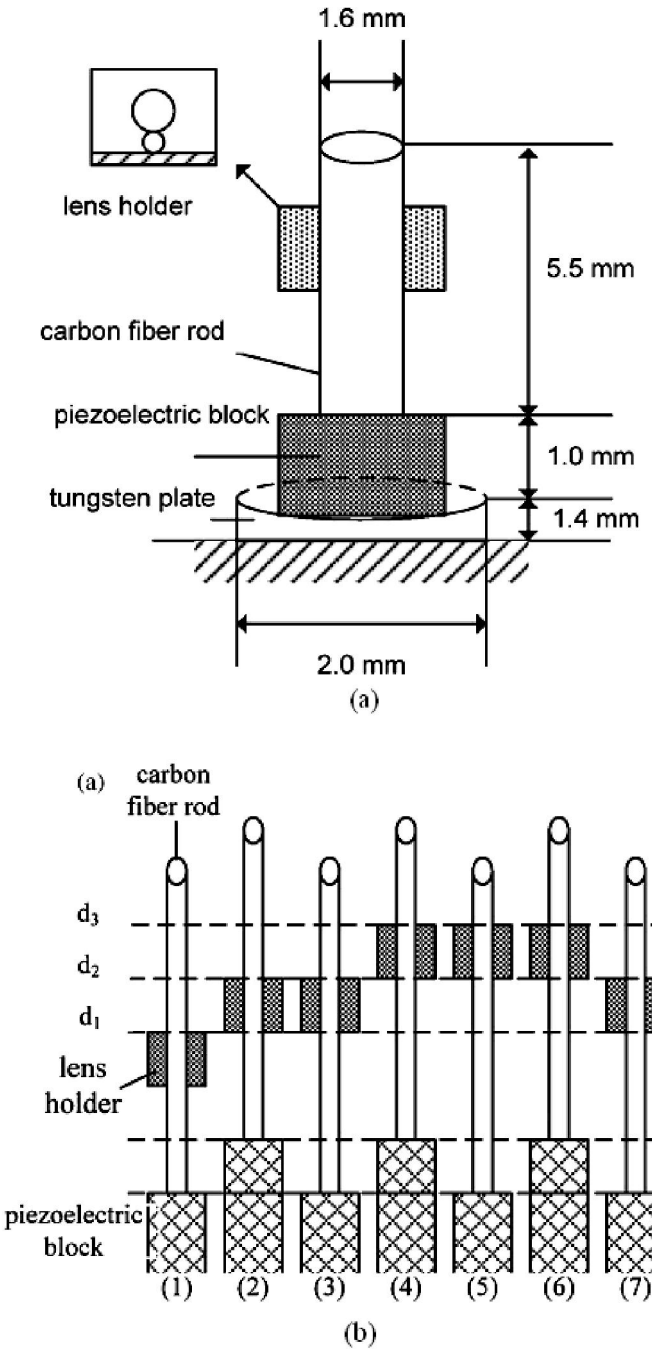

Figure 1.6 The impact ultrasonic linear motor a) structure of the motor b) the operation principle of motor [8].

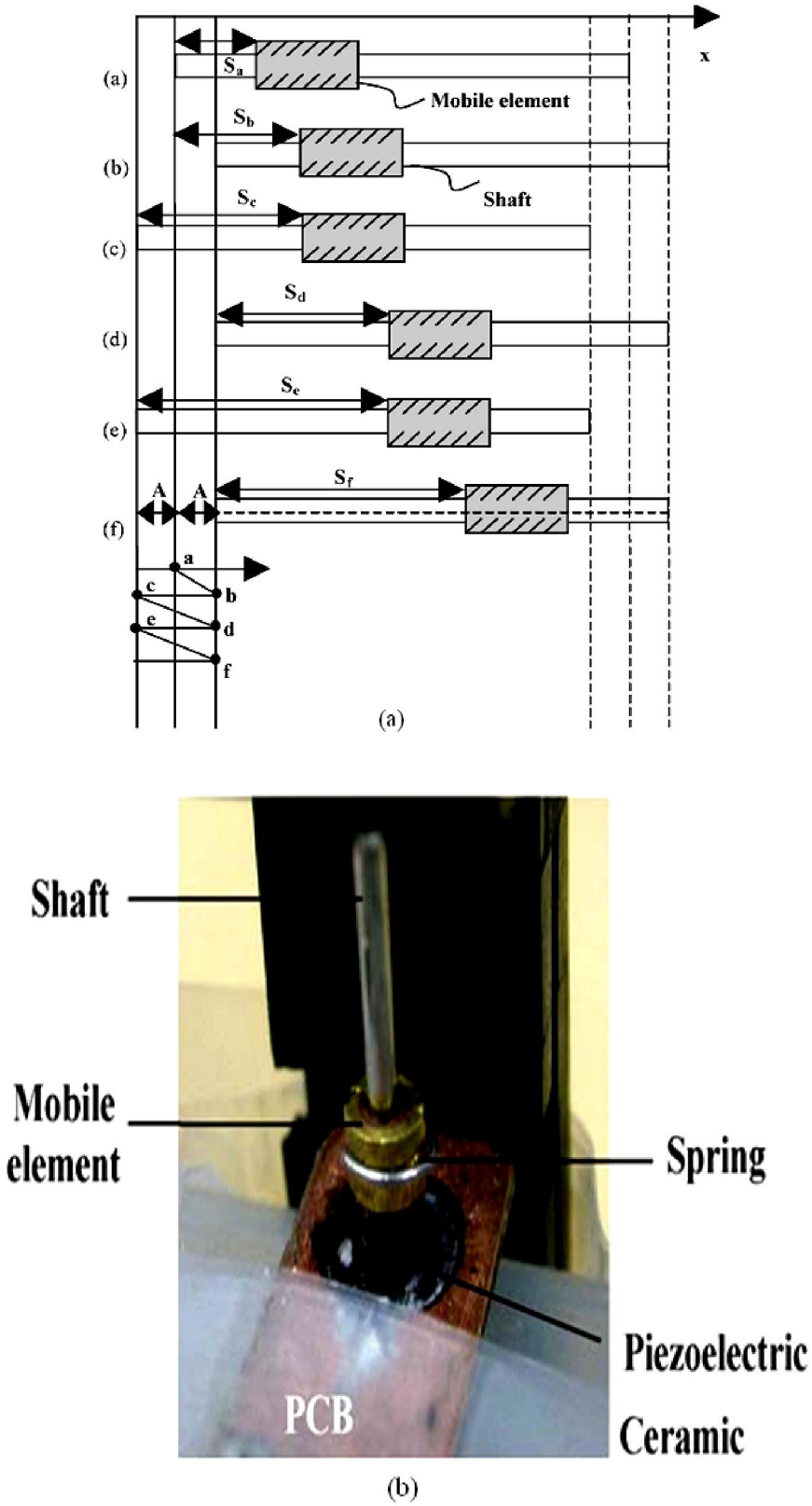

Figure 1.7 The impact ultrasonic linear motor a) principle of the inertia displacement b) structure of the motor [10].

1.3.2.3 Multi-mode type ultrasonic linear motor

The inverse piezoelectric effect is the principle of making the piezoelectric material to be an oscillator in ultrasonic motor. Projection of a point on the actuator surface is an elliptical path [17, 39]. By pressing the oscillator against a slider, friction force between the oscillator and the slider occurs, resulting the oscillator drives the slider. Another way to create the elliptical trajectory is to use bending mode in the transverse direction as proposed by [15-16]. Other stators work by using bimodal vibration: longitudinal vibration mode and the bending vibration mode [15]. Figures 1.8 to 1.10 show the schematics diagram of multi-mode type ultrasonic linear motor.

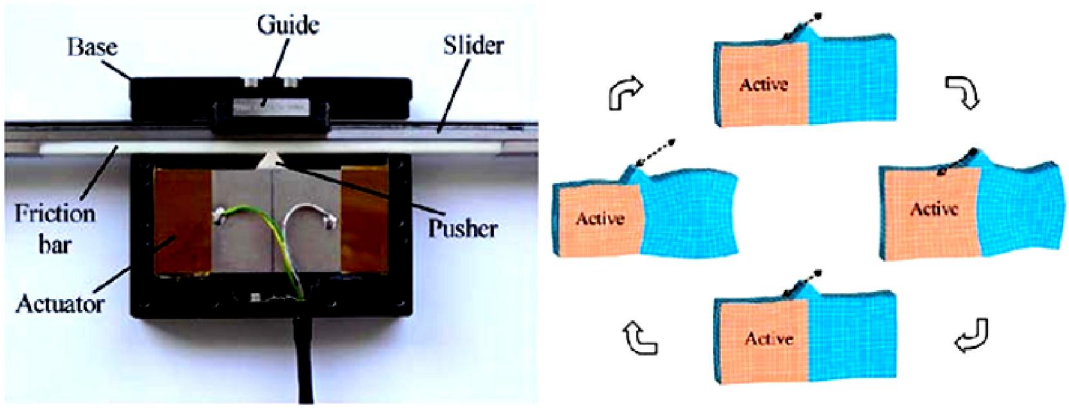

Figure 1.8 The multi-mode motor by Physikinstrumente [17].

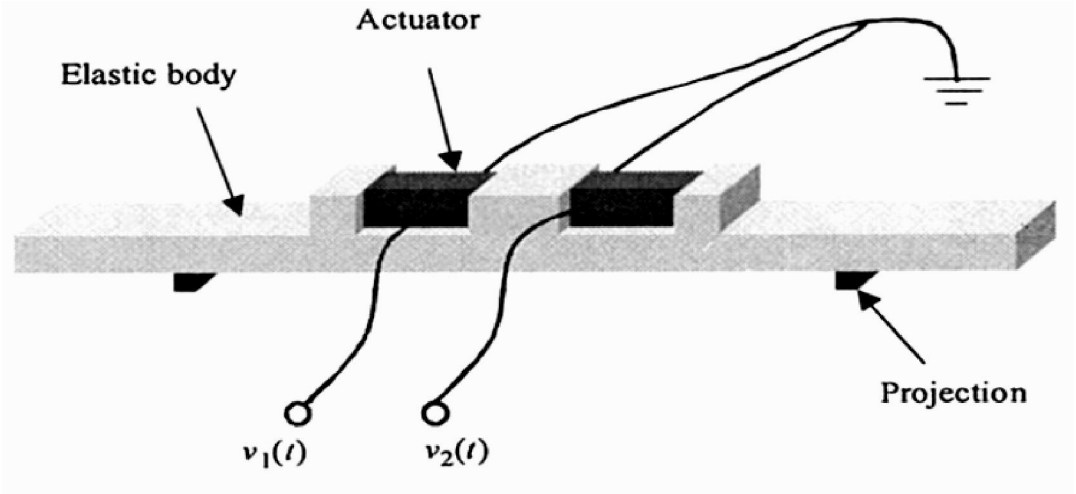

Figure 1.9 The multi-mode stator by B. Zhai et al., [16].

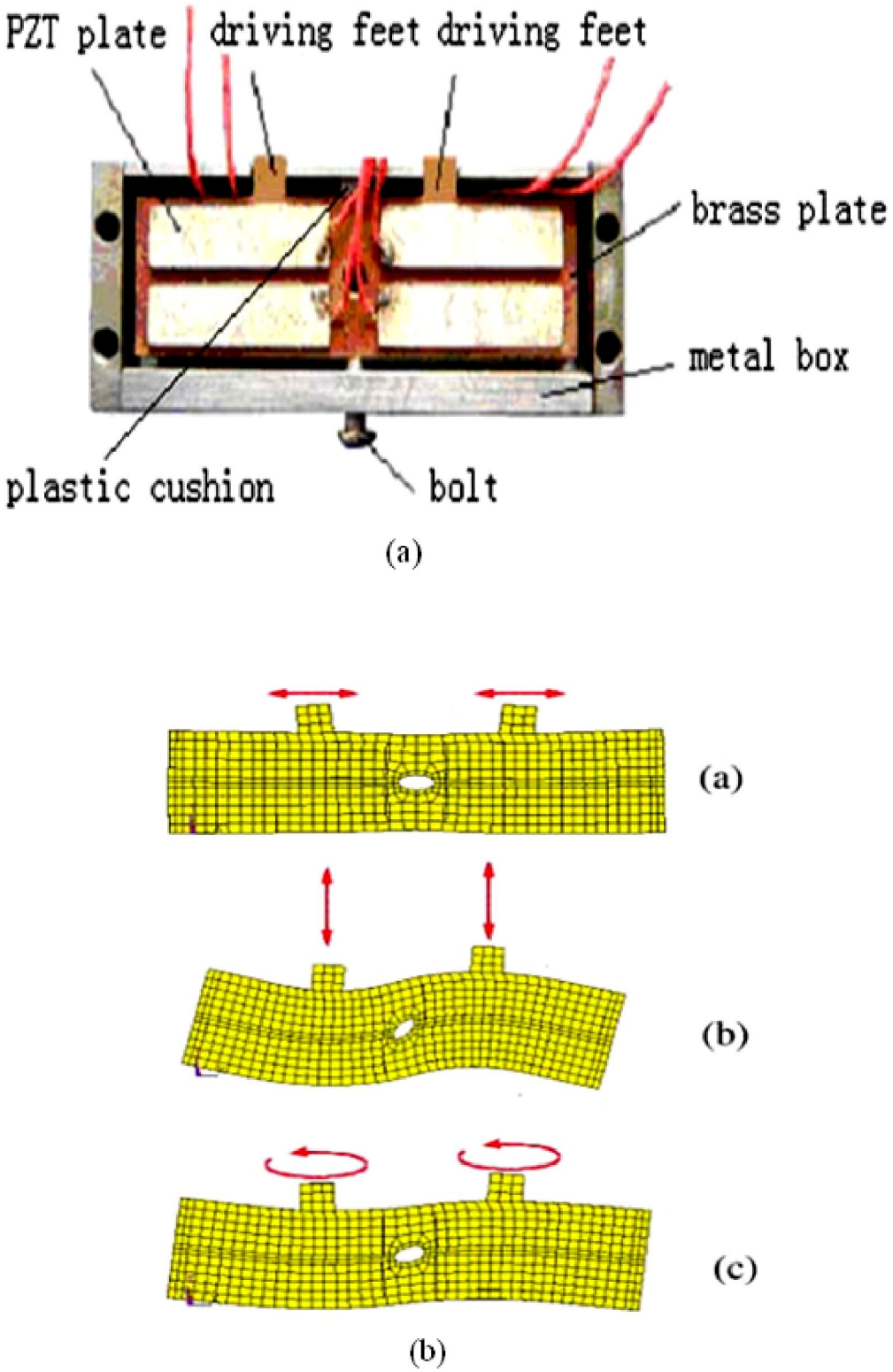

Figure 1.10. Prototype and vibration mode of the multi-mode stator by C. Lu et al., [15].

1.3.2.4 Traveling wave ultrasonic linear motor

The traveling wave ultrasonic motor relies on wave propagation through a stationary elastic media, the point on its surface undergo elliptical motion. This phenomenon is illustrated in Figures 1.11 to 1.13. The material of the media does not move only the wave that propagates. The compression preload between movable and stationary parts creates frictional driving force around the anti-node of the wave. Propagation of traveling wave shifts the contact area between rotor and stator propagation. The velocity of a traveling wave ultrasonic motor is directly proportional to the velocity of the traveling wave and distance from neutral plane of the stator to the contact surface [40].

Operating principle of the traveling wave ultrasonic linear motor based on the use of the converse piezoelectric effect as well. The transformation of the ultrasonic vibration to mechanical movement is obtained through the elliptic motion on the stator which penetrates the stator-to-rotor contact layer and generates driving force of the stator surface, and the force exciting in the contact zone between the stator and the rotor [12,20, 41].

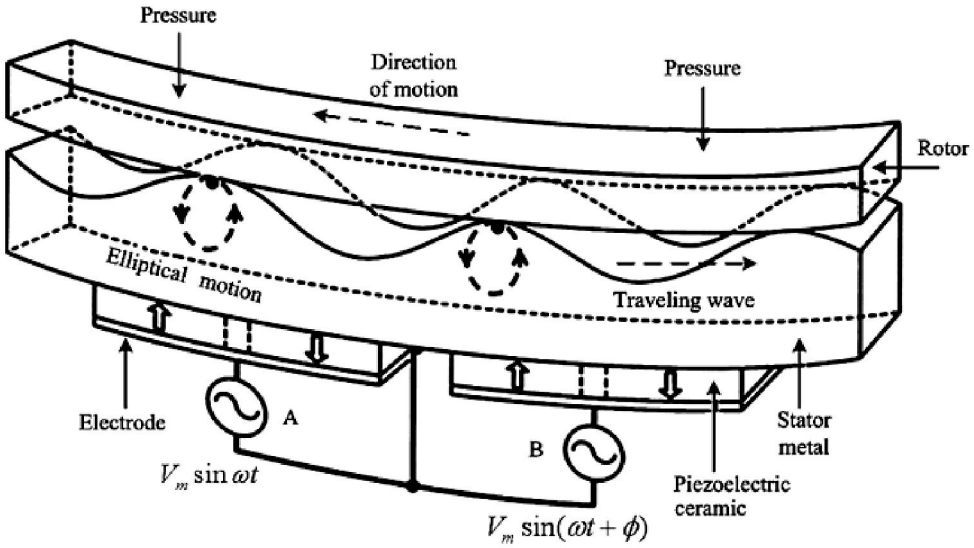

Figure 1.11 Fundamental of the traveling wave ultrasonic motor [18].

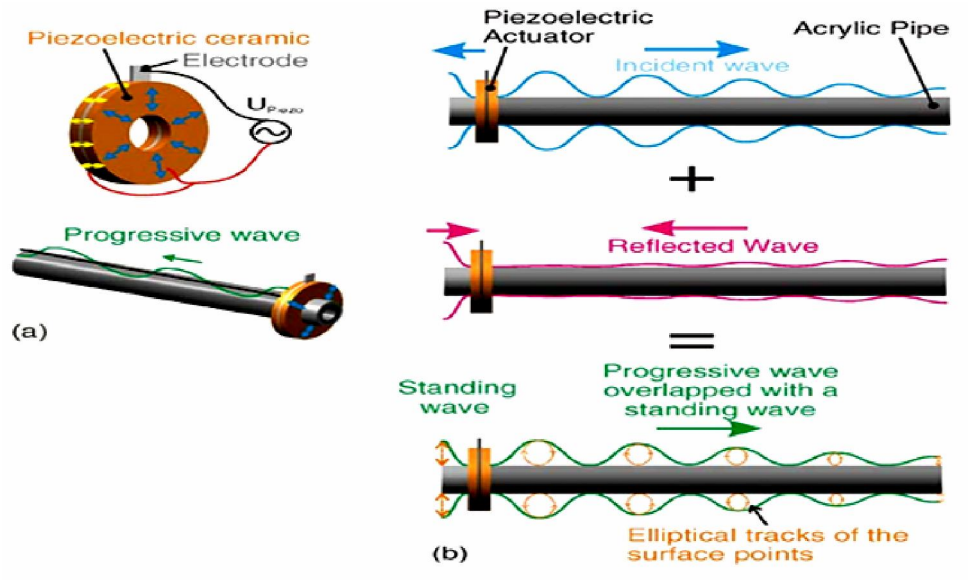

Figure 1.12 Traveling wave in an acrylic pipe [12].

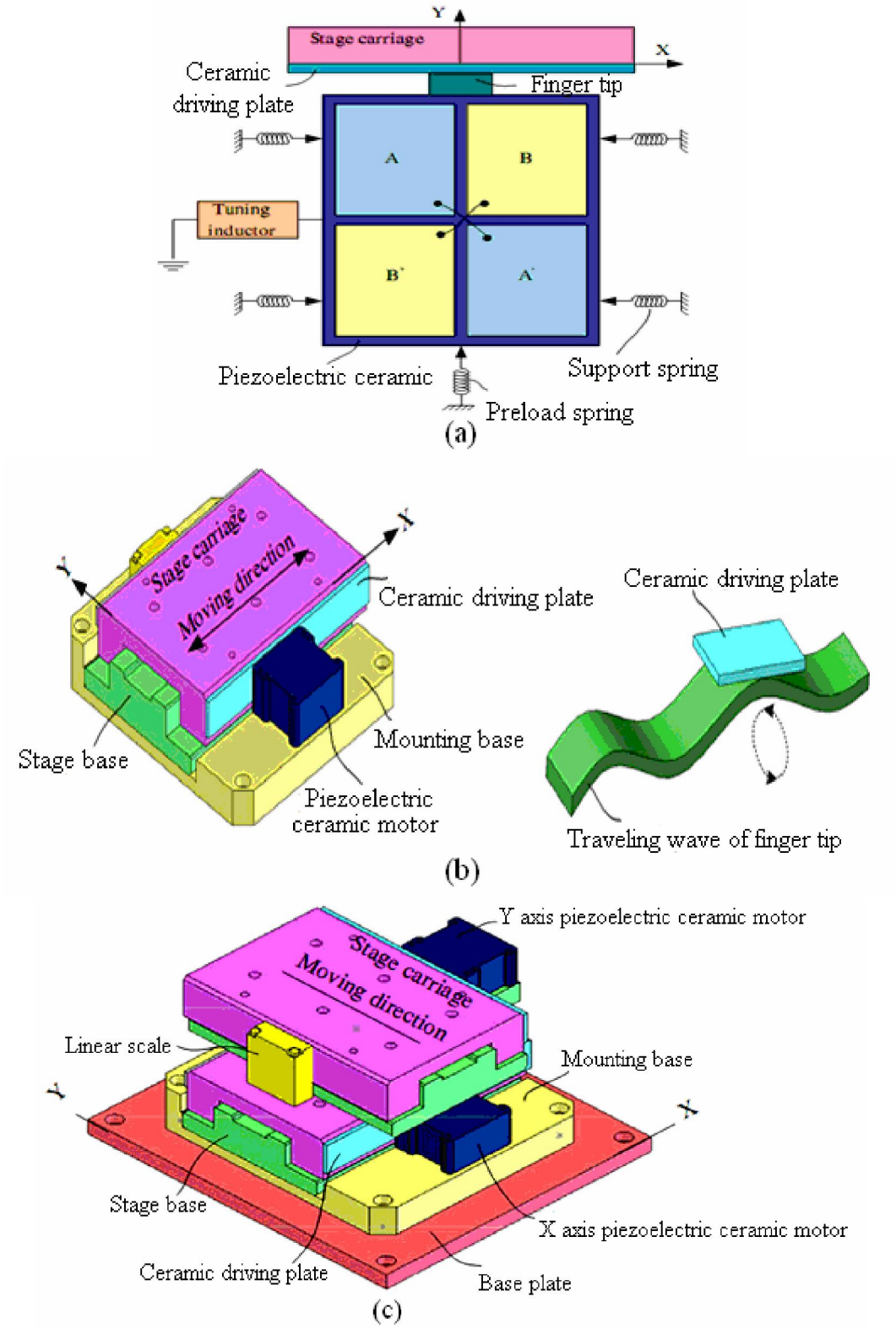

Figure 1.13 The linear piezoelectric stator a) structure of the piezoelectric motor b) driving principle c) configuration of the two axis piezo-motor stage [42].

1.3.2.5 Surface acoustic wave ultrasonic motor

A basic construction of the surface acoustic wave (SAW) motor is shown in Figures 1.14 and 1.15. The stator is a surface acoustic wave device made of lithiumniobate. At each end, interdigital transducers are deposited. Rayleigh wave is excited by the interdigital transducer with a high frequency electrical power source. A driving frequency is the resonance frequency which is determined by the pitch of the electrode. The driving frequency is approximately 10 to 100 MHz. The elliptical motion on the media surface due to the traveling Rayleigh wave is applicable to a traveling wave ultrasonic motor. The basic principle is the same as the traveling wave ultrasonic motor, however the vibration displacement of the wave is totally different [19, 21, 22, 43].

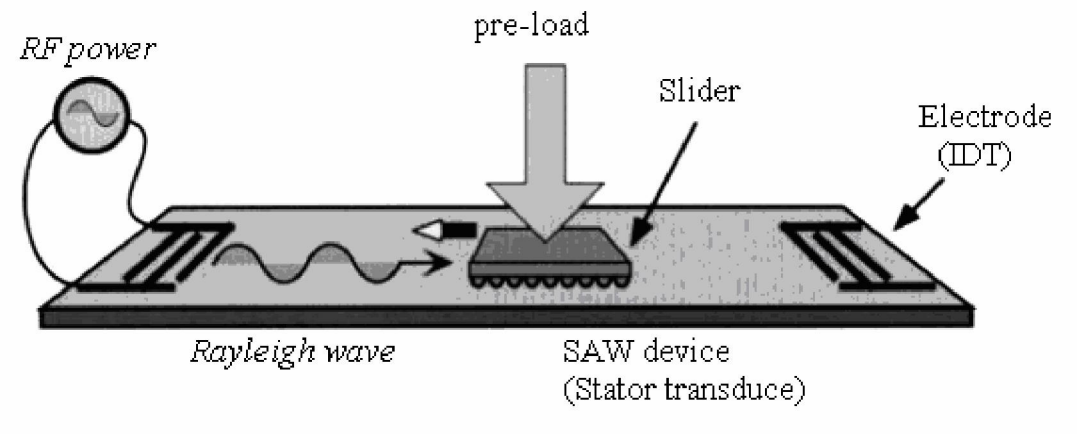

Figure 1.14 Operation principle of the SAW motor [21].

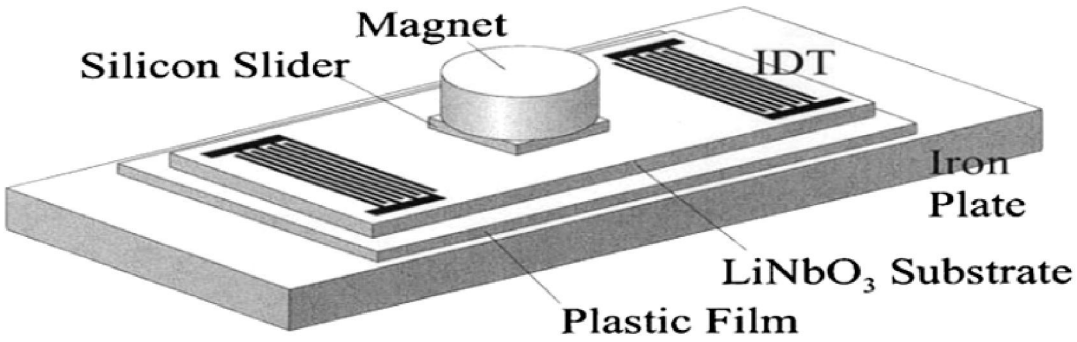

Figure 1.15 Miniaturized SAW linear motor [22].

1.3.2.6 Standing wave ultrasonic linear motor

The standing wave ultrasonic motor is also referred as a vibration-couple or a woodpecker motor, where the vibrator is connected to the piezoelectric driver and a tip portion generates flat elliptical movement [20,16] as shown in Figure 1.16. Vibration displacement of $u_x = u_0 \sin(\omega t + \alpha)$ is excited at a active piezoelectric vibrator. The vibrator piece generates bending force because of restriction at the rotor, causing the tip to move along the rotor face as shown in Figure 1.16. There are two types of the standing wave ultrasonic motor. One has a single set of active piezoelectric element and the other has two sets of active piezoelectric elements [44]. The single unit piezoelectric element can generate coupled vibration according to the geometry of the vibrator. For example, a longitudinal vibrator is able to excite bending vibration or a torsional/twist motion. This can produce by using nonsymmetrical transducers. There are two vibration directions for exciting the rotor. One is the direction normal to the vibration surface and the other is in the tangential

direction. For the multi-vibration mode, two sets of active piezoelectric elements can share work of friction control and driving force. Usually, the two vibrators are arranged in an orthogonal setup [45] as shown in Figure 1.18.

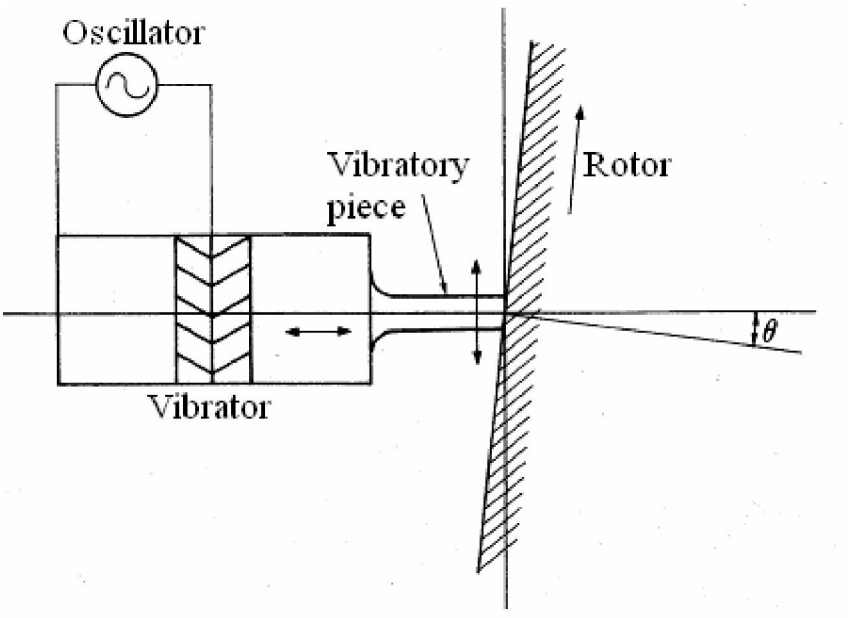

Figure 1.16 Standing wave ultrasonic motor [44].

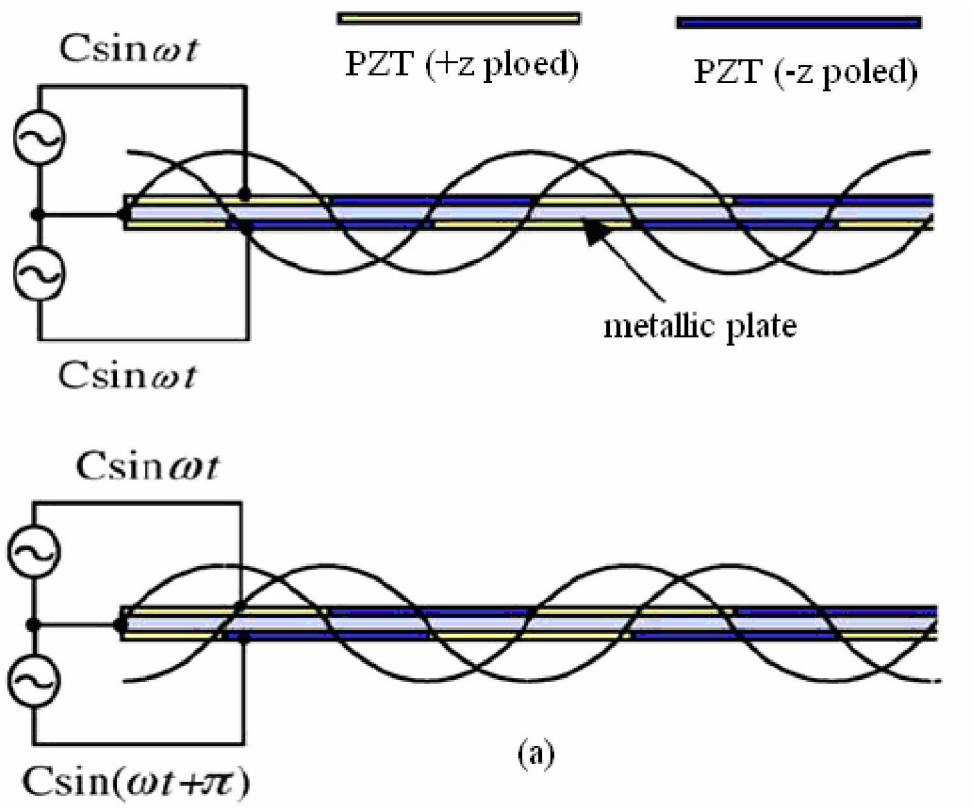

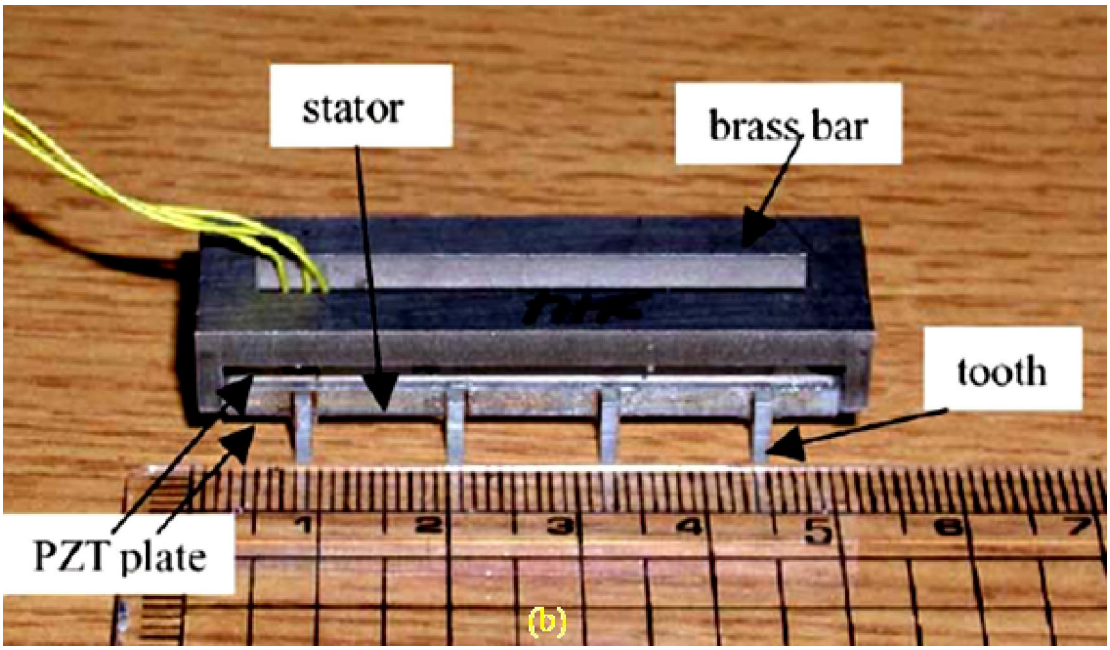

Figure 1.17 The standing wave ultrasonic motor: (a) two electrode patterns patch bonded on stator; (b) prototype of a standing wave ultrasonic motor [13].

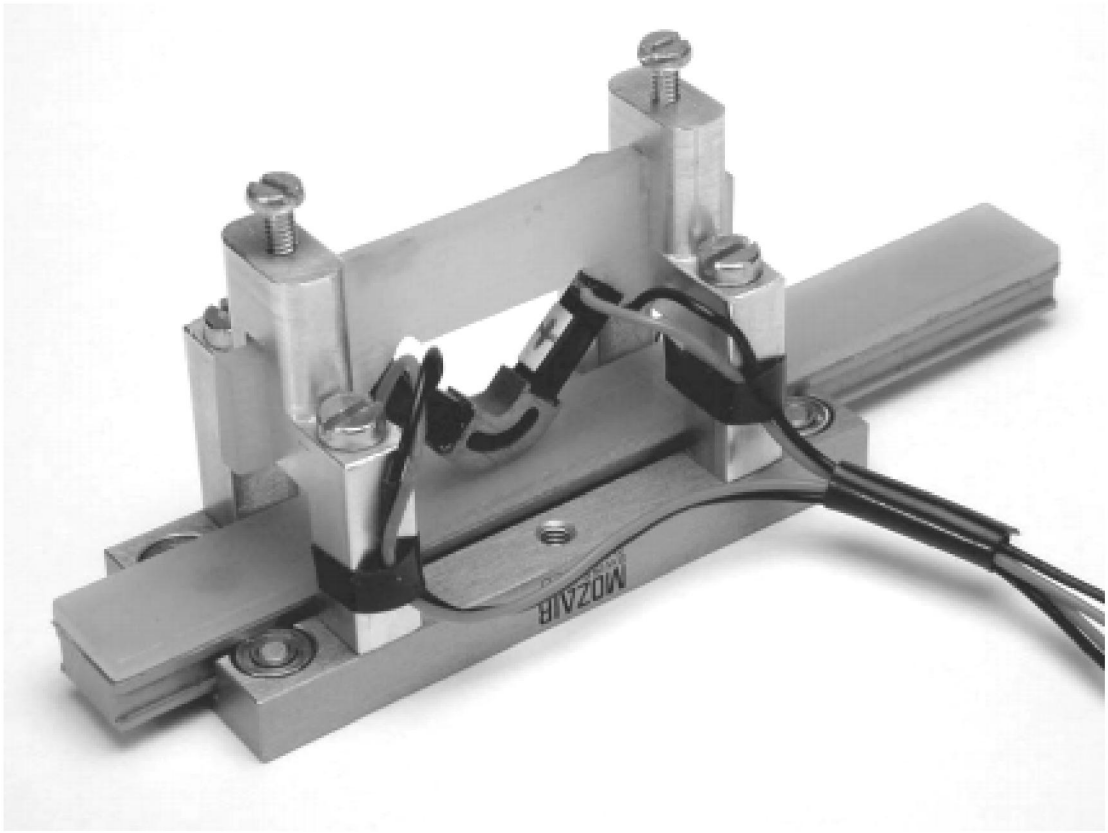

Figure 1.18 Prototype of the standing wave ultrasonic motor [45].

1.4 Performance Parameters of Ultrasonic Motors

Generally, performance of ultrasonic motors depends on two main factors. They are heat generation due to motor operation and properties of the friction material. The discussion is as follows.

1.4.1 Heat generation

A problem of ultrasonic motors is heat generation during operation, which sometimes temperature is upto 120 ^{o}C during operation. This can cause a serious degeneration of the motor characteristics through depolarization of piezoelectric

material. Therefore, ultrasonic motor should require a very hard type piezoelectric material with a high mechanical quality factor Q, to surpass the depolarization temperature during operation. It is also notable that the actual mechanical vibration amplitude at the resonance frequency is directly proportional to the mechanical quality factor (Q) [33, 46].

1.4.2 Friction material

Efficiency of ultrasonic motors strongly depends on the force transmission at stator-to-rotor interface. Hence, improvement of the friction material yields the better force transmission. The high friction layer between a stator and a rotor causes increased efficiency and performance. There are many types of the friction coating material such as glass embedded Teflon (GET), titanium aluminum nitride (TiAIN), titanium nitride (TiN), diamond like carbon (DLC) and silicon incoporated-dimond like carbon (Si-DLC) [33, 47-53]. Furthermore, dynamic properties and lifetime of the ultrasonic motors are also related to the friction coating material used in the sliding interface [33, 47, 50-53].

1.5 Other parameters

The actuator patterns bonded on a stator of the curvilinear ultrasonic motors were reported by [6]. The fundamental principle of the curvilinear motor is the traveling wave ultrasonic motors. In the study, number and size of the actuator patches are the same for both actuator patterns in order to investigate the system

response at the same amount of excitation. There are two different patterns. One is partially laminated in the middle of the arc stator span, pattern 1 (Figure 1.19); the other is partially laminated near the supports, pattern 2 (Figure 1.20). Each pattern has three pair, respectively, bonded on top and bottom surfaces. Location shift between the actuator on top and bottom surfaces is a half of actuator length. For both bottom and top actuator groups are excited by a pair of electrical signals: Asin(ωt) and Acos(ωt), where A is the signal amplitude and ω is the driving frequency. The result found that the configuration of partially bonded piezoelectric actuators near the stator supports (pattern 2) can generate effective traveling waves because it has less wave fluctuation as compared with those generated in pattern 1.

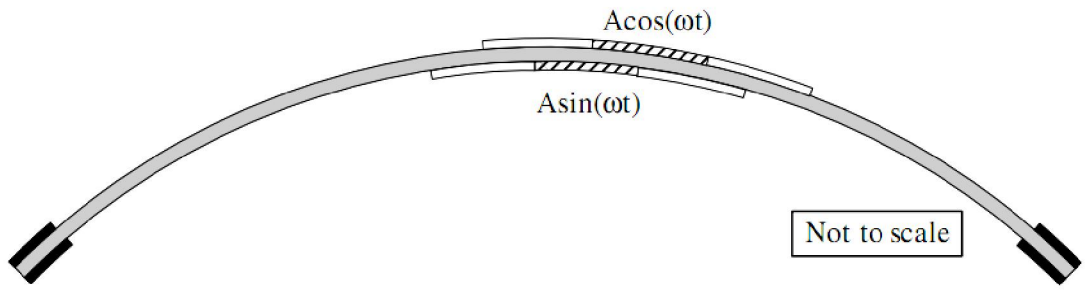

Figure 1.19 The partially laminated arc stator with piezoelectric actuators in the middle of the arc span (pattern 1) (▭: steel; ▬: damping material; ▭: PZT + polarity; ▨: PZT – polarity.) [6].

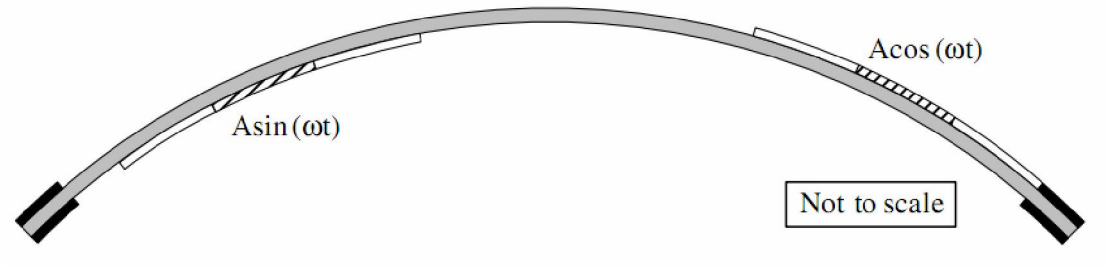

Figure 1.20 The partially laminated arc stator with piezoelectric actuators near the supports (pattern 2) (▭: steel; ■: damping material; ▭: PZT + polarity; ▨: PZT – polarity.) [6].

Ultrasonic linear motors can be applied for many applications as mentioned before. Several types of ultrasonic linear motor have been developed for improving in performance perspective e.g., increasing driving force, synergetic positioning a bundled miniature [4, 7, 9, 54-55], adjustment the shapes of the stator and increasing the tooth on the stator surface for increasing the motor performance [15, 56], improving design by using a bimorph cantilever beam as an actuator [57-58], changing design the principle based on inertia displacement [8, 10, 12]. Furthermore, patterns of the actuator bonded on the stator surface have been reported by [6, 59]. In practical applications, partially bonded actuators can reduce weight, material cost, power consumption and required maintenance of ultrasonic motors. However, the arc motor reported by [6] still has large number of actuators bonded on the stator causing high structural stiffness. This directly effects power consumption of the ultrasonic motor. However, a parameter of the energy consumptions for the ultrasonic linear motor has not been completely reported. At the present, electronic device and components are in small-sized; the ultrasonic linear motor with low energy consumption is required to be a low-energy-consumption operating device. The goal of this research is to reduce number of the piezoelectric actuators used in the linear

ultrasonic motor and to study parameters that affect the motor performance. In this research, the traveling wave type ultrasonic motor is selected because it has high propagation wave amplitude, implying high driving force, when driving at the natural frequency [28].

1.6 Objectives of Research

1. To design an ultrasonic linear motor by reducing the number of piezoelectric actuators in order to reduce energy consumption.
2. To study performance parameters and relationship of dynamic characteristic of the ultrasonic linear motor.

1.7 Scopes of Research

1. Investigate and analyze characteristics of the ultrasonic linear motor by using finite element and experimental methods.
2. Fabricate a laboratory prototype of the ultrasonic linear motor for demonstration and testing.

1.8 Expected Results

1. A new design of the ultrasonic linear motor with reducing number of piezoelectric actuators
2. Parametric relationships and characteristics of the ultrasonic linear motor.

In the following chapter, fundamental theory and knowledge will be provided as a basis understanding before designing and testing the ultrasonic linear motor later on.

Chapter 2

Piezoelectric Material

2.1 Introduction

In this chapter, characteristic of the piezoelectric material is studied. The piezoelectric material has two effects which are the direct and inverse piezoelectric effects. The direct piezoelectric effect is phenomenon of a material that has ability to generate and electrical charge in proportional to the external applied force. The inverse piezoelectric effect is a phenomenon when an electric field applies in parallel with polarization direction of the material and that induces expansion of the material. In other words, the inverse piezoelectric effect means that the material changes its geometry or dimension when an electrical voltage is applied. The direct piezoelectric effect means that the material generates an electrical voltage when a mechanical force is applied.

In the present, the piezoelectric ceramics (PZT) are made by many different manufacturers with variety of processes to achieve certain material properties. In general, the PZT ceramics are divided into two groups: soft and hard. Important properties of the piezoelectric ceramic related to the design of ultrasonic motors are given in Table 2.1.

The behavior of a PZT plate polarized along its axis is illustrated in Figure 2.1. For clearness, the magnitude of the effect has been overstated. Figure 2.1(a) shows the PZT plate under no-load condition. Afterwards, if an external force (compressive or

tensile) is applied on the material, then the PZT plate generates voltage between the electrodes that effect is called the direct piezoelectric effect. Conversely, if an electrical voltage is applied on the material, then the dimensions of PZT plate are changed increasingly or decreasingly depended on either positive or negative field, respectively. This effect is called the inverse piezoelectric effect as depicted in Figure 2.1(b).

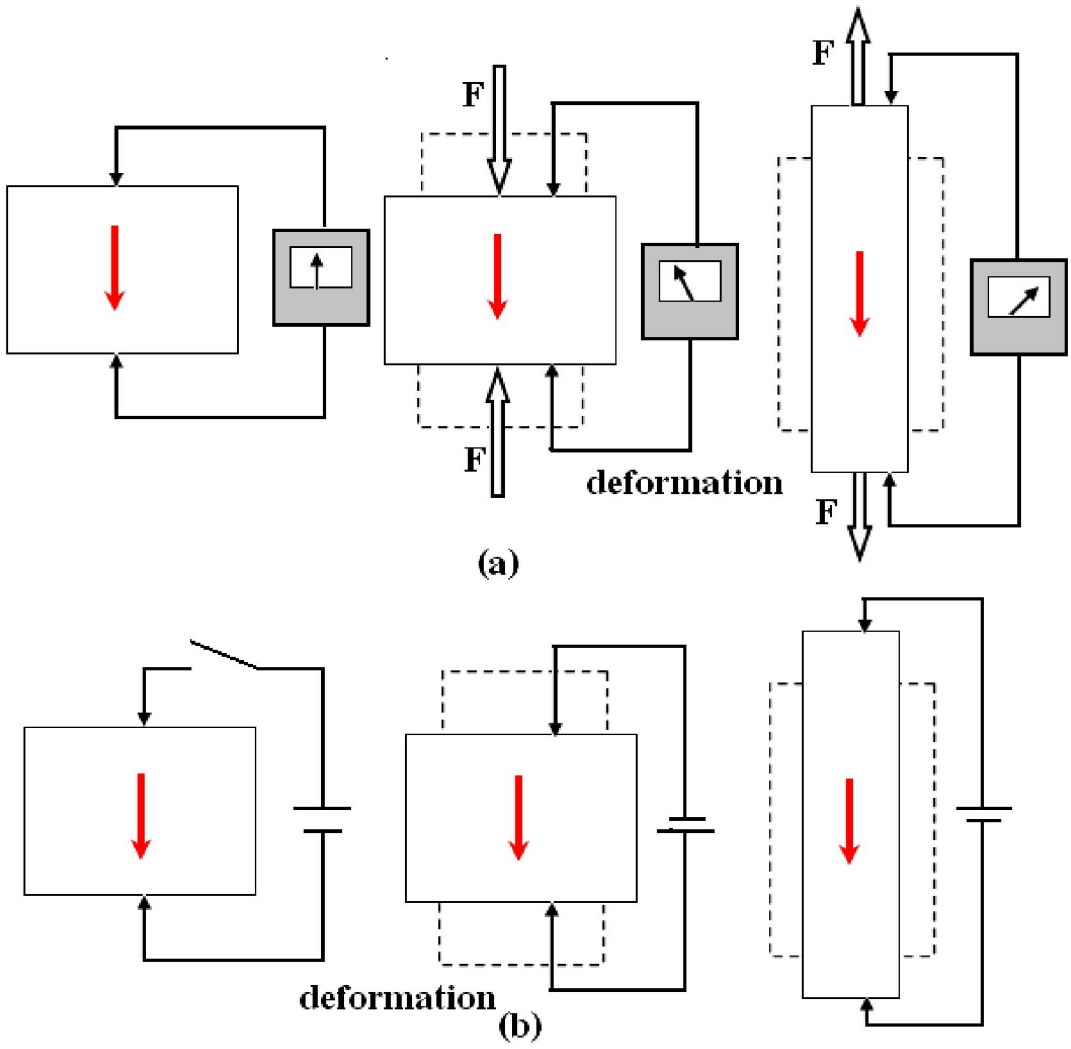

Figure 2.1 Piezoelectric effects: (a) direct effect and (b) inverse effect

Table 2.1 Properties of soft and hard piezoelectric materials

Soft PZT	Hard PZT	Effect on
High dielectric constant	Low dielectric constant	Actuator capacitance (causes of electric loss)
High dielectric loss	Low dielectric loss	Electric loss
Low mechanical quality factor Q (~50)	High mechanical quality factor Q (~900)	Resonance amplification (High Q~low damping)
Low Young's modulus	High Young's modulus	Actuator stiffness
High strain coefficient	Low strain coefficient	Actuator stroke

*Markus G. Bauer., 2001

The hard piezoelectric ceramic is normally selected for designing of ultrasonic piezoelectric motors. The purpose is to excite the motor at one of its mechanical resonance, which should be above 20 kHz to avoid audible noise. The actuation stroke is amplified at this resonance. Although the hard piezoelectric ceramic has the higher strain coefficient (smaller stroke), but its exhibit the lower damping losses which increases vibration amplitude at resonance and also minimizes heat generation during operation [40].

The classification of the crystallographic material can be divided into thirty two classes. Eleven of these classes have a centre of symmetry and twenty one non-centrosymmetric classes as shown in Figure 2.2. The twenty one of non-centre symmetric class can be divided into twenty piezoelectric and one non-piezoelectric class. The twenty piezoelectric classes can be divided into ten unique polar axis and ten spontaneously polarized class. Their spontaneous polarization is decreased by

increasing of temperature. Therefore, these materials are named pyroelectric. Moreover, the ferroelectric is a subclass of the pyroelectrics which has two or more orientation stages. The orientation stage can be switched from one state to another by an electric field. These two orientation states have identical crystal structure, but differ only in their electric polarization vectors at zero electric field. All ferroelectric materials are piezoelectric material, but not all piezoelectric materials are ferroelectric material [60-61].

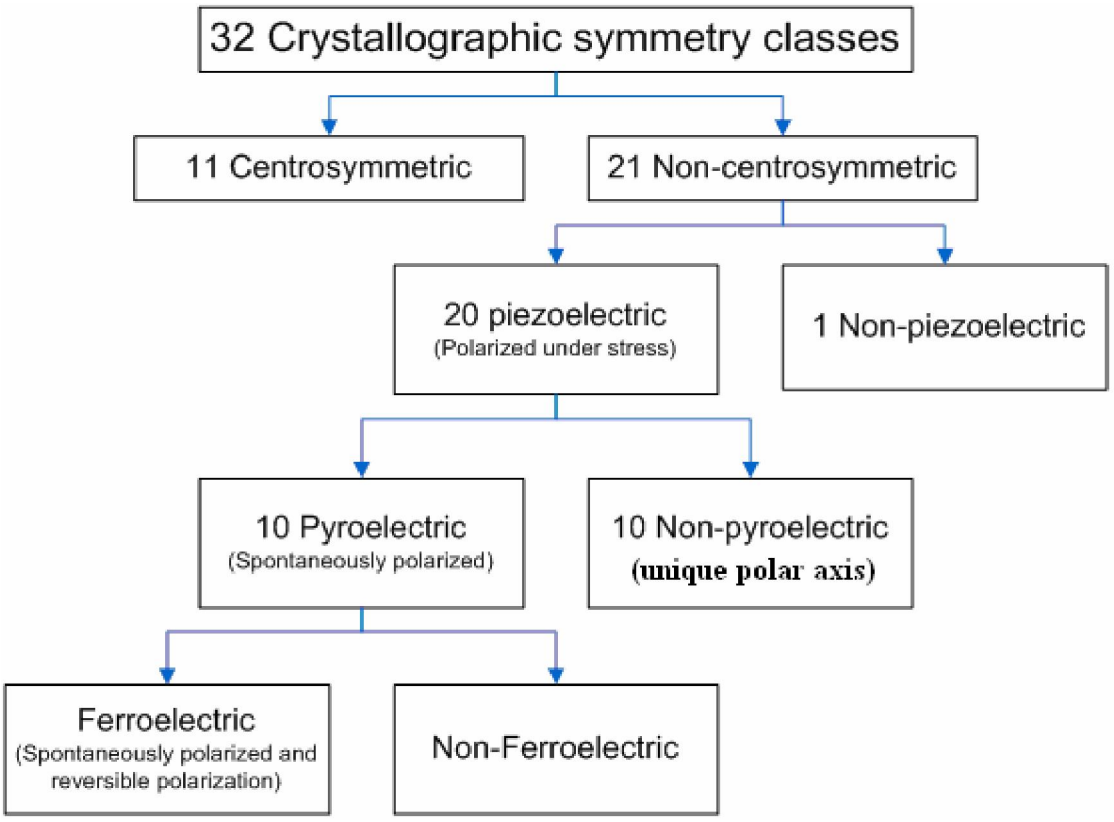

Figure 2.2 Classification of symmetry relating piezoelectric, pyroelectric and ferroelectric materials [61].

For selection of the piezoelectric material in applications should be consider high piezoelectric coefficient because its yield large strain and vibration amplitude. The direct piezoelectric effect can be used for transformer and igniter applications. Meanwhile, the inverse piezoelectric effect can be used for actuator and ultrasonic motor applications.

2.2 Polarization of Piezoelectric Material

Generally, piezoelectric material has electrical dipoles arranged in random direction. In order to obtain useful macroscopic response, the dipoles must be permanently aligned with one another through a poling process. In the poling process, the material is heated above its Curie temperature with a strong electric field applied on them. Curie temperature is a property of a piezoelectric material whereas the dipole can be changed orientation in the solid phase when heated. When the material is cooled below Curie temperature, the dipoles are still maintained permanently. After a poling process, the material has a residual polarization and piezoelectric characteristic. A change of geometric dimensions (expansion or contraction) of the piezoelectric material resultant a change of electrical charges.

A working temperature of the piezoelectric material is usually well below its Curie temperature [62]. If the piezoelectric material is heated above the Curie temperature with non electric field applied, dipoles of the material are revert to random orientation. Even at lower temperature, the application of very strong electric field can cause dipole shifting out of preferred alignment. Figure 2.3 illustrates procedure of poling process.

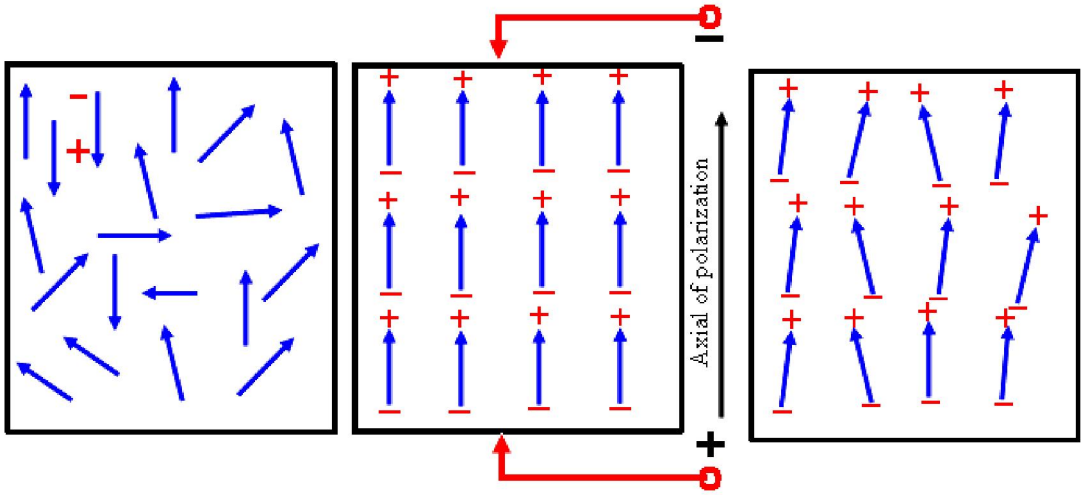

Figure 2.3 Polarization of the piezoelectric material.

2.3 Piezoelectric Properties

The piezoelectric ceramic is an orthotropic material. Therefore, physical properties are related to both directions of an applied mechanical force and electrical field. Hence, the piezoelectric properties have an index with two subscripts describing directions of two related quantities, such as applied strain electrical potential.

2.3.1 Piezoelectric charge constant

The piezoelectric charge constant, d, is an important indicator in selection of material for strain-dependent applications. Definition of the piezoelectric charge constants are described below.

d_{33} is the induced polarization in the 3-direction per unit stress applied in the 3-direction in unit of [C/N] or the induced strain in the 3-direction per unit electric field applied in the 3-direction in unit of [m/V].

d_{31} is the induced polarization in the 3-direction per unit stress applied in the 1-direction in unit of [C/N] or the induced strain in the 1-direction per unit electric field applied in the 3-direction in unit of [m/V].

d_{15} is the induced polarization in the 3-direction per unit shear stress applied in the 2-direction in unit of [C/N] or the induced shear strain in the 2-direction per unit electric field applied in the 1-direction in unit of [m/V].

.

2.4 Elastic Compliance

The elastic compliance of the piezoelectric material can be defined by the relationship between stress and strain by mean of Hook's law as

$$x_{ij} = s_{ijkl} X_{kl} \tag{2.1}$$

where s_{ijkl} is the elastic compliance (m^2/N), x_{ij} is the strain and X_{ij} is the stress (N/m^2), respectively.

2.5 Piezoelectric Effects

Two effects of the piezoelectric material are direct and inverse piezoelectric effects. The piezoelectric effects occur when the voltage or mechanical force applies on its. Relationship between stress (X_{ij}) and charge density (D_i) of the piezoelectric material can be defined as follows,

$$D_i = d_{ijk} X_{jk} \tag{2.2}$$

$$D_i = \varepsilon_{ij} E_j \tag{2.3}$$

$$D_i = p_i \Delta T \tag{2.4}$$

where d_{ijk} is the third rank tensor of the piezoelectric coefficients; ε_0 is the dielectric permittivity of vacuum, P_i is the polarization of the piezoelectric element, ε_{ij} is the dielectric permittivity, p_i is the pyroelectric coefficient, E_j is electric field and ΔT is the difference temperature. Furthermore, the inverse piezoelectric effect depends on an electrical applied voltage on the piezoelectric material. The relationship between strain and electric field of the inverse piezoelectric effect is defined as follow,

$$x_{ij} = d_{kij} E_k = d^t_{ijk} E_k \tag{2.5}$$

where d^t is the transposed matrix of the inverse piezoelectric coefficient. However, sign of charge density and strain depended on direction of the mechanical force and electric field. Therefore, the piezoelectric coefficients have positive and negative sign.

Normally, the piezoelectric coefficient that measured in the same electrical filed direction is called the longitudinal coefficient. In the other hand, the piezoelectric coefficient that measured in the orthogonal to the electrical field direction is called the transverse coefficient. The piezoelectric coefficient that measured in plane of piezoelectric material is called shear coefficient.

2.6 Matrix Notation

The tensor of elastic compliance and piezoelectric coefficients can be written in a matrix short form as shown in Table 2.2.

Table 2.2 Matrix notation of piezoelectric coefficients.

Tensor notation	Name	Matrix notation
$x_{ii} = 11, 22, 33$	strain	$x_m,\ m = 1,2,3$
x_{ij} = 23 or 32, 13 or 31, 12 or 21	shear strain	$x_m,\ m = 4,5,6$
S_{ijkl}	elastic compliance (m^2/N)	S_{mn}, m and n = 1,2,3
$2S_{ijkl}$	elastic compliance (m^2/N)	S_{mn}, m and n = 4,5,6
$4S_{ijkl}$	elastic compliance (m^2/N)	S_{mn}, m and n = 4,5,6
d_{ijk}	piezoelectric coefficient (C/N)	$d_{im}, m = 1,2,3$
d_{ijk}	piezoelectric coefficient (C/N)	$\frac{1}{2} d_{im}, m = 4,5,6$

Accordingly, Equations (2.1), Equation (2.2) and Equation (2.5) can be written in the matrix form as

$$x_m = S_{mn} X_n \tag{2.6}$$

$$D_i = d_{im} X_m \tag{2.7}$$

$$x_m = d_{im} E_i \tag{2.8}$$

where i = 1,2,3 and m,n = 1,2,...,6, respectively.

2.7 Piezoelectric Constitutive Equations

The relationship between thermal property, mechanical property and electrical property of the piezoelectric material is considered through thermodynamic principle. Hence, this relationship is important for modeling and understanding response of the piezoelectric material. The first and second laws of thermodynamic define the energy change as follow,

$$dU = TdS + X_{ij} dx_{ij} + E_i dD_i \tag{2.9}$$

where dU is the internal energy, T is the temperature, dx is the revolution of strain, dD is the dielectric displacement and dS is the entropy.

Integrating Equation (2.9) leads to

$$\int dU = \int TdS + \int X_{ij} dx_{ij} + \int E_i dD_i \tag{2.10}$$

$$U = TS + X_{ij} x_{ij} + E_i D_i \tag{2.11}$$

Gibbs free energy (G) defined from Equation (2.11) can be written as

$$G = U - TS - X_{ij} x_{ij} - E_i D_i . \tag{2.12}$$

The derivative of Gibbs free energy in Equation (2.12) is given by

$$dG = -SdT - x_{ij}dX_{ij} - D_i dE_i \,. \tag{2.13}$$

Each terms of Equation (2.13) can be written as

$$S = -\left(\frac{\partial G}{\partial T}\right)_{X,E} \tag{2.14}$$

$$x_{ij} = -\left(\frac{\partial G}{\partial X_{ij}}\right)_{T,E} \tag{2.15}$$

$$D_i = -\left(\frac{\partial G}{\partial E_i}\right)_{T,X} . \tag{2.16}$$

Therefore Equation (2.14) to (2.16) can be written as

$$dS = \left(\frac{\partial S}{\partial T}\right)_{X,E} dT + \left(\frac{\partial S}{\partial X_{ij}}\right)_{T,E} dX_{ij} + \left(\frac{\partial S}{\partial E_i}\right)_{T,X} dE_i \tag{2.17}$$

$$dx_{ij} = \left(\frac{\partial x_{ij}}{\partial T}\right)_{X,E} dT + \left(\frac{\partial x_{ij}}{\partial X_{ij}}\right)_{T,E} dX_{ij} + \left(\frac{\partial x_{ij}}{\partial E_k}\right)_{T,X} dE_k \tag{2.18}$$

$$dD_i = \left(\frac{\partial D_i}{\partial T}\right)_{X,E} dT + \left(\frac{\partial D_i}{\partial X_{ij}}\right)_{T,E} dX_{ij} + \left(\frac{\partial D_i}{\partial E_j}\right)_{T,X} dE_j . \qquad (2.19)$$

The revolution of strain of Equation (2.18) can be defined as follow

$$dx_{ij} = \left[\frac{\partial x_{ij}}{\partial T}\right]_{X,E} dT + \left[\frac{\partial x_{ij}}{\partial X_{ij}}\right]_{T,E} dX_{ij} + \left[\frac{\partial x_{ij}}{\partial E_k}\right]_{T,X} dE_k$$

where $\alpha_{ij} = \left[\frac{\partial x_{ij}}{\partial T}\right]_{X,E} dT$ is thermal expansion.

$$\left[\frac{\partial x_{ij}}{\partial X_{ij}}\right]_{T,E} dX_{ij} = \left[\frac{dx_{ij}}{dX_{ij}}\right]_{T,E} dX_{ij} \qquad (2.20)$$

where $x_{ij} = s_{ijkl} X_{kl}$

$$\left[\frac{\partial x_{ij}}{\partial X_{ij}}\right]_{T,E} dX_{ij} = \frac{d\left(s_{ijkl} X_{kl}\right) \quad dX_{ij}}{dX_{ij}}$$

$$\left[\frac{\partial x_{ij}}{\partial X_{ij}}\right]_{T,E} dX_{ij} = \left[s_{ijkl} \frac{d\left(X_{kl}\right)}{dX_{ij}} + X_{kl} \frac{d\left(s_{ijkl}\right)}{dX_{ij}}\right]_{T,E} dX_{ij}$$

$$\left[\frac{\partial x_{ij}}{\partial X_{ij}}\right]_{T,E} dX_{ij} = s_{ijkl}{}^{T,E} dX_{kl} \qquad (2.21)$$

$$\left[\frac{\partial x_{ij}}{\partial E_K}\right]_{T,X} dE_K = \left[\frac{dx_{ij}}{dE_K}\right]_{T,E} dE_K \tag{2.22}$$

where $x_{ij} = d_{kij} E_K$;

$$\left[\frac{\partial x_{ij}}{\partial E_K}\right]_{T,X} dE_K = \frac{d\left(d_{kij} E_k\right)_{T,E}}{dE_k} dE_K$$

$$\left[\frac{\partial x_{ij}}{\partial E_K}\right]_{T,X} dE_K = \left[d_{kij}\frac{dE_k}{dE_k} + E_k \frac{d\left(d_{kij}\right)}{dE_k}\right]_{T,E} dE_K$$

$$\left[\frac{\partial x_{ij}}{\partial E_K}\right]_{T,X} dE_K = d_{kij} dE_k \,. \tag{2.23}$$

Substituting Equations (2.20) to (2.23) into Equation (2.18) yields

$$dx_{ij} = \alpha_{ij}^{X,E} dT + s_{ijkl}^{T,E} dX_{kl} + d_{kij}^{T,X} dE_k \,. \tag{2.24}$$

Integrating Equation (2.24) leads to

$$x_{ij} = \alpha_{ij}^{X,E} \Delta T + s_{ijkl}^{T,E} X_{kl} + d_{kij}^{T,X} E_k \,. \tag{2.25}$$

The dielectric displacement of the Equation (2.19) can be defined as follows

$$dD_i = \left(\frac{\partial D_i}{\partial T}\right)_{X,E} dT + \left(\frac{\partial D_i}{\partial X_{ij}}\right)_{T,E} dX_{ij} + \left(\frac{\partial D_i}{\partial E_j}\right)_{T,X} dE_j$$

where $D_i = p_i T$;

$$\left[\frac{\partial D_i}{\partial T}\right]_{X,E} dT = \frac{\partial (p_i T)}{\partial T} dT = \frac{d(p_i T)}{dT} dT$$

$$\left[\frac{\partial D_i}{\partial T}\right]_{X,E} dT = \left[p_i \frac{dT}{dT} + T \frac{dp_i}{dT}\right]_{X,E} dT$$

$$\left[\frac{\partial D_i}{\partial T}\right]_{X,E} dT = p_i dT \tag{2.26}$$

where $D_i = d_{ijk} X_{jk}$;

$$\left[\frac{\partial D_i}{\partial X_{ij}}\right]_{T,E} dX_{ij} = \left[\frac{dD_i}{dX_{ij}}\right]_{T,E} dX_{ij}$$

$$\left[\frac{\partial D_i}{\partial X_{ij}}\right]_{T,E} dX_{ij} = \frac{d(d_{ijk} X_{jk})}{dX_{ij}} dX_{ij}$$

$$\left[\frac{\partial D_i}{\partial X_{ij}}\right]_{T,E} dX_{ij} = \left[d_{ijk}\frac{dX_{jk}}{dX_{ij}} + X_{jk}\frac{d\left(d_{ijk}\right)}{dX_{ij}}\right]_{T,E} dX_{ij}$$

$$\left[\frac{\partial D_i}{\partial X_{jk}}\right]_{T,E} dX_{ij} = d_{ijk}\,dX_{jk} \tag{2.27}$$

where $D_i = \varepsilon_{ij}E_j$;

$$\left[\frac{\partial D_i}{\partial E_j}\right]_{T,X} dE_j = \left[\frac{dD_i}{dE_j}\right]_{T,X} dE_j$$

$$\left[\frac{\partial D_i}{\partial E_j}\right]_{T,X} dE_j = \left[\frac{d\left(\varepsilon_{ij}E_j\right)}{dE}\right]_{T,X} dE_j$$

$$\left[\frac{\partial D_i}{\partial E_j}\right]_{T,X} dE_j = \left[\varepsilon_{ij}\frac{dE_j}{dE_j} + E_j\frac{d\varepsilon_{ij}}{dE_j}\right]_{T,X} dE_j$$

$$\left[\frac{\partial D_i}{\partial E_j}\right]_{T,X} dE_j = \varepsilon_{ij}^{T,X} dE_j\,. \tag{2.28}$$

Substituting Equation (2.26) to (2.28) into Equation (2.19) can be expressed as

$$dD_i = p_i^{X,E} dT + d_{ijk}^{T,E} dX_{jk} + \varepsilon_{ij}^{T,X} dE_j\,. \tag{2.29}$$

Integrating Equation (2.29) leads to

$$D_i = p_i^{X,E}\Delta T + d_{ijk}^{T,E} X_{jk} + \varepsilon_{ij}^{T,X} E_j \tag{2.30}$$

where p_i is the Pyroelectric coefficient (C/m^2.K), α_{ij} is thermal expansion tensor. In the case of the temperature constant process, the first term of Equation (2.25) and Equation (2.30) are zero.

Hence, Equation (2.25) and Equation (3.30) can be written as follows,

$$x_{ij} = s_{ijkl}^{T,E} X_{kl} + d_{kij}^{T,X} E_k \tag{2.31}$$

$$D_i = d_{ijk}^{T,E} X_{jk} + \varepsilon_{ij}^{T,X} E_j . \tag{2.32}$$

In addition, the above equations can be written in matrix forms as

$$x_m = s_{mn}^{T,E} X_n + d_{im}^{T,X} E_i \tag{2.33}$$

$$D_i = d_{im}^{T,E} X_m + \varepsilon_{ij}^{T,X} E_j . \tag{2.34}$$

Consequently, strain or charge of piezoelectric material must be measured at the stress or electric field equal to zero, respectively. It is well known that the above equations, Equations (2.33) and (2.34), are ***the piezoelectric constitutive equations***.

2.8 Piezoelectric Power Consumption

The power consumption is very important issue in application of design piezoelectric device especially for small power electronic device [63-66]. The power consumption of the piezoelectric actuator is depended on its geometry, material properties, driving voltage and frequency [65, 67-68]. Interaction between the piezoelectric actuator and its host structure can be described by using the structural mechanics. The system is integrated with actuator and host structure. The mechanical impedance includes mass, damping, boundary condition, rigidity and spatial coordinate are also considered in the system equation [63]. The general methodology to study the power consumption of a piezoelectric system integrated with induced strain actuators by mean of coupled electro-mechanic analysis has been reported by [63-65, 67-68].

The electrical power is a product of voltage and current which can be written as

$$P = IV \tag{2.35}$$

where P is the electrical power, V is the applied voltage and I is the current, respectively. The apparent power using the magnitude of the electrical admittance is defined as

$$Y = \frac{I}{V} \tag{2.36}$$

where Y is the electrical admittance. Analytical development of power consumption focuses on development of the electrical admittance of piezoelectric actuators.

Furthermore, the electrical admittance is directly developed from the piezoelectric constitutive equations as written below

$$x_1 = \frac{1}{Y_{11}^E} X_1 + d_{31} E_k \tag{2.37}$$

$$X_1 = Y_{11}^E \left(x_1 - d_{31} E_k \right) \tag{2.38}$$

$$D_3 = \varepsilon_{33} E_k + d_{31} X_1 \tag{2.39}$$

where x_1 is the strain of piezoelectric actuator, Y_{11}^E is the elastic modulus of piezoelectric material, X_1 is the stress acting on piezoelectric actuator, d_{31} is the piezoelectric constant, E_k is the electric field, D_3 is the electric displacement and ε_{33} is the dielectric constant. Furthermore, the electric field is defined by $E = V/h_a$ where h_a is the actuator thickness. Accordingly, the charge and current can be defined as

$$Q = \iint_{xy} D_3 dx dy = b_a l_a \left(\varepsilon_{33} E_k + d_{31} X_1 \right) \tag{2.40}$$

$$I = \frac{dQ}{dt} = \frac{d}{dt} \left[\varepsilon_{33} E_k + d_{31} X_1 \right] b_a l_a = \frac{d}{dt} \left[\left(\varepsilon_{33} - d_{31}^2 Y_{11} \right) E_k + d_{31} Y_{11} x_1 \right] b_a l_a \tag{2.41}$$

where b_a is the actuator width and l_a is the actuator length. It is assumed that strain of the actuator is the same as strain of the host structure. Thus, the strain of the piezoelectric actuator can be written as

$$x_1 = \frac{\Delta l_a}{l_a} = \frac{x}{l_a} \quad . \tag{2.42}$$

If the strain of Equation (2.40) is equal to zero, the admittance of piezoelectric actuator can be written as

$$\frac{\tilde{I}(s)}{\tilde{V}(s)} = \tilde{Y}(s) = s\left(\varepsilon_{33} - d_{31}^2 Y_{11}^E\right)\frac{b_a l_a}{h_a} = sC \, . \tag{2.43}$$

The constant C is the effective capacitance of piezoelectric actuator. Moreover, the effective capacitance is related to dielectric and piezoelectric properties. The effective capacitance can be expressed as

$$C = \left(\varepsilon_{33} - d_{31}^2 Y_{11}\right)\frac{b_a l_a}{h_a} \, . \tag{2.44}$$

The admittance of Equation (2.43) in complex domain can be transformed to that of the frequency domain as

$$Y(\omega) = \omega\left(\varepsilon_{33} - d_{31}^2 Y_{11}^E\right)\frac{b_a l_a}{h_a} = \omega C \tag{2.45}$$

The estimation of magnitude of the piezoelectric power consumption can be defined as follows

$$P_{\max} = \frac{1}{2}\omega_{\max} V_{\max}^2 \sum_{i=1}^{n} C_i \tag{2.46}$$

$$C_{total} = \sum_{i=1}^{n} C_i \tag{2.47}$$

where C_i is the effective capacitance of the actuator i, n is the number of actuators being used. To accurately predict the maximum power consumption by using Equation (2.46), the maximum effective capacitance of the piezoelectric actuators must be measured [65].

2.9 Electromechanical Coupling Coefficient

The electromechanical coupling factor, k_{ij}, is an indicator of the effectiveness in consumption of an electrical energy into mechanical energy, or vice versa. The first subscript to k_{ij} denotes direction along the applied electrodes; the second subscript denotes the direction along the applied or developed mechanical energy. The electromechanical coupling coefficient values provided by supplier's specifications typically are theoretical maximum values. At low input frequencies, a typical piezoelectric ceramic can convert 30 – 75% of the energy conversion in one form to another, depending on composition of the ceramic and direction of forces involved. A high electromechanical coupling coefficient usually is desirable for efficient energy

conversion, but the electromechanical coupling coefficient value does not account dielectric or mechanical losses, nor recovery of unconverted energy. The accurate measurement of efficiency is the ratio of useable energy delivered by the piezoelectric element to the total energy taken up by the element. The piezoelectric ceramic elements in well designed systems can exhibit efficiency exceed 90%. The dimensions of a piezoelectric element can dictate value of electromechanical coupling factor (k_{ij}). For a thin disc of piezoelectric element, a planar coupling factor, k_p, expresses by a radial coupling which is the coupling between an electric field parallel to the 3-direction in which the element is polarized and mechanical effects that produce radial vibrations, orthogonal to the direction of polarization (the 1-and-2-directions). For discs or plates that have large surface dimensions relative to its thickness, the thickness coupling factor, k_t or k_{33} represents a coupling between an electric field in the 3-direction and mechanical vibrations in the same direction. Furthermore, resonance frequencies in the thickness direction of discs or plate element are much higher than resonance frequencies in the transverse direction. Meanwhile, strongly attenuation of transverse vibration at the high resonance frequency, a result of the transverse contraction/expansion that accompanies the expansion/contraction in thickness, make k_t lower than k_{33}, the corresponding factor for longitudinal vibrations of a thin rod of the same material, for which a much lower longitudinal resonance frequency more closely matches the transverse resonance frequency [69]. Each of the electromechanical coupling coefficients is explained as follows,

k_{33} is the electromechanical coupling coefficient for electric field in the 3-direction (parallel to direction in which ceramic element is polarized) and longitudinal vibrations in the 3-direction (ceramic rod, length >10x diameter)

k_t is the electromechanical coupling coefficient for electric field in the 3-direction and vibrations in the 3-direction (thin disc, surface dimensions large relative to thickness; $k_t < k_{33}$)

k_{31} is the electromechanical coupling coefficient for electric field in the 3-direction (parallel to direction in which ceramic element is polarized) and longitudinal vibrations in the 1-direction (perpendicular to direction in which ceramic element is polarized) (ceramic rod)

k_p is the electromechanical coupling coefficient for electric field in the 3-direction (parallel to direction in which ceramic element is polarized) and radial vibrations in the 1-direction and 2-direction (both perpendicular to direction in which ceramic element is polarized) (thin disc)

The electromechanical coupling coefficient represents efficiency of converting electrical energy into mechanical energy, or converting mechanical energy into electrical energy [62]. The k-value defined in terms of k^2 as

$$k^2 = \frac{w_1}{w_2}. \tag{2.48}$$

In the case of direct piezoelectric effect, w_1 is the mechanical energy output, w_2 is electrical energy input. Conversely, for the inverse piezoelectric effect, w_1 is

the electrical energy output and w_2 is the mechanical energy input. Since piezoelectricity is an interaction between electrical and mechanical transformation the electromechanical coupling coefficient can be defined as [62]

$$k^2 = \frac{d^2}{\varepsilon^T x^E} \tag{2.49}$$

where d is the piezoelectric constant, ε^T is the dielectric constant at constant stress and x^E is the elastic compliance at constant electric field, respectively.

2.10 Depolarization of Piezoelectric Material

The piezoelectric material after a poling treatment, it will be permanently polarized. It must be handling with care to ensure that the piezoelectric ceramic will not depolarized, since this would resultant in partial or even total loss of its piezoelectric properties. The depolarization of piezoelectric materials depends on electrical, mechanical or thermal effect [33, 62]. All kinds of piezoelectric depolarization are described next.

2.10.1 Electrical depolarization

Exposure to a strong electric field in the opposite direction of exciting will cause depolarization of a piezoelectric material. Level of depolarization depends on grade of piezoelectric material, exposure time, temperature, but electric fields of 200-500 V/mm or greater typically have a significant depolarizing effect. An alternating

current also have a depolarizing effect during each half cycle that opposite the exciting piezoelectric domain [69].

2.10.2 Mechanical depolarization

Mechanical depolarization occurs when a mechanical stress applies on a piezoelectric element high enough to excite orientation of the domains, and hence destroy alignment of the dipole. The limit of mechanical stress should be considered for each material grade.

2.10.3 Thermal depolarization

Thermal depolarization occurs when a piezoelectric material is heated to its Curie temperature, the domains will become disordered and the material will be depolarized. The recommended upper operating temperature for a piezoelectric ceramic should be approximately half-way between 0°C and the Curie temperature. Within the recommended operating temperature range, temperature-associated changes in the orientation of the domain are reversible. On the other hand, these domain changes can create charge displacements and electric fields. However, temperature fluctuations can generate relatively high voltages, capable of depolarizing the ceramic element. A capacitor can be incorporated into the piezoelectric device to accumulate the superfluous electrical energy. For a particular material, the pyroelectric charge constant (the change in polarity for a given change in temperature) and the pyroelectric field strength constant (the change in electric field for a given change in temperature) are indicators of the vulnerability of the material to pyroelectric effects. A high piezoelectric charge constant (pyroelectric charge

constant) or high piezoelectric voltage constant (pyroelectric field strength constant) indicates good resistance to pyroelectric effect [69].

2.11 Applications of the Piezoelectric Material

A piezoelectric device or system can be constructed for any application that based on a electromechanical transducer principle. For a particular application however, limitations include size, weight, and cost of the system. Piezoelectric devices can be applied on four categories of application, i.e., generator, sensor, actuator, and transducer. Characteristics for each category are summarized in this section.

2.11.1 Generators

Piezoelectric ceramics can generate sufficient charge to spark across an electrode gap, and thus they can be used as ignitors in lighters, gas stoves, welding equipments, and similar apparatus. Piezoelectric ignition systems are small and simple. These are advantages of the piezoelectric ignitor over kinds of ignitors such as permanent magnet, high voltage transformer and capacitor ignitors. Alternatively, electrical energy generated by a piezoelectric element can be stored. A technique of making multilayer capacitors has been used to construct multilayer piezoelectric generators as well. Such piezoelectric generators are excellent solid state batteries for electronic circuits [33,69].

2.11.2 Sensors

A sensor converse a physical parameter, such as acceleration or pressure, into an electrical signal. In some sensors, the physical parameter can act directly on the piezoelectric element. In other devices, an acoustical signal establishes vibration in the piezoelectric element and the vibrations is, in turn, converted into an electrical signal. Moreover, the sensor provides a visual, audible, or physical response to the shock vibration input, for example, automobile seatbelt locking system response to a rapid deceleration [33,69].

2.11.3 Actuators

A piezoelectric actuator converts an electrical signal into a precisely controlled physical displacement. It is well suitable for adjusting precision machining tools, lenses, or mirrors. Piezoelectric actuators are also used to control hydraulic valves, spray valves, act as small-volume pumps or special-purpose motors, and other precision required applications. Piezoelectric motors are unaffected by energy efficiency loss that limited in miniaturization of electromagnetic motors. Piezoelectric motor can be constructed to sizes less than 1 cm^3. An important advantage of piezoelectric motors is absence of electromagnetic noise. Alternatively, if the physical displacement is prevented, the piezoelectric actuator will generate a useable force [18,69].

2.11.4 Transducers

Piezoelectric transducers converse electrical energy into mechanical vibration energy, oftenly in a from of sound or ultrasound to perform a task. Piezoelectric

transducers can be generated audible sounds. The significant advantages over the electromagnetic speaker are that compact, simple, reliable, and minimal energy input can produce a high level of sound. These characteristics are ideally matched to needs of battery-powered devices because the piezoelectric effect is reversible, a transducer can be a generator of both ultrasound and a sensor to convert incoming sound into an electrical signal. Some devices are designed for measuring distance, flow rate, or fluid level by incorporate a single piezoelectric transducer in the signal-sending and-receiving roles; meanwhile, other designs incorporate two transducers and separate these roles. Piezoelectric transducers are also used to generate ultrasonic vibration for cleaning, atomizing liquids, drilling or milling ceramics or other materials, welding plastics, medical diagnostics, etc [69].

2.12 Chapter Summary

This chapter has provided study of the piezoelectric material characteristics in the piezoelectric ultrasonic linear motor and other applications. The topics are history, polarization, piezoelectric effects, piezoelectric constitutive equation, electromechanical coupling coefficient, depolarization and applications of the piezoelectric material, respectively. All characteristics of piezoelectric material are very important for design a well performance ultrasonic motor. However, performances of an ultrasonic motor are not only depended on the active piezoelectric material, but it is also depended on the contact interface between a stator and a rotor. The contact interface between a rotor and a stator will be studied in the next chapter.

Chapter 3

Mathematical Model of the Contact Interface

3.1 Introduction

In the research on ultrasonic motors, mathematical modeling of the contact mechanics and operational characteristics of the motors have been the issue for selection of contact materials and design parameters [70]. Mathematical models of the contact mechanic between the stator and rotor have been reported [71]. Furthermore, the Hertzian contact model for a linear ultrasonic motor has been studied [72], while evaluation of the motor performance of a traveling wave ultrasonic motor based on a model of a visco-elastic friction layer on stator and a rigid rotor has been presented [49, 73-78]. At the same time, some researchers presented performance estimation of an ultrasonic motor with a contact model of distributed liner spring between the stator and rotor interface [37, 79-84].

The purpose of this chapter is to study the mathematical model between stator and rotor for estimating performance of the piezoelectric ultrasonic linear motor; especially, the motor velocity and the driving force generated. Contact mechanics of ultrasonic motors is rather complicated due to the fact that many parameters should be taken to account. The operational characteristics depend on the geometry, frequency and vibration amplitude of the stator, stiffness and damping of the contact layer, flexibility of the rotor, normal pre-load force, static deflection of stator and rotor and frictional characteristics of the contact material as well as their surface topology and

microstructure [69]. However, mathematical models are able to guide for choice of the contact layer material and useful for understanding operational characteristics of the ultrasonic motors under action of a compressive force [85]. A spatial fixed reference frame $(\hat{x},\hat{z})$ is used. The model can be formulated in a moving reference frame by using the transformation of $\hat{x} = x + v_w t$, where the wave propagation velocity is $v_w = \lambda\omega/2\pi$. The moving reference frame moves with the wave crest and the description becomes independent in time [74].

In this study, the mathematical models of the linear ultrasonic motor, both visco-elastic friction layer and the linear spring are later used to compare with the experimental results.

3.2 Basic Modeling Assumption of the Ultrasonic Linear Motor

The structure and driving mechanism of a piezoelectric ultrasonic linear motor are related. Those include a lot of non-linear and uncertain factors. Moreover, all causes are very complicated. In order to simplify the problem, a model of visco-elastic foundation is being used. The following assumptions have been made for the contact layer analysis [49, 85-86].

1) The natural plane of the moves in the same way of an ideal traveling wave.

2) The variation of the model in depth direction can be ignored. Hence, the three-dimensional model is replaced by a two-dimensional model and the line contact is able to use for description.

3) The rotor is a rigid body and its surface is smooth. In addition, the friction material is visco-elastic and its surface is smooth, (the surface roughness is neglected.)

4) The surface of stator teeth is a continuous sinusoidal wave and the influence of the tooth space is neglected.

5) The motor runs at steady state (the starting and stopping motor effects are not considered.)

6) Coulomb friction law is valid on the contact interface between stator and rotor.

7) The friction layer is divided into tangential and normal component independently, which do not influence each other.

3.3 Natural Frequencies and Mode Shapes

Mode shape function and natural frequencies of a beam are functions of integer index (i) which may be associated with number of flexural haft-wave in the mode shape, there is a natural frequency and mode shape for each i. The bending mode shape and natural frequency of a beam are defined as follows [87],

$$f_i = \frac{\lambda_i^2}{2\pi L^2}\sqrt{\frac{E_b I_b}{m}}, \quad i = 1,2,3... \tag{3.1}$$

where λ_i is a dimensionless parameter which is a function of boundary conditions applied to the beam and $\lambda_i = (2i+1)\pi/2; \quad i\rangle 5$, m is the mass per unit length of the

beam, L is the length of the beam, E_b is the modulus of elasticity of the beam and I_b is the area moment of inertia of beam about neutral axis, respectively.

3.4 The Contact Interface Modeling

The first one, the contact layer of an ultrasonic motor was described by a visco-elastic fundamental model. It incorporates stiffness and damping parameters in both normal and tangential directions. Furthermore, influence of the inertia of the friction layer has been considered in this model. Figure 3.1 illustrates the visco-elastic fundamental model. In addition, normal equivalent stiffness C_N and tangential equivalent stiffness C_T result from shear deformation (U_x^k) and normal deformation (U_z^k) of an element of the contact layer with the width dx as shown in the Figure 3.2. The both stiffness components of the contact layer are defined as follows,

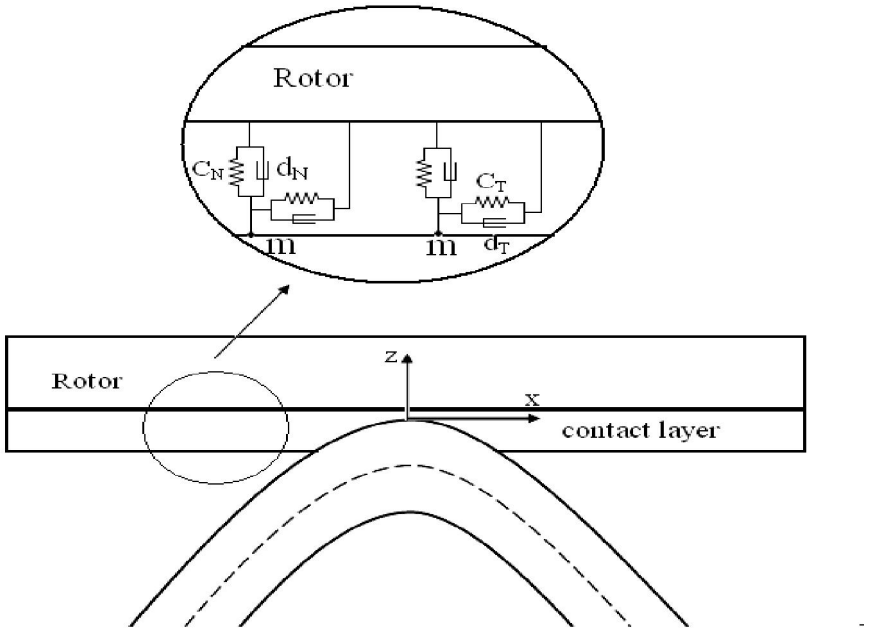

Figure 3.1 The visco-elastic contact model.

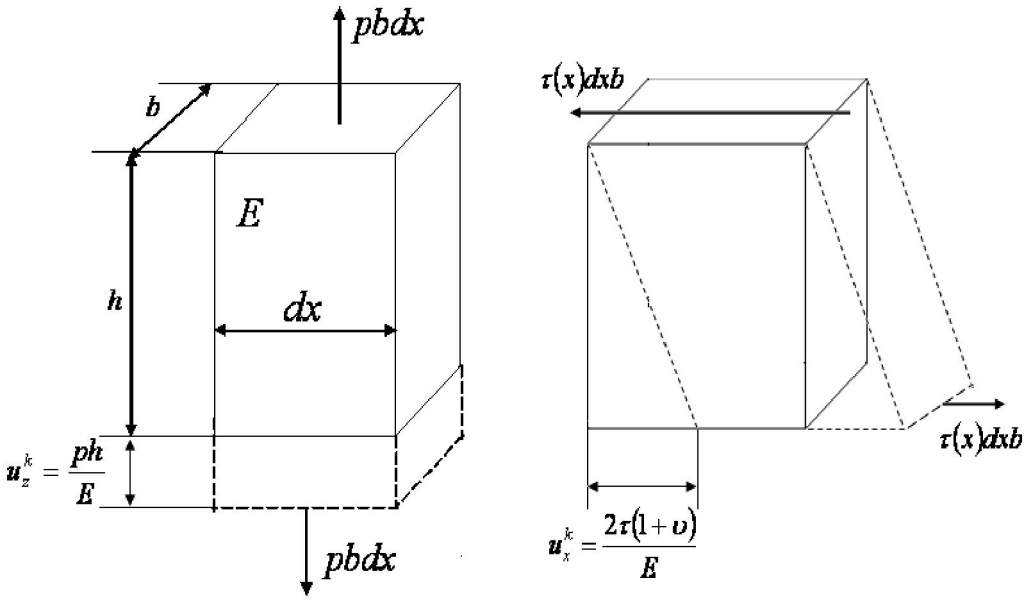

Figure 3.2 Displacements in normal and tangential directions.

$$C_N = \frac{Eb}{h_c} \tag{3.2}$$

$$C_T = \frac{Eb}{2h_c(1+\nu)} \tag{3.3}$$

where C_N is the normal equivalent stiffness; C_T is the tangential equivalent stiffness; D_N is the normal equivalent damping; D_T is the tangential equivalent damping; $m = \frac{1}{2}\rho_c b h_c$ is the equivalent mass; ρ_c is the density of the contact layer; h_c is the height of the contact layer; U_x^k is the shear deformation; U_z^k is the normal deformation; E_b is modulus of elasticity; υ is the Poisson's ratio; τ_x is the tangential stress in the x-direction and P is the normal stress in the z-direction. As assumed previously, the three-dimensional coordinate system is simplify two-dimensional system. The motion of the neutral plane of the stator with amplitude then becomes [30, 75, 77]

$$W(\hat{x}, t) = A \cos\left(\frac{2\pi\hat{x}}{\lambda} - \omega t\right) \tag{3.4}$$

where A denotes the amplitude of vibration and λ is the wavelength of the traveling wave.

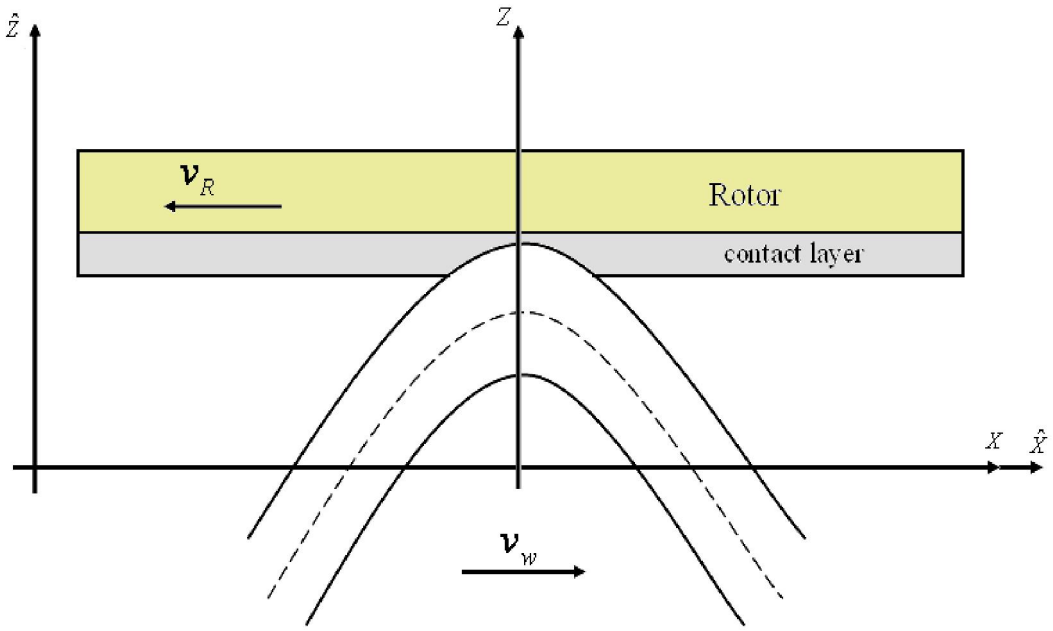

Figure 3.3 Contact mechanics between the stator and the rotor.

A frame of references is fixed on the neutral plane of the stator (x,z) as shown in Figure 3.3. The transformation between the fixed frame and moving frame can be expressed as $\hat{x} = x + V_w t$, where the wave propagation velocity is $V_w = \frac{\lambda\omega}{2\pi}$. Then, Equation (3.4) can be simplified as

$$w(x,t) = A\cos\left\{\frac{2\pi}{\lambda}(x + Vwt) - \omega t\right\} \tag{3.5}$$

$$w(x,t) = A\cos\left\{\frac{2\pi}{\lambda}\left(x + \frac{\lambda\omega}{2\pi}t - \omega t\right)\right\} \tag{3.6}$$

$$w(x,t) = A\cos\left\{\frac{2\pi x}{\lambda} + \frac{2\pi\lambda\omega}{\lambda 2\pi}t - \omega t\right\} \tag{3.7}$$

$$w(x,t) = A\cos\left[\frac{2\pi x}{\lambda}\right] \tag{3.8}$$

The normal displacement of a point on stator surface is

$$U_z(x) = A\cos\left[\frac{2\pi x}{\lambda}\right] + a \tag{3.9}$$

where a denotes the distance between surface of stator tooth and neutral plane of stator. The tangential displacement of a point on stator surface is

$$U_x(x) \approx -a\frac{d(w(x))}{d(x)} \tag{3.10}$$

$$U_x(x) = -a\frac{d}{d(x)}\left[A\cos\left\{\frac{2\pi x}{\lambda}\right\}\right] \tag{3.11}$$

$$U_x(x) = aA\frac{2\pi}{\lambda}\sin\left(\frac{2\pi x}{\lambda}\right) \tag{3.12}$$

The rotor is assumed to be a rigid body without normal displacement, and rotate at uniform speed of V_R. The rotor is pressed on the stator by a preload F_N and

compresses the friction layer on the stator. Figure 3.4 shows wave penetration into the contact layer. The displacement in the normal direction is constant because the rotor is a rigid body. For a compression force on the rotor, elliptical trajectory of point at the contact surface propels the rotor. The elliptical motion at the contact surface of the tooth tip is occurred by coupling the tangential and transverse displacements. The force transmission from the stator to the rotor is illustrated in Figure 3.4, where V_w is the velocity of traveling wave, V_R is the rotor velocity, K and L are the boundary conditions of the contact layer and stator.

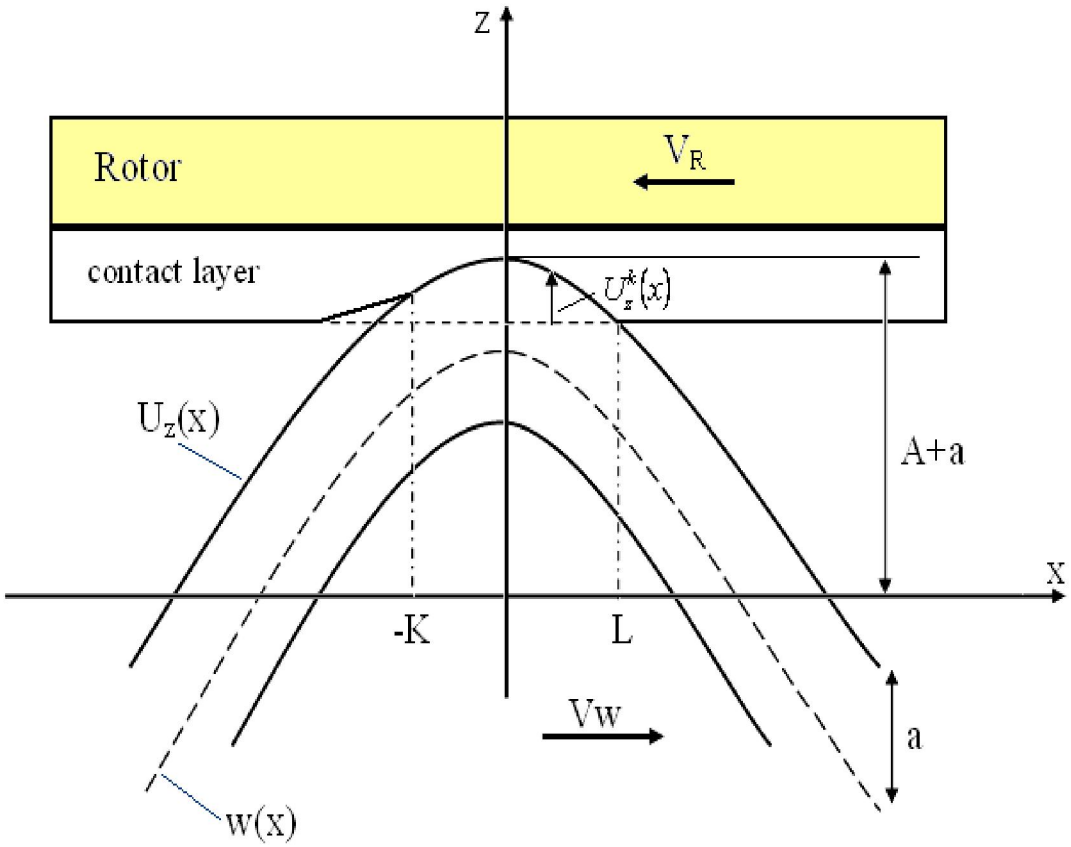

Figure 3.4 Wave penetration into the contact layer.

The normal displacement $U_z^k(x)$ of the contact layer surface is defined by Equation (3.9). Furthermore, velocity and acceleration of the contact layer are described by Equation (3.15) and Equation (3.16), respectively.

$$U_z^K(x) = U_z(X) - U_z(L) = \left(w(x) + a - w(x) + a\right) \tag{3.13}$$

$$U_z^K(x) = A\cos\left[\frac{2\pi x}{\lambda}\right] - A\cos\left[\frac{2\pi L}{\lambda}\right] \qquad -K\langle x\langle L \tag{3.14}$$

$$\dot{U}_z^K(x) = \frac{d}{dt}U_z^K(x) = A\frac{2\pi}{\lambda}V_w \sin\left[\frac{2\pi x}{\lambda}\right] \tag{3.15}$$

$$\ddot{U}_z^K(x) = \frac{d}{dt}\dot{U}_z^K(x) = -A\left[\frac{2\pi}{\lambda}\right]^2 V_w^2 \cos\left[\frac{2\pi}{\lambda}\right] \tag{3.16}$$

This visco-elastic model is called Kevin's model [73] which developed based on the visco-elastic friction between the stator and the rotor interface.

For the normal pressure of an infinitesimal contact layer of the width dx, the Newton's second law can be applied. A free body diagram of the contact layer is shown in Figure 3.5. Dynamics of the contact zone can be written in Equation (3.18).

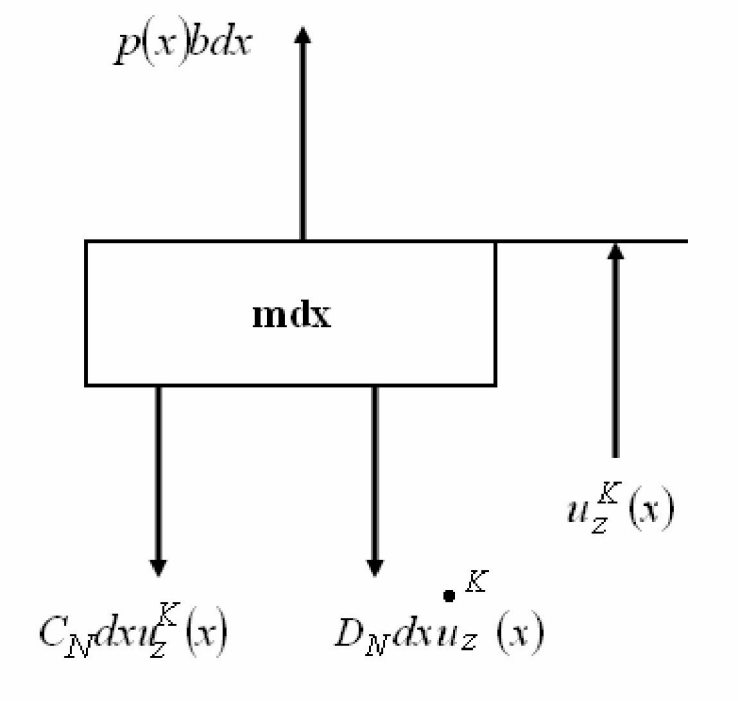

Figure 3.5 The free body diagram of the contact layer in the normal direction.

$$\sum F_y = m_y a \tag{3.17}$$

$$mdx\ \ddot{U}_z^K(x) = p(x)dxb - C_N dx U_z^K(x) - d_N dx \dot{U}_z^K(x) \tag{3.18}$$

$$p(x)dxb = mdx\ddot{U}_z^K(x) + C_N dx U_z^K(x) + d_N dx \dot{U}_z^K(x) \tag{3.19}$$

The Equation (3.19) is divided by *dx* and can be written as:

$$p(x)b = m\ddot{U}_z^K(x) + C_N U_z^K(x) + d_T \dot{U}_z^K(x) \tag{3.20}$$

$$p(x)=\frac{1}{b}\left\{-mA\left[\frac{2\pi}{\lambda}\right]^2 V_w^2\cos\left(\frac{2\pi x}{\lambda}\right)+C_N A\left(\cos\left[\frac{2\pi x}{\lambda}\right]-\cos\left[\frac{2\pi L}{\lambda}\right]\right)+d_N A\left[\frac{2\pi}{\lambda}\right]V_w\sin\left[\frac{2\pi x}{\lambda}\right]\right\} \tag{3.21}$$

where $\omega=\left[\frac{2\pi}{\lambda}\right]V_w$;

$$p(x)=\frac{A}{b}\left\{-m.\omega^2\cos\left[\frac{2\pi x}{\lambda}\right]+C_N\cos\left[\frac{2\pi x}{\lambda}\right]-C_N\cos\left[\frac{2\pi x}{\lambda}\right]+d_N\omega\sin\left[\frac{2\pi x}{\lambda}\right]\right\} \tag{3.22}$$

$$p(x)=\frac{A}{b}\left\{\left(C_N-m\omega^2\right)\cos\left[\frac{2\pi x}{\lambda}\right]+d_N\omega\sin\left[\frac{2\pi x}{\lambda}\right]-C_N\cos\left[\frac{2\pi x}{\lambda}\right]\right\} \tag{3.23}$$

The second contact model between the stator and the rotor on half wavelength of an ultrasonic motor is shown in the Figure 3.6. The contact layer is set on the surface of rigid rotor regarded as a distribution linear spring [30, 37, 79, 84]. By fixing a coordinate on the stator, the normal displacement of a point on surface of the stator can be written as

$$U_z(x)=A\cos\left[\frac{2\pi x}{\lambda}\right] \tag{3.24}$$

where, A is the amplitude of the stator, λ is the wave length. When the preload (F_N) is applied on the half of wavelength of the rotor, the contact zone of the stator and the rotor is within the range of $[-x_O, x_O]$. This can be seen in the Figure 3.6. The

contact points on the stator have the same tangential velocity as the rotor is in the range of $[-x_r, x_r]$.

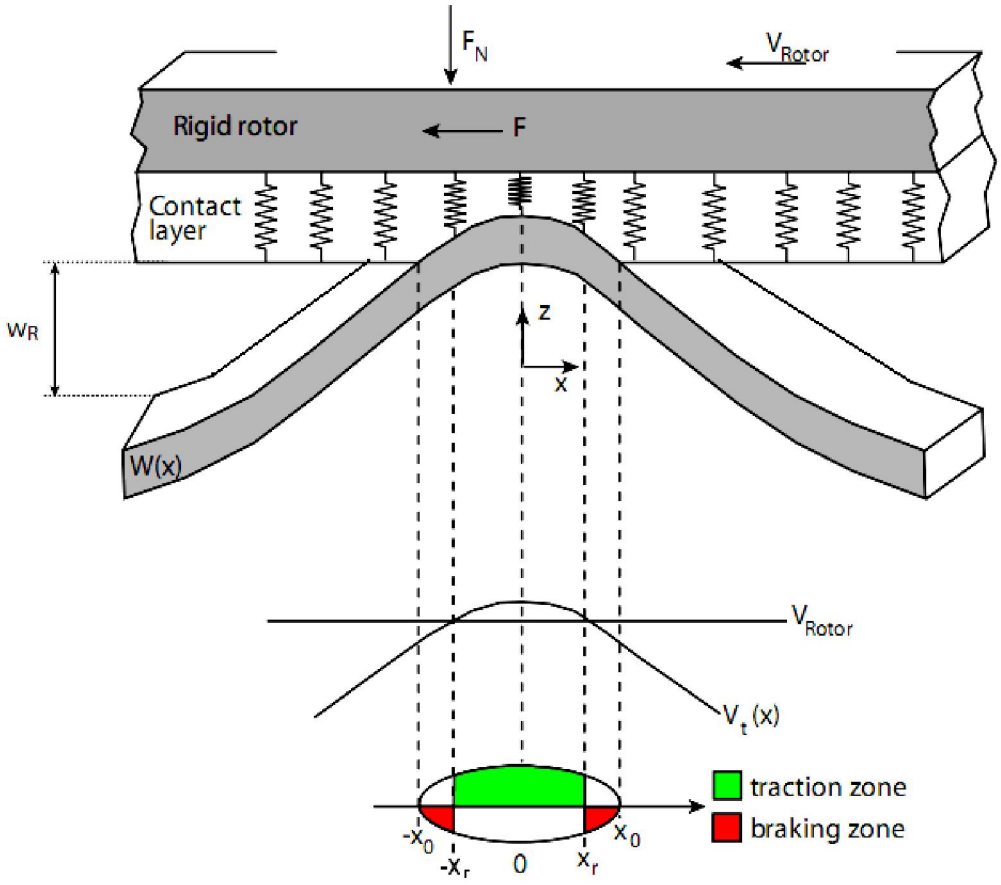

Figure 3.6 Schematic diagram of the contact model between the stator and the rotor of an ultrasonic motor [83].

Depending on the vibration amplitude of the stator and the speed of the rotor, three cases can be classified. First, the maximum driving force is transmitted to rotor when the tangential velocity of the stator in the whole contact area is larger than that of the rotor velocity. Second, the tangential velocity of the stator in the whole contact

area is less than that of the rotor velocity. Therefore, the maximum breaking force is transmitted. Third, there are two points at $-x_r$ and x_r where the stator and the rotor have the same tangential velocity. Therefore, the contact area can be divided into three regions. In this case, the central region $x \langle x_r$ the rotor is driven by the stator and the outer regions contact, where $-x_0 \langle x \langle -x_r$ and $x_r \langle x \langle x_0$ the rotor is stopped by the stator.

Penetration of the stator into the contact layer of the rotor causes generation of normal contact pressure force $p(x)$ along the contact zone. Consequently, the contact pressure force is distributed along of the contact region $-x_r \le x \le x_r$ which can be written as

$$p(x) = k_f A\left(\cos\frac{2\pi x}{\lambda} - \cos\frac{2\pi x_o}{\lambda} \right) \tag{3.25}$$

and

$$k_f = \frac{E_c b}{h_c} \tag{3.26}$$

where k_f is the normal equivalent stiffness, E_c is the elastic modulus of the contact layer, h_c is the thickness of the contact layer and b is width of contact region.

In the normal direction, the normal force can be written as

$$F_N = NAk_f \int_{-x_o}^{x_o} \left(\cos\frac{2\pi x}{\lambda} - \cos\frac{2\pi x_o}{\lambda} \right) dx \tag{3.27}$$

where N is the number of contact wave crest. It is assumed that Coulomb's friction is valid in the contact interface between the stator and rotor and the friction coefficient μ_k is constant. The driving force is generated by the friction at the contact region. Therefore, the driving force occurred within the contact region can be expressed as

$$F_T = \mu_k NAk_f \int_{-x_o}^{x_o} \operatorname{sgn}\left|Vs(x) - V_R\right| \left(\cos\frac{2\pi x}{\lambda} - \cos\frac{2\pi x_o}{\lambda} \right) dx \tag{3.28}$$

Direction of the driving force depends on the sign of the relative velocity between the surface points of the stator and the velocity of the rotor ($\Delta V = Vs(x) - V_R$). That is, the driving force drives the rotor when the tangential velocity of the stator $V_s(x)$ is larger than that the rotor velocity V_R. Conversely, the driving force breaks the rotor when the tangential velocity of the stator is less than the rotor velocity.

The power output of the rotor (P_R) is defined as

$$P_R = F_T V_R = V_R \mu_k NAk_f \int_{-x_o}^{x_o} \operatorname{sgn}\left|Vs(x) - V_R\right| \left(\cos\frac{2\pi x}{\lambda} - \cos\frac{2\pi x_o}{\lambda} \right) dx \tag{3.29}$$

Furthermore, the efficiency of the ultrasonic motor is defined as

$$\eta = \frac{Mechanical \quad output}{Electrical \quad input} x100\% \tag{3.30}$$

Mathematical models of an ultrasonic motor are adopted to predict the motor performance such as motor velocity and driving force. For the accurate prediction of motor performance, several parameters must be measured. Those are friction coefficient, number of contact waves, thickness of friction material, and contact area between the stator and the rotor. In the case of the linear spring model, it is unable to comprehensively evaluate characteristic of an ultrasonic linear motor due to the contact region between the stator and the rotor is not spring phenomenon. Nevertheless, the linear spring model is still able to predict of characteristic of the linear ultrasonic motor at the no-load speed and the maximum driving force.

3.5 Chapter Summary

The mathematical models of the ultrasonic linear motor were described in this chapter. Generally, the mathematical model of the ultrasonic motor is called contact model and later used for verification the experimental and finite element results. The validated results would be relationship between applied voltage and velocity and characteristic curve (the relationship between driving force and velocity). In this study, results of the ultrasonic linear motor are obtained from finite element method and experiment which will be and discussed in the later (Chapter 5 and Chapter 6). In Chapter 4, the experimental setup and performance testing of the piezoelectric linear ultrasonic motor, such as relationship between applied voltage and velocity, applied voltage and driving force, applied voltage and pre-load and driving force and velocity will be discussed and studied.

Chapter 4

Methodology of Research

4.1 Introduction

In Chapter 2, the piezoelectric properties, piezoelectric effects and governing equation of the piezoelectric material were studied. In Chapter 3, the mathematical model of the contact interface between the stator and the rotor of the piezoelectric ultrasonic linear motor was studied to investigate the motor performance. Afterwards, the analytical results will be used to compare with simulation and experimental results. In this chapter, the research methodology for studying characteristic and performance of the piezoelectric ultrasonic linear motor is described. The study can be divided into two parts, they are finite element and experiment studies. Three finite element analyses are used to investigate the motor characteristic. They are modal, harmonic and transient analyses, respectively. Meanwhile, the experimental study is used to investigate the motor performances. They are relationships between applied voltage and velocity, driving force and velocity, applied voltage and driving force and suitable preload. Other properties such as effective capacitance of the piezoelectric actuator and natural frequency of the system of ultrasonic piezoelectric linear motor are also measured.

4.2 Procedure of the Research

All of procedures are finite element modeling, experiment, analysis of the result, verification and conclusion. The procedure of the research is shown in Figure 4.1. First, two new designs of the linear ultrasonic motor with laminate piezoelectric actuator is established. That is, the design of the motor with dual actuators and single actuator. Then, the stator of the motor is modeled by using finite element method to study the vibration characteristics. The analyses used in the finite element method are modal analysis, harmonic analysis and transient analysis. After that, necessary parameters of finite element results are used to estimate the motor performance based on the mathematical model discussed in the previous chapter. Then, a prototype of the piezoelectric ultrasonic linear motor is fabricated based on the finite element parameters. Afterwards, the prototype of the piezoelectric ultrasonic linear motors is tested. Finally, the finite element and experimental results are compared and discussed for validation and conclusion.

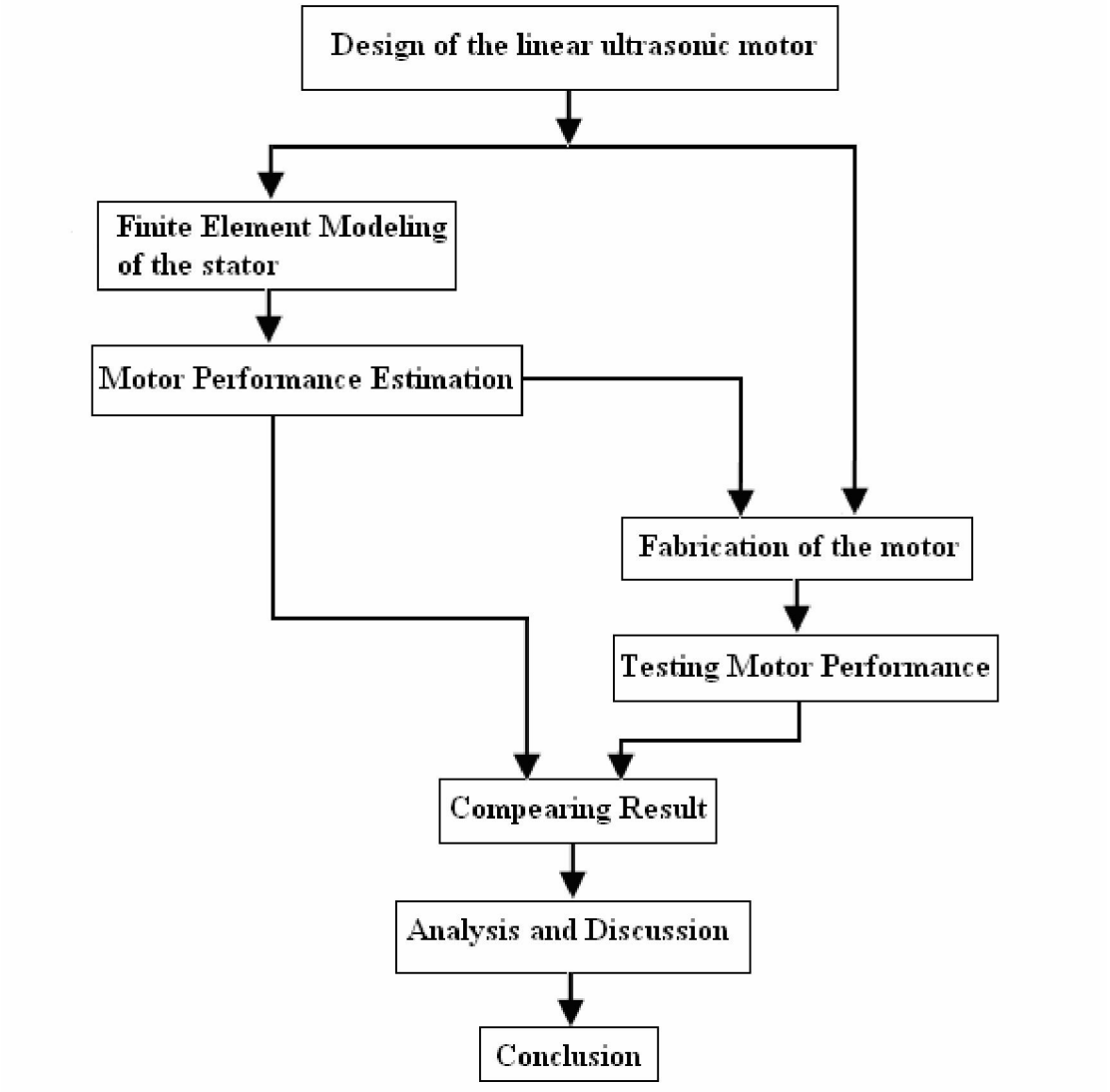

Figure 4.1 Procedure of the research.

4.3 Finite Element Analysis

To predict the experimental result, the stator of the linear ultrasonic motor is modeled by using the finite element software package, MSC.Marc. Dimensions of the finite element model are illustrated in Figure 4.2 for a dual piezoelectric actuator motor and Figure 4.3 for a single piezoelectric actuator motor. For the dual piezoelectric actuator motor, the stator is bonded with damping material patches at the supported boundaries to prevent the wave reflection. The boundary conditions of the stator are fixed on both sides (fixed the nodal displacement for all directions). The excitation applied voltages on the piezoelectric actuators are Asin(ωt) on the left actuator and Acos(ωt) on the right actuator. Meanwhile, the single piezoelectric actuator ultrasonic linear driver, the stator is bonded with only one active piezoelectric actuator on the left side near the supported boundary. Other boundary conditions are fixed, similar to the dual actuators motor. The excitation voltage is Asin(ωt) applied on the active piezoelectric actuator. The excitation frequency is varied to determine the operating frequency that generates a traveling wave. All material properties and dimensions of the finite element model are assigned according to Table 4.1. To determine the system response, the finite element models are simulated based on the boundary conditions and excitations as mentioned before.

Steps of calculation the results of the finite element models are mesh generation, identification of material properties, identification of contact table properties, identification of boundary conditions, loadcase analysis and job calculation, respectively.

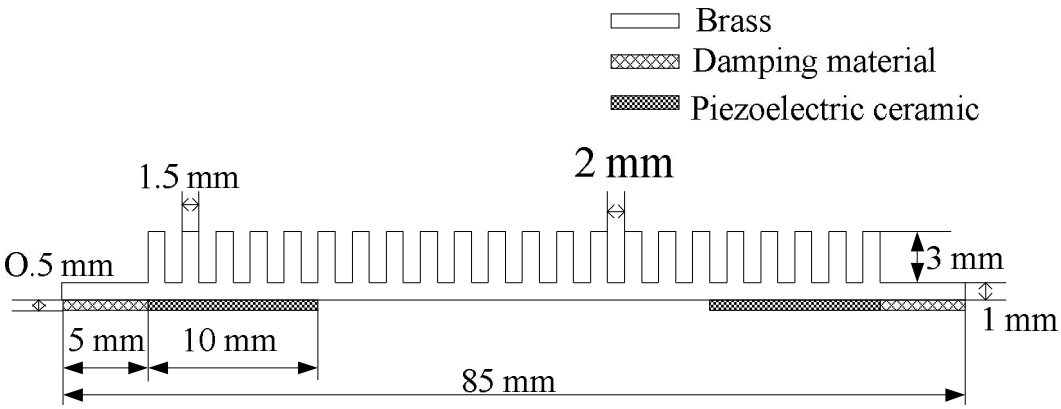

Figure 4.2 Schematic diagram of the dual actuator linear stator.

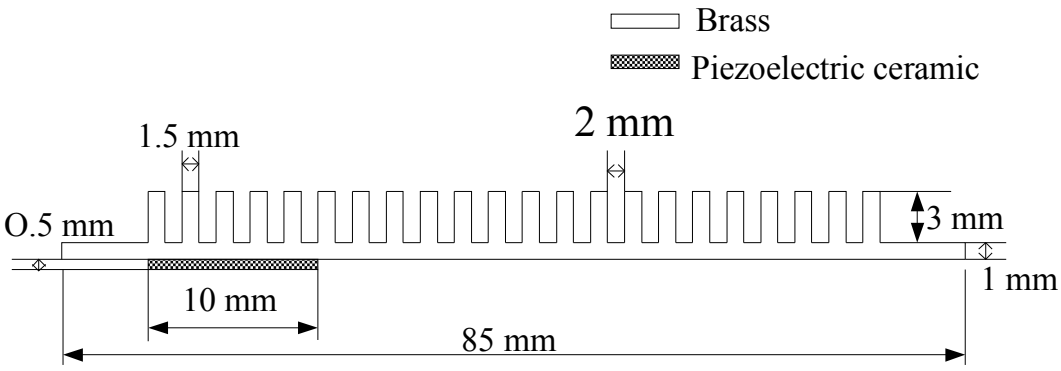

Figure 4.3 Schematic diagram of the single actuator linear stator.

4.3.1 Mesh generation

In this section, the finite element models of the ultrasonic linear motors are created according to the actuator pattern that bonded on a stator. There are two piezoelectric actuator patches for a dual actuator motor. The right one generates cosine wave and the other one generates sine wave. Meanwhile, the actuator of a single actuator motor generates only sine wave because it has one actuator bonded with the stator. The piezoelectric material type PZT-4 (S.P.K. Electronics CO., LTD. TAIWAN) is used to be actuator in this research. Dimensions of the piezoelectric actuator are width of 6 mm, thickness h^a of 0.5 mm and length of 10 mm. Brass is used for stator material. The stator dimensions are width of 6 mm, length of 85 mm and thickness of 1 mm. For a dual actuator motor, the damping material is bonded on the both ends of the stator for protection of wave reflection when the wave reached the ends of the supports. Dimensions of a damping material patch are width of 6 mm, length of 5 mm and thickness of 0.5 mm. Furthermore, the stator tooth is made to amplify of the wave amplitude and elliptical locus. The size of a tooth is width of 6 mm, height of 3 mm and thickness of 1.5 mm. Figure 4.2 and Figure 4.3 illustrate all dimensions of the piezoelectric ultrasonic linear stators. Accordingly, Figure 4.4 and Figure 4.5 show the finite element models of the dual actuator and single actuator stators.

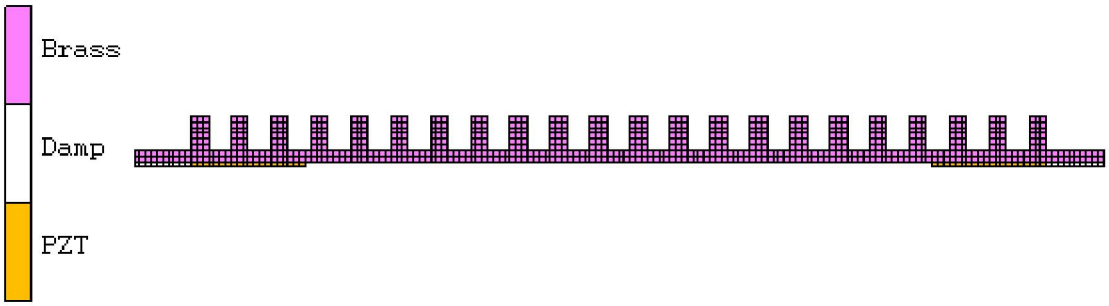

Figure 4.4 Finite element model of the dual actuator linear stator.

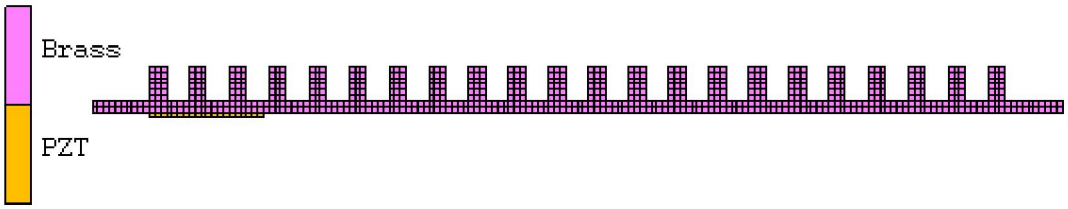

Figure 4.5 Finite element model of the single actuator linear stator.

The full integration (161) is selected for element type of piezoelectric ceramic actuator, and plane strain full integration (11) is selected for stator and damping material. Furthermore, the element class of Quad 4 is used for all elements in the models. Total number of elements of a dual actuator motor and a single actuator motor are 796 and 756 elements, respectively.

4.3.2 Material properties

The materials used in the finite element models and ultrasonic linear motor systems are brass, damping material and piezoelectric ceramic. All material properties are described in Table 4.1.

Table 4.1 Material properties of the linear ultrasonic motor

	PZT-4 actuator	Brass stator	Silicon Rubber Damping material	Unit
Modulus of Elasticity	(Orthotropic)	(Isotropic)	(Isotropic)	
Y_{11}	79	96	4.2×10^{-3}	GPa
Y_{33}	66	96	4.2×10^{-3}	GPa
Density	7700	8400	1510	kg/m^3
Poisson's ratio	0.33	0.35	0.45	
Damping coefficient	0.0013	0.0005	0.05	
Piezoelectric constant				
e_{33}	17.56	-	-	C/m^2
e_{31}	-4.38	-	-	C/m^2
Permittivity	1.018×10^{-8}	-	-	F/m
Capacitance	2096	-	-	pF
			-	

4.3.3 Contact model

The contact conditions are identified in this section. Figure 4.6 shows the contact table for the dual actuators piezoelectric ultrasonic linear motor. Figure 4.7 illustrates the contact table of the single actuator piezoelectric ultrasonic linear motor. The glue contact condition (G) is applied for attaching damping materials and piezoelectric actuators with the stator as a perfect bonding assumption.

Figure 4.6 Contact table of the dual actuator linear ultrasonic motor.

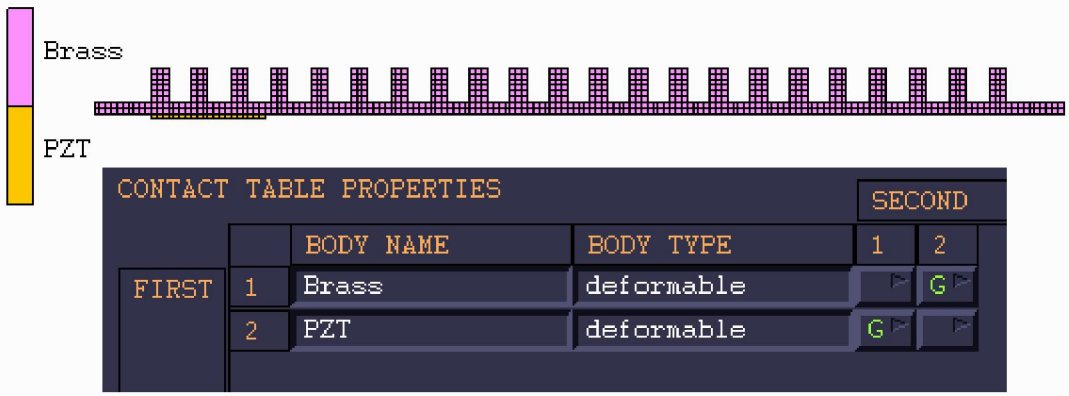

Figure 4.7 Contact table of the single actuator linear ultrasonic motor.

4.3.4 Boundary conditions

Boundary conditions of the finite element models are both mechanical and electrical. The fixed nodal displacement (all directions) are applied on ends of the stator according to the physical motor as shown in Figure 4.8. The electrical voltage boundary conditions are applied on the piezoelectric actuators as follow, Asin(ωt) is applied on the open surface of the left actuator and Acos(ωt) is applied on the open surface of the right actuator. For the single actuator motor, the electrical applied voltage boundary condition is excited on the open surface of the left actuator as Asin(ωt). The stator is electrical ground. In the analysis section, excitation frequency and applied voltage can be varied. Figure 4.9 illustrates the applied boundary condition of the single actuator motor. Then, applied electrical boundary conditions of the dual and single actuator motor are depicted in Figure 4.10 and Figure 4.11.

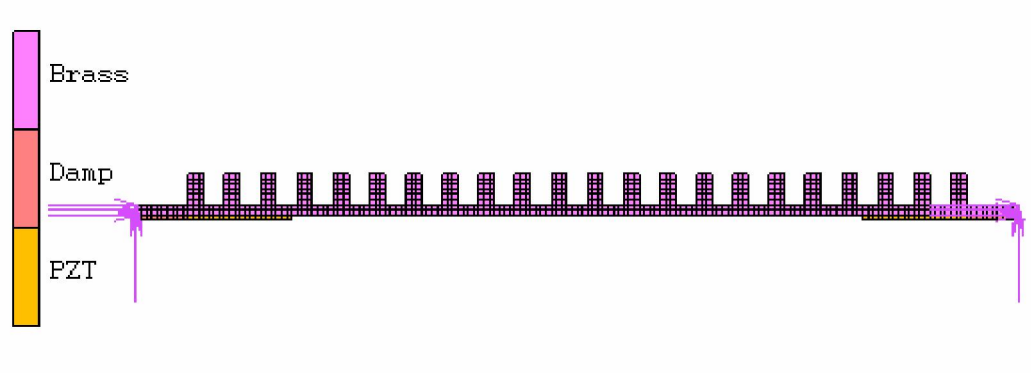

Figure 4.8 The fixed boundary condition of the dual actuator linear motor.

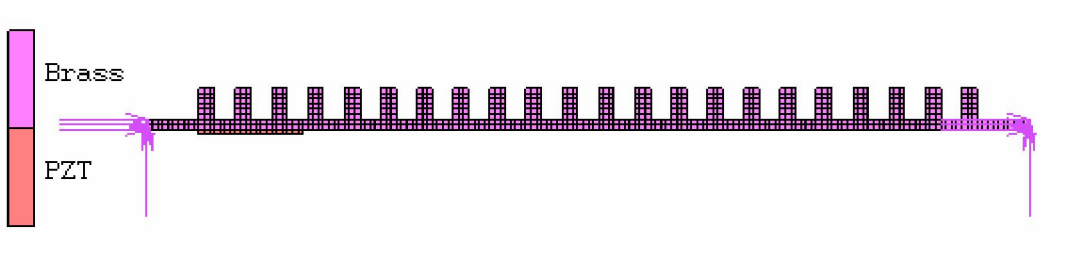

Figure 4.9 The fixed boundary condition of the single actuator linear motor.

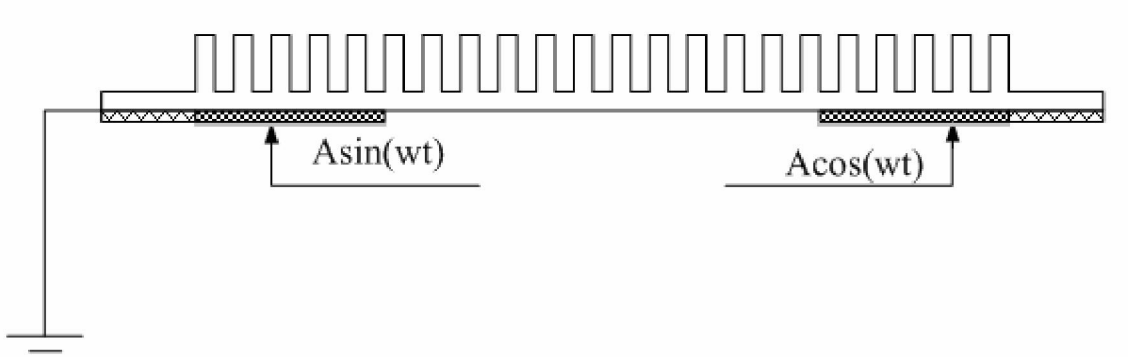

Figure 4.10 The applied electrical voltage on piezoelectric actuators of the dual actuator linear motor.

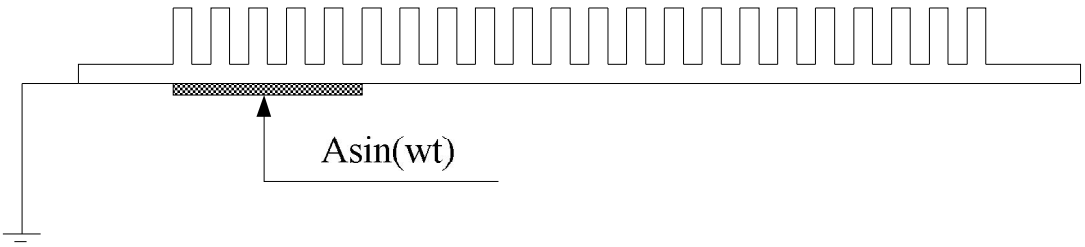

Figure 4.11 The applied electrical voltage on a piezoelectric actuator of the single actuator linear motor.

4.3.5 Finite element analysis

For MSC.Marc, there are two steps of preparation of the finite element input before the numerical calculation. First, the loadcases setting is a selection of the loads boundary conditions, and assumptions which are used in the calculation. Second, jobs setting are a selection of the analysis cases which are modal, harmonic, or transient analysis. All cases of the finite element analyses are described below.

4.3.5.1 Modal analysis

The modal analysis in the finite element method gives results of the system natural frequency and mode shape. This analysis, sometimes, is called free vibration analysis. Important parameters that effect of the modal analysis are all material properties (piezoelectric ceramic, brass and damping material), geometry and boundary conditions.

4.3.5.2 Harmonic analysis

Frequency responses of the finite element models are investigated through the harmonic analysis. In the case study, the piezoelectric actuators bonded on the stator are subjected to sinusoidal electrical excitations with amplitude of 54 V. For the dual actuators linear motor, the electrical signal of 54sin (ωt) is applied on the left actuator and the electrical signal of 54cos (ωt) was applied on the right actuator. For the single actuator electrical signal of 76sin (ωt) is applied. The change of vibration amplitude of the motors when the excitation frequency ω is varied from 20,000 to 35,000 Hz. That is the harmonic response investigated in this research.

4.3.5.3 Transient analysis

The transient analysis gives the result of system response in time domain. In this study, the transient analysis is used for investigation of the system response of wave propagation and operating frequency, because, in the experiment, the propagation wave occurred on the tooth surface of the stator can not be easily seen or measured. Moreover, the transient analysis yields the most effective way to find the actuator pattern patch that generates propagation wave at the operating frequency.

4.4 Experimental Setup of the Linear Ultrasonic Motors

In this research, the suitable actuator patterns and dimensions of piezoelectric ultrasonic linear motors are determined by using finite element method. Afterwards, the prototypes of the dual and single actuator linear motors are built for evaluation of motor performance. The interested parameters in the testing of the motor performance are relationships between preload and motor velocity, electrical applied voltage and motor velocity, driving force and electrical applied voltage, driving force and motor velocity. All these relationships will be discussed in the next chapter.

4.4.1 Fabrication of the piezoelectric ultrasonic linear motor

Figure 4.12 and 4.13 show prototypes of the dual actuator and single actuator ultrasonic linear motors fabricated in this research. The two motors have the same dimensions of the stator and teeth. The dimensions of the stator are width of 6 mm,

length of 85 mm and thickness of 1 mm. The tooth dimensions are width of 6 mm, thickness of 1.5 mm and height of 3 mm which is used for amplification the propagation wave amplitude. Figure 4.14 and Figure 4.15 show the stators with the dual actuators and single actuator, respectively.

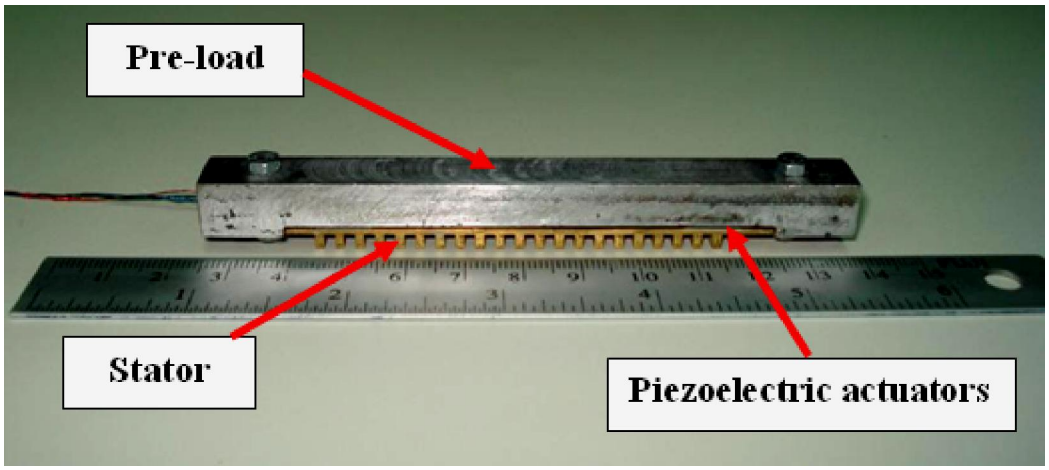

Figure 4.12 Prototype of the dual actuator ultrasonic linear motor.

Figure 4.13 Prototype of the single actuator ultrasonic linear motor.

Figure 4.14 Stator with the dual piezoelectric actuators.

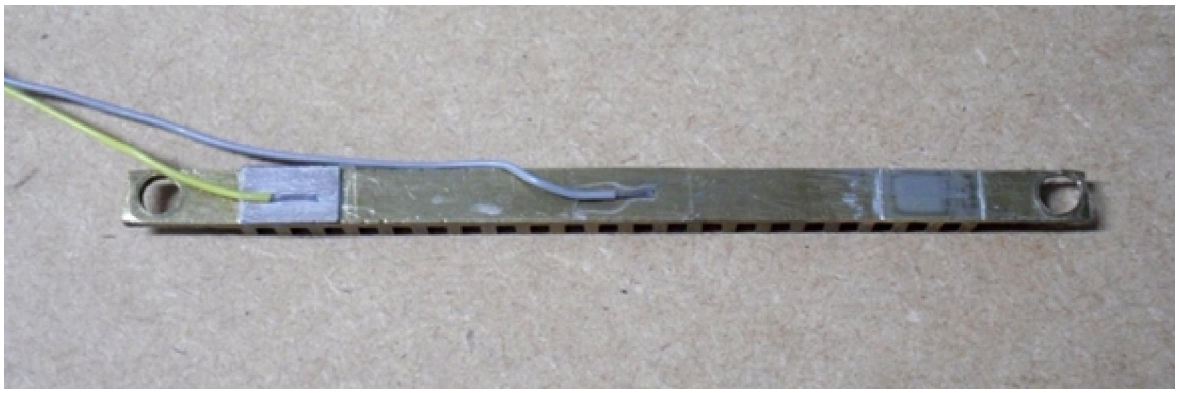

Figure 4.15 Stator with the single piezoelectric actuator.

4.4.2 Implementations of research

As mentioned in the methodology, the steps of research consist of the finite element modeling and experiment. The finite element method provides estimation of essential parameters and prediction of the operating frequency. Accordingly, the motor is fabricated for testing the performance. Instruments of the experiment setup for investigation the motor performance consist of two high voltage amplifiers, an impedance analyzer and a digital time sensor, a function generator, a data acquisition module and software. Details for all instruments are described next.

4.4.2.1 High voltage amplifier

The electrical input signals ($A\sin(\omega t)$ and $A\cos(\omega t)$) for exciting the piezoelectric actuators are generated by using Labview software sending though the data acquisition I/O module, but this can only generate the maximum electrical signal amplitude upto 10 V, while the experiment requires more than that. Therefore, the electrical signal has to be amplified. Accordingly, the high voltage amplifier is used to amplify the electrical signal before exciting the piezoelectric actuator. The high voltage amplifier is very important for this research. Two high voltage amplifiers model A-301 HS of A.A. Lab System, are used in the setup. Figure 4.16 shows the high voltage amplifier model A-301 HS of A.A. Lab System.

Figure 4.16 The high voltage amplifier (model A-301 HS).

4.4.2.2 Data acquisition module and software

In this research, a data I/O and acquisition program, Labview, is used to generate two electrical signals which are Asin(ωt) and Acos(ωt) for driving the piezoelectric actuators. A data acquisition module of the National Instrument company model NI USB-6215 is selected to converse the generated signal from digital input to analog output. The data acquisition module is illustrated in Figure 4.17. The block diagram of Labview program for generating the two electrical signals is illustrated in Figure 4.18, and the parameter control front panel is illustrated in the Figure 4.19.

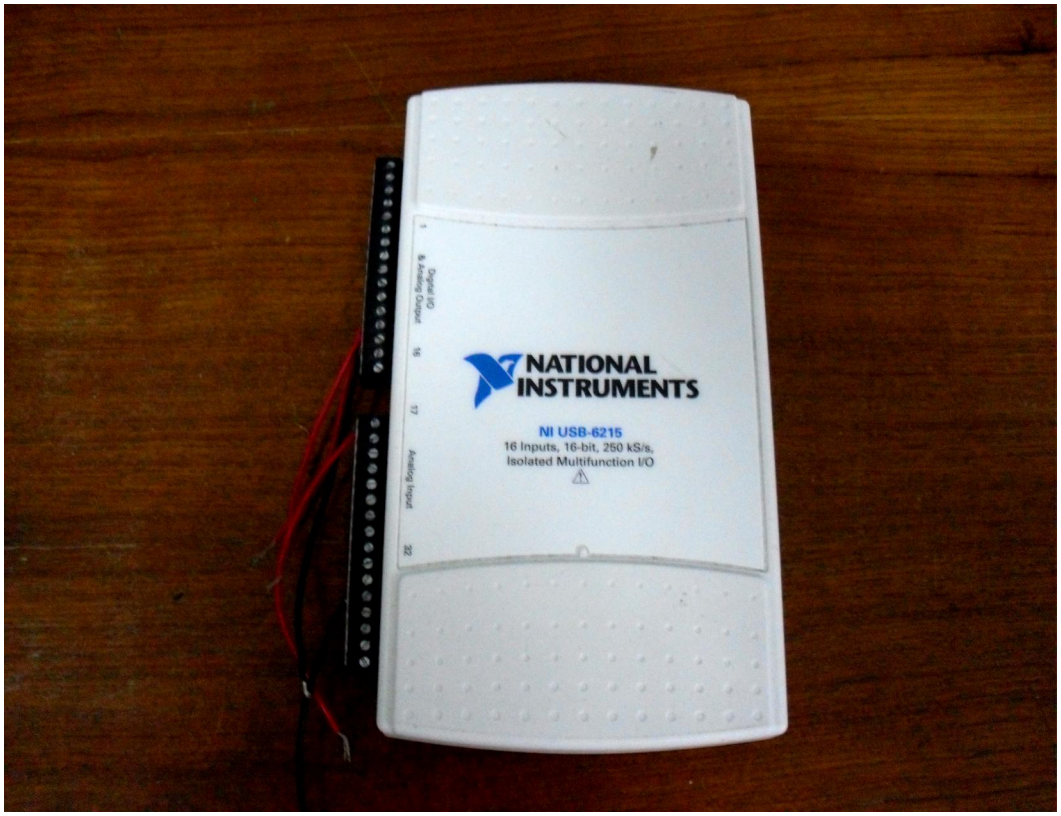

Figure 4.17 The data acquisition module (model NI USB-6215).

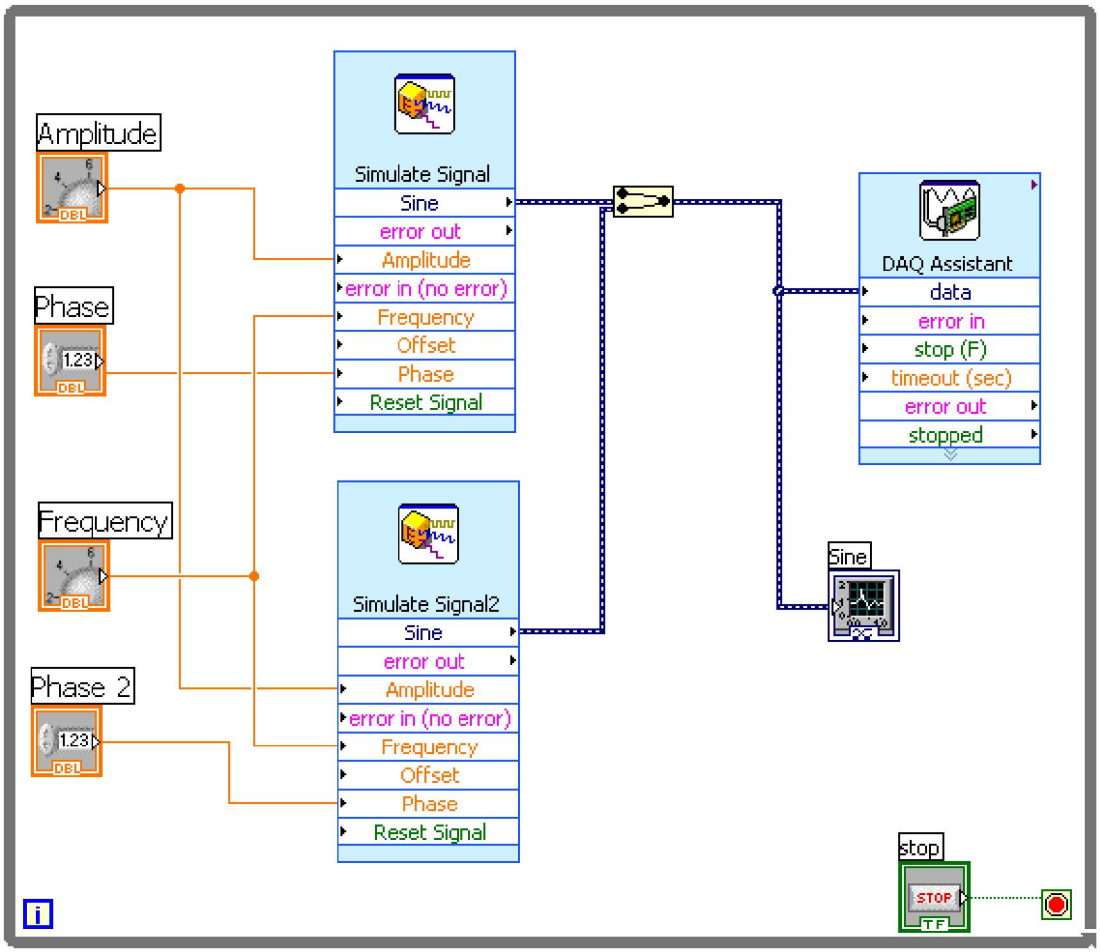

Figure 4.18 Block diagram for generating two harmonic signals.

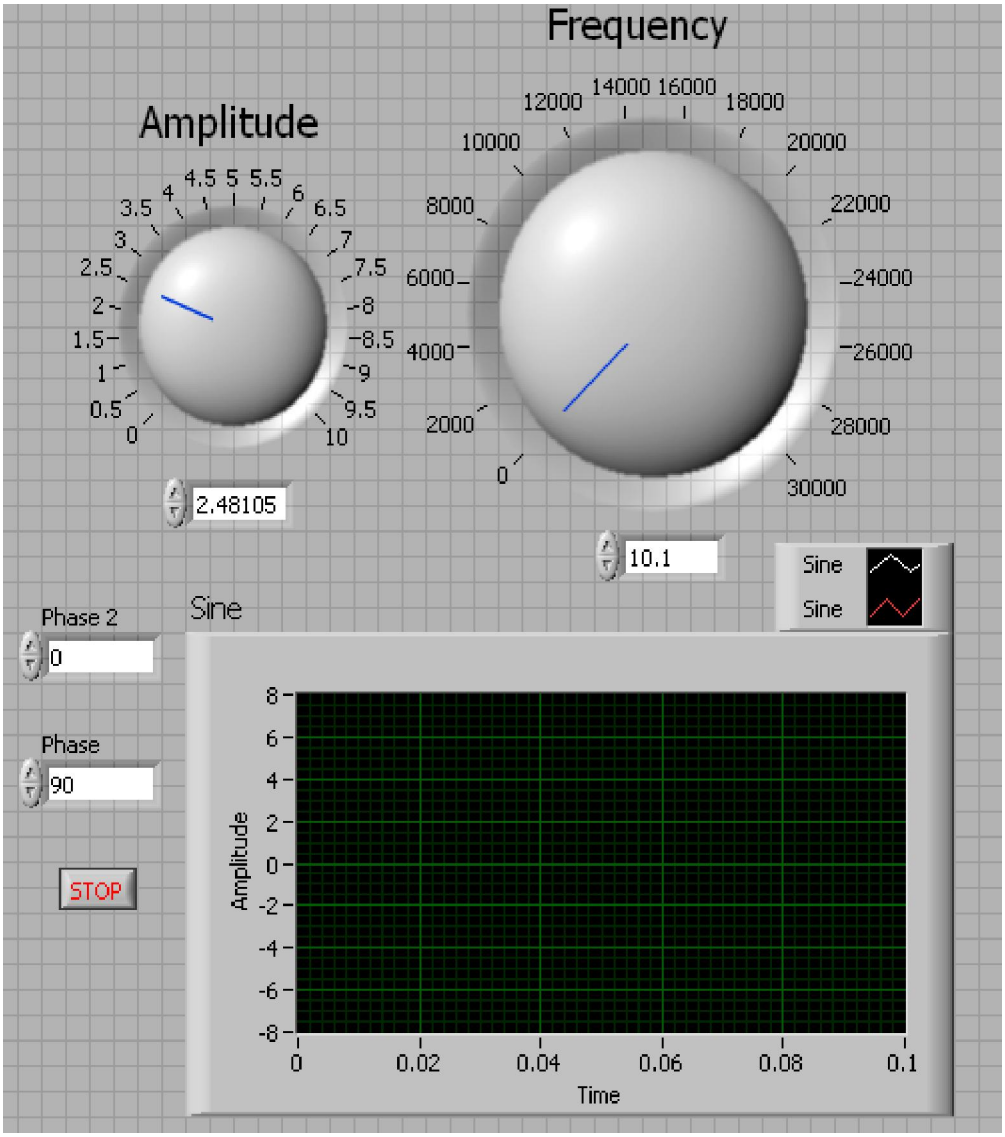

Figure 4.19 The parametric control front panel of the Labview program.

4.4.2.3 Impedance analyzer

An impedance analyzer machine model 4194A made by Hewlett Packard company is used to measure natural frequency of the system for both dual actuator and single actuator linear motors. The natural frequency measured by this machine is later compared and validated with the natural frequency of the finite element and analytical results. The Hewlett Packard Impedance analyzer is shown in Figure 4.20.

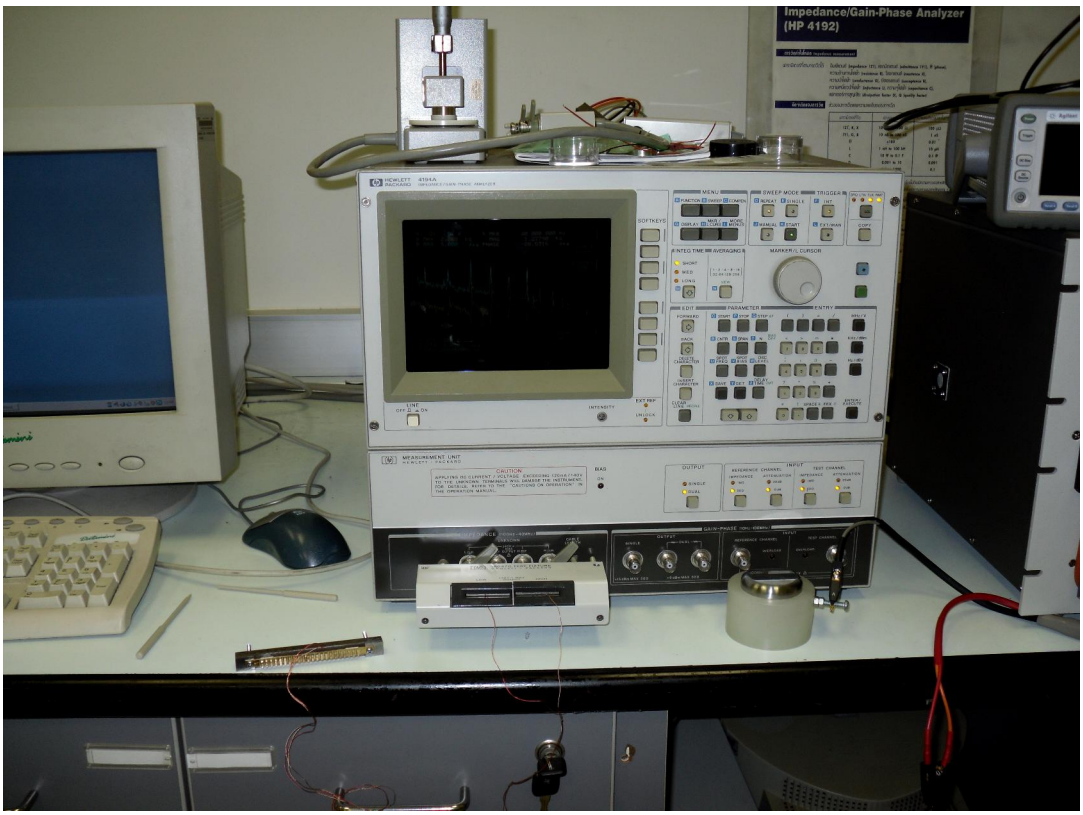

Figure 4.20 Hewlett Packard Impedance analyzer (model 4194A).

4.4.2.4 Digital time sensor

A digital time sensor is illustrated in Figure 4.21. It is for measuring the time of travel of the motor in a specific distance. Then, that time is calculated to be the average velocity of the motor.

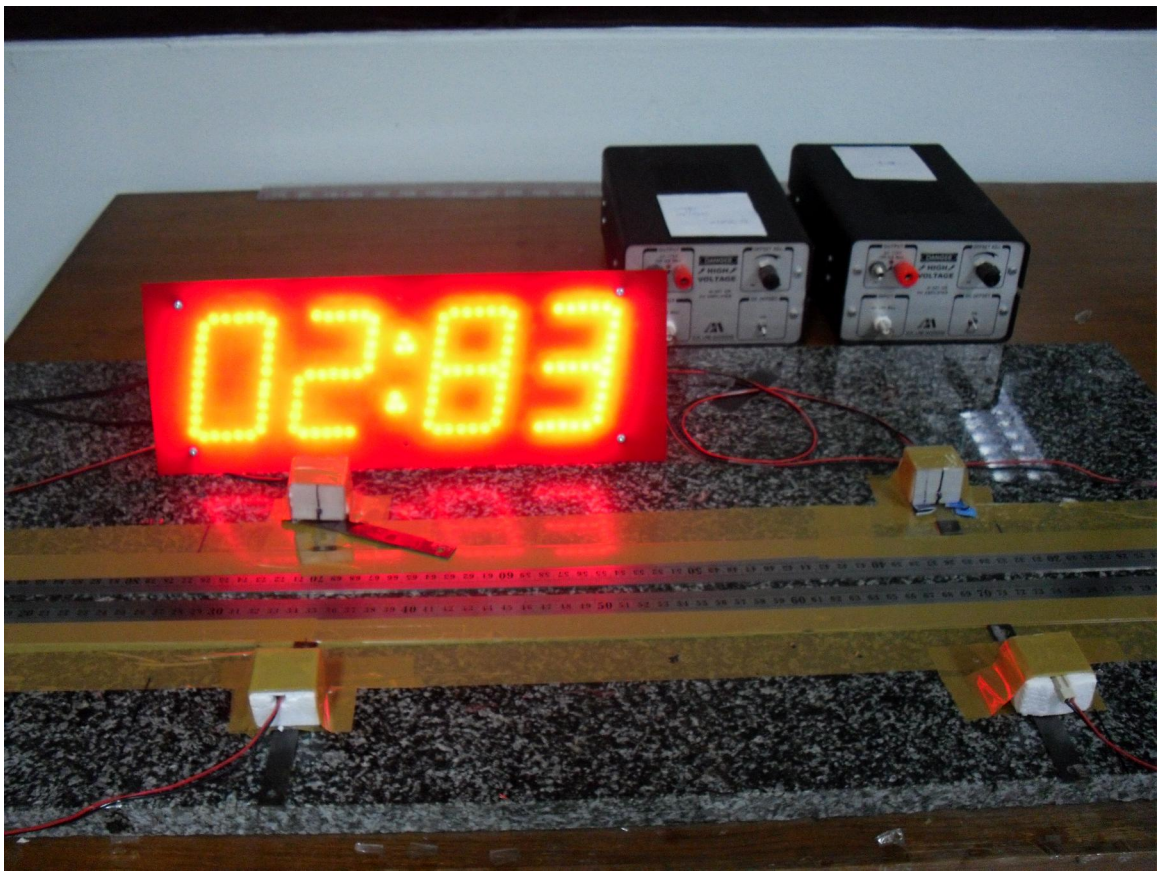

Figure 4.21 The digital time sensor.

4.4.3 Experimental setup

As mentioned above, all instruments in the experiment has already been described. The experimental setup for testing the motor performance is prepared. The apparatus consists of two power amplifiers for dual actuator linear motor (only one amplifier for single actuator), a data acquisition, a digital time sensor, a laptop computer, Labview program, a motor preload and a driving load. For testing the motor characteristics, the motor is set on a flat base made from granite. Then, the electrical applied voltages are excited on the piezoelectric actuators. The operating frequency is adjusted by the input excitation signal. The operating frequency is a frequency that generates traveling wave moving the stator in one direction. Furthermore, the direction of the traveling wave can be controlled by alternating the phase difference between the two control signals for the dual actuator motor, but the single actuator motor can not.

The important parameters that have effect on the motor performance are investigated. They are the optimum preload, the relationship between velocity and electrical applied voltage, motor velocity and driving force. Afterwards, all results from the experiment will be compared with the finite element and analytical results. All experiments for evaluation of the motor performance are described below.

4.4.3.1 Investigation of the optimum pre-load

The optimum pre-load of the piezoelectric ultrasonic linear motors is determined via the experiment. Generally, the optimum pre-load of the ultrasonic motor is the

required compression force that generates the maximum of the motor velocity. The pre-load is varied from 0 to 250 g. Generally, velocity of the motor increases when the pre-load is increased upto a certain value and decreases afterward. The maximum velocity of the motor is generated at the optimum pre-load.

4.4.3.2 Relationship between the electrical applied voltage and motor velocity

The relationship between the electrical applied voltage and motor velocity is studied. The optimum pre-load of 101.5 g taken from the previous investigation is used. For this test, the moving distance of the motor from start to stop is 35 cm. The time of travel is measured by a digital time sensor, and then calculated to be the average motor velocity. At each electric voltage that applied, the velocity is determined.

4.4.3.3 Relationship between the electrical applied voltage and driving force

The relationship between the electrical applied voltage and driving force criteria is investigated. The variable parameter is the electrical applied voltage. The procedure for testing the relationship is as follows. The first step, the electrical applied voltage is excited on the piezoelectric actuator to determine the motor velocity. Subsequently, increasing the driving load until the motor can not move forward, the driving load at this point is the maximum driving force of the motor. Then, change the applied voltage and determine the maximum driving force for each

applied voltage. Accordingly, the relationship between electrical applied voltage and driving force of the motor is plotted.

4.4.3.4 Relationship between the velocity and driving force

The relationship between the motor velocity and driving force of the motor is determined and discussed. The controlled parameters are the pre-load, moving distance, operating frequency and applied voltage. All quantities of the controlled parameters are set as the pre-load of 101.5 g, the moving distance of 35 cm, the applied voltage of 54 V and the operating frequency of 28.21 kHz for dual actuators while the operating frequency of 31.32 kHz the applied voltage of 76 V for single actuator ultrasonic linear motors. The motor velocity is then determined for each value of driving load.

4.4.3.5 Measurement of the natural frequency

Natural frequencies of the motor are measured by using an impedance analyzer machine (Hewlett Packard, model 4194A).The impedance of the stator is measured on one piezoelectric actuator while another actuator is open-circuit. There stator is put on the flat floor to emulate the working condition. The voltage for measuring the stator impedance is set at 1 Vrms. The natural frequencies of the both motors are later compared with the finite element and analytical results.

4.4.3.6 Capacitance of the piezoelectric material

Generally, the electrical power requirement of piezoelectric actuators is depended on geometry, material properties, applied voltage and frequency. The capacitance of the piezoelectric actuator directly effected the electrical power consumption [65]. The capacitance of piezoelectric actuator can be determined by the calculation and measurement via a LCR machine. In Chapter 2, Equation 2.44 is for calculation the effective capacitance value of the piezoelectric actuator. To accurately predict the maximum power consumption by using Equation 2.46, the measured maximum capacitance of the piezoelectric actuators must be taken [64-65]. The LCR meter (GW Instek model LCR-821) is used in this research as illustrated in Figure 4.23.

Figure 4.22 The LCR meter (GW Instek model LCR-821).

4.5 Chapter Summary

The methodology of the research has been described to study the motor performance both dual and single actuator linear motors. The finite element and experiment methods are used for studying and evaluation the motor performance. The finite element method is for the modal, harmonic and transient analyses. The analytical results from the finite element model are the natural frequency, amplitude of propagation wave and operating frequency. Furthermore, the experimental method is for evaluation of the motor performance, which are the optimum pre-load, relationships between electrical applied voltage and motor velocity, electrical applied voltage and driving force, motor velocity and driving force; natural frequency and effective capacitance of the piezoelectric actuator. Moreover, all apparatus and experimental setups used in this research have been described in this chapter. The results of the both dual actuator and single actuator piezoelectric linear motors received from the finite element analyses and experiments will be discussed in the next chapters.

Chapter 5

Ultrasonic Linear Motor with Dual Piezoelectric Actuators

5.1 Introduction

An ultrasonic motor usually consists of a stator and a rotor. The stator drives the rotor by means of traveling wave at the contact area, as mentioned in previous chapters. The traveling waves are generated by piezoelectric actuators which are bonded with the stator. The electrical excitation applied to the piezoelectric actuator induces deformation on the piezoelectric actuator and stator [5-6]. Generally, conventional ultrasonic motors have been using certain numbers of active piezoelectric actuator to create mechanical vibration on the stator. A large number of piezoelectric actuators will cause not only high energy consumption but also undesired system stiffness, resulting in requirement of high applied voltage for the generation of effective vibration on the stator. At the same time, the high applied voltage would raise temperature of the system during operation and would possibly cause depolarization of the piezoelectric actuators [25]. For this reason, one of the main objectives of this study is to reduce the number of piezoelectric actuators, so that it will be the simpler structure for fabrication, requires lower applied voltage and consumes less excitation energy. Hence, a design of ultrasonic linear motor with dual piezoelectric actuators is introduced in this chapter. The principle of operation of the

ultrasonic linear motor is discussed. In addition, vibration characteristics of the linear stator are investigated by using finite element method. In addition, the performance of the ultrasonic linear motor with dual piezoelectric actuators is assessed. Key relationships among performance parameters such as velocity, pre-load weight, applied voltage and driving force are reported. Topics of discussion are presented in detail in the following sections.

5.2 Design and the Principle of Operation

An ultrasonic linear motor with dual piezoelectric actuators consists of a beam stator with rectangular teeth, damping material patches and two piezoelectric actuators bonded with the beam structure near both ends of the beam, as shown in Figure 5.1. The actuator design is that the length of the actuator is equal to the wave length (λ). The phase difference of the two harmonic excitations on the piezoelectric actuators is 90 degree, so that the rotor can be driven efficiently [18, 25].

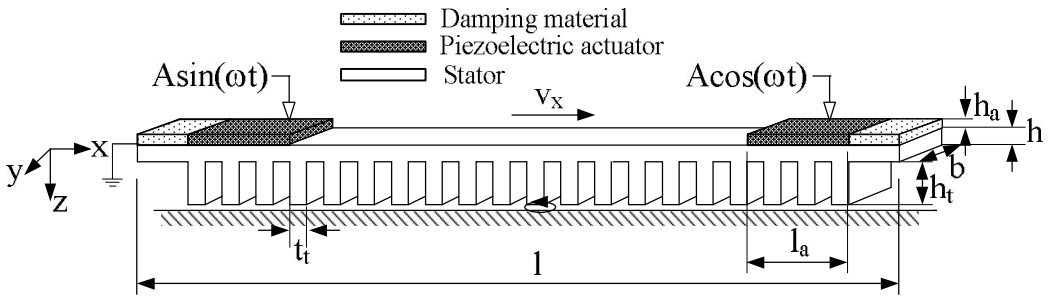

Figure 5.1 Design of the ultrasonic linear motor with dual piezoelectric actuators.

The stator generates traveling waves when the piezoelectric actuators are excited by harmonic excitations. The wave should propagate on the stator in one direction with consistency in wave amplitude. However, traveling waves reflect when they hit a physical boundary at the end of the stator. This distorts the pattern of the traveling waves. Accordingly, damping material patches are attached to the stator at both ends of the stator next to the fixed supports in order to prevent wave reflections. The piezoelectric ceramic actuators are polarized in the thickness direction. The two harmonic excitations are Asin(ωt) and Acos(ωt) signals, where A is the signal amplitude, ω is the driving frequency and t is the time. The body of the stator is grounded. Direction of the traveling waves can be controlled by alternating the phase difference between the two control signals. Teeth on the stator are designed to expand the wave amplitude and to create elliptical motions at the tips of the teeth. The elliptical motions at the tips generate driving forces against the contact surface [18, 20]. Velocity of the motor can be controlled by adjusting the amplitude of excitation voltages on the piezoelectric actuators.

The stator is assumed to be a thin beam. Hence, vibration theory of the elastic thin beam is applicable to analyze the characteristics of the stator. The governing equation of a homogeneous isotropic solid beam [88] is expressed as follow,

$$Y_b I \frac{\partial^4 u_3}{\partial x^4} + \rho A_C \frac{\partial^2 u_3}{\partial t^2} = 0, \tag{5.1}$$

where Y_b is the Young's modulus, $I = bh^3/12$ is the area moment of inertia of the beam cross-section, b is the beam width, h is the beam thickness, u_3 is the transverse

displacement, ρ is the mass density and A_c=bh is the cross-section area. The solution of the governing equation above is

$$u_3(x,t) = A_z \sin(\omega t - kx), \tag{5.2}$$

where $k = 2\pi/\lambda$ is the wave number, λ is the wavelength and A_z is the transverse wave amplitude. In addition to the transverse displacement, the variation in the longitudinal direction (x-axis) is given by

$$\sigma(x,z,t) = -z\frac{\partial u_3}{\partial x} = aA_z k\cos(\omega t - kx), \tag{5.3}$$

where a is the distance from the beam neutral surface to the teeth contact surface. Based on (5.2) and (5.3), the trajectory of a point at the teeth tip can be achieved as

$$\left(\frac{\sigma}{A_z ak}\right)^2 + \left(\frac{u_3}{A_z}\right)^2 = 1. \tag{5.4}$$

Equation (5.4) shows that the trajectory of the point is elliptical. When the stator is pressed against the surface, the stator moves itself by the friction force exerting at the contact surface. The velocity in the x-direction is obtained by the derivate of (5.3) as

$$v_x = -aA_z k\omega\sin(\omega t - kx). \tag{5.5}$$

Equation (5.5) represents the maximum speed reachable by the motor. The motor moves in opposite direction to the wave direction. Thus, the motor can move in another direction by reversing the wave direction. The natural frequency of the beam with fixed-fixed boundary condition can be written as [87].

$$f_i = \frac{\lambda_i^2}{2\pi L^2}\sqrt{\frac{Y_b I_b}{m}}\ ;\ \lambda_i = \frac{(2i+1)\pi}{2} \text{ for } i > 5 \tag{5.6}$$

where L is the length of the beam and m is the mass per unit length of the beam. In the case study, the mass of the teeth on the linear stator is also included into the mass per unit length of the beam. In order to verify the theoretical analysis, the ultrasonic linear motor with dual piezoelectric actuators is studied employing a finite element software package. The finite element model of the ultrasonic motor is discussed next.

5.3 Finite Element Model of the Ultrasonic Linear Motor with Dual Piezoelectric Actuators

According to the design described above, the stator of the ultrasonic linear motor is modeled to study the vibration characteristics, the frequency response and the local motion of the teeth tip. The linear stator is made of brass. The dimensions of the stator are width b of 6 mm, length l of 85 mm and beam thickness h of 1 mm. The teeth dimensions are height h_t of 3 mm, width b_t of 6 mm and thickness t_t of 1.5 mm. The teeth are used for amplifying the elliptical trajectory at the surface contact. The

piezoelectric actuator is made of Lead Zirconate Titanate (PZT-4). The actuator dimensions are length l_a of 10 mm, width b_a of 6 mm and thickness h_a of 0.5 mm as shown in Figure 5.1. The length of the actuator is equal to the wave length. The two piezoelectric actuators are located one at each end of the stator. The actuators are excited by a pair of electrical signals, $A\sin(\omega t)$ and $A\cos(\omega t)$. Capacitance of the piezoelectric actuator is measured by using a LCR meter (GW Instek LCR-821). The damping coefficient of the damping material is assumed to be 0.05 or 5%. The stator is made of brass because it is practical in manufacturing and processing. Other properties of the stator, the actuators and the damping materials are described in Table 5.1. Furthermore, it is assumed that the piezoelectric actuator (PZT-4) is an orthotropic material. The related shear modulus can be calculated based on the given modulus of elasticity and Poisson's ratio.

Table 5.1 Material properties of the ultrasonic linear motor with dual piezoelectric actuators

	PZT-4 actuator	Brass stator	Silicon Rubber Damping material	Unit
Modulusof Elasticity	(Orthotropic)	(Isotropic)	(Isotropic)	
Y11	79	96	4.2 x 10-3	GPa
Y33	66	96	4.2 x 10-3	GPa
Density	7700	8400	1510	kg/m3
Poisson's ratio	0.33	0.35	0.45	
Damping coefficient	0.0013	0.0005	0.05	
Piezoelectric constant		-	-	
e_{33}	17.56	-	-	C/m^2
e_{31}	-4.38	-	-	C/m^2
Permittivity	1.018x10-8	-	-	F/m
Capacitance	2096		-	pF

To predict the experimental result, the stator is modeled and simulated by using a finite element software package, MSC.Marc. The finite element model of the linear stator with dual piezoelectric actuators is illustrated in Figure 5.2. The stator is bonded with damping material patches at supported boundaries to prevent wave reflections. The model is assumed to be a two-dimensional plain strain problem. The boundary conditions of the stator are stipulated to be fixed at both ends. The excitation voltages are 54sin(ωt) on one actuator and 54cos(ωt) on the other one. The excitation frequency is varied to determine the operating frequency that generates a traveling wave. All material properties and dimensions of the finite element model are assigned according to the previous descriptions (Table 5.1).

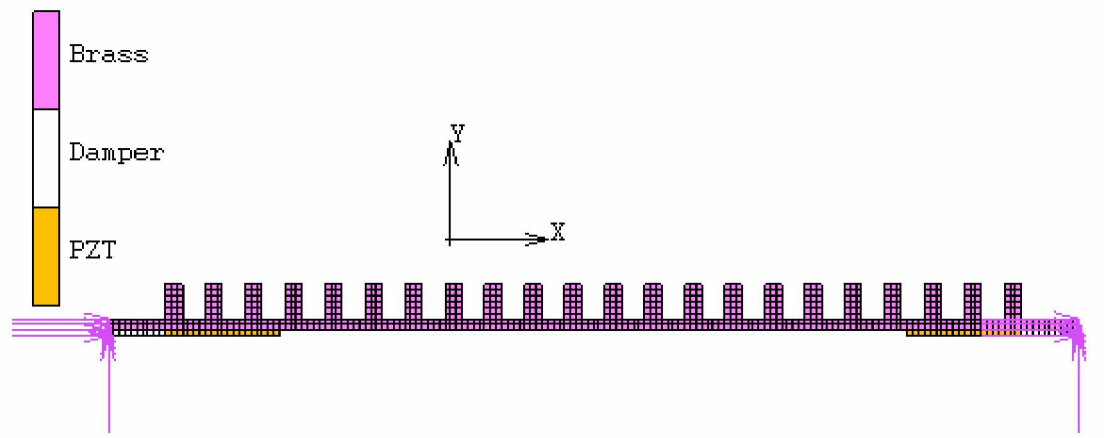

Figure 5.2 Finite element model of the stator with dual piezoelectric actuators.

5.4 Vibration Characteristics of the Stator

Analytical and finite element models of the stator with dual piezoelectric actuators are carried out and simulated to determine the system response based on the

boundary conditions and excitations as operated. Details of the experimental testing are discussed in the next section. The modal analysis is conducted to study the free vibration characteristics of the system. Natural frequencies of the stator for the analytical, finite element and experimental results are presented in Table 5.2. Natural frequencies are obtained in the early range of ultrasonic frequency (just above 20 kHz). Reasons are to avoid causing audible noises at the lower frequency operation, and that a power amplifier circuit has a limited capability for generating signals at higher frequency operation.

Table 5.2 Natural frequencies of the ultrasonic linear stator

Mode	Natural frequency (kHz)		
	Analytical	Finite element	Experimental
12	23.41	22.21	20.85
13	27.30	24.82	23.79
14	31.50	27.25	26.88
15	35.99	29.53	29.53
16	40.79	31.53	31.97

Figure 5.3 illustrates the finite element result of the 14^{th} mode shape which is close to the operating frequency. The wave configuration could be expected based on its natural mode shape because the structure tends to behave closely to the natural mode shape when the system is operated near its natural frequency. The traveling wave of the ultrasonic linear motor is generated by combining two standing waves occurred on a stator. Moreover, the desirable traveling wave must move in one direction along the stator with consistency in wave amplitude, and the wave direction can be controlled by alternating the phase difference of the excitation signals.

Figure 5.3 The 14th vibration mode shape of the stator at 27.25 kHz.

Following this, frequency response of the stator is investigated. The dual actuators are subjected to two sinusoidal voltages with an amplitude of 54 V. These are 54sin(ωt) and 54cos(ωt) for the left and the right actuators, respectively. The excitation frequency ω is varied from 20 to 35 kHz in order to investigate the system response and to determine the operating frequency. Results show that the linear stator creates pure standing waves with high wave amplitude when the system is excited at natural frequencies. Likewise, there are ultrasonic motors that work near the natural frequency and yield superb performances because the systems response with high wave amplitude at the natural frequency [15, 54, 85, 89-90].

Harmonic analysis is employed for the determination of displacement response of the wave. The wave configuration can be determined by transient analysis. In this case study, the operating frequency that yields the traveling wave is at 29.2 kHz which is in between the 14th and 15th modes. At operating frequency of 29.2 kHz, the system yields the highest transverse displacements as illustrated in Figure 5.4.

An elliptical motion at the contact surface of a tooth tip is induced by the coupling of longitudinal and transverse displacements. Figure 5.5 shows the calculated elliptical trajectory of the middle tooth tip at the contact surface based on the finite element result when the system is excited at the operating frequency of 29.2

kHz. Recalling that the motor moves in opposite direction to the trajectory path, the friction force generated on the contact surface is dependent on the transverse displacement, while the velocity of the motor depends on the longitudinal displacement. Hence, size of the elliptical trajectory is important to the motor performance.

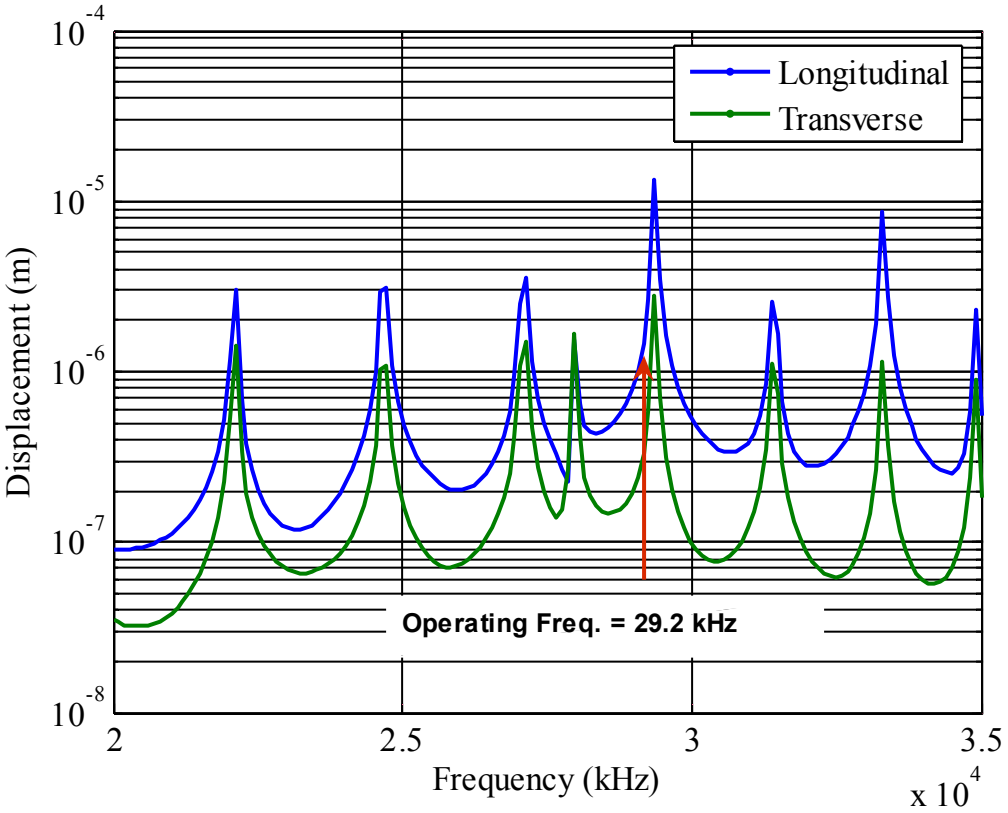

Figure 5.4 Harmonic response of the linear stator with dual piezoelectric actuators.

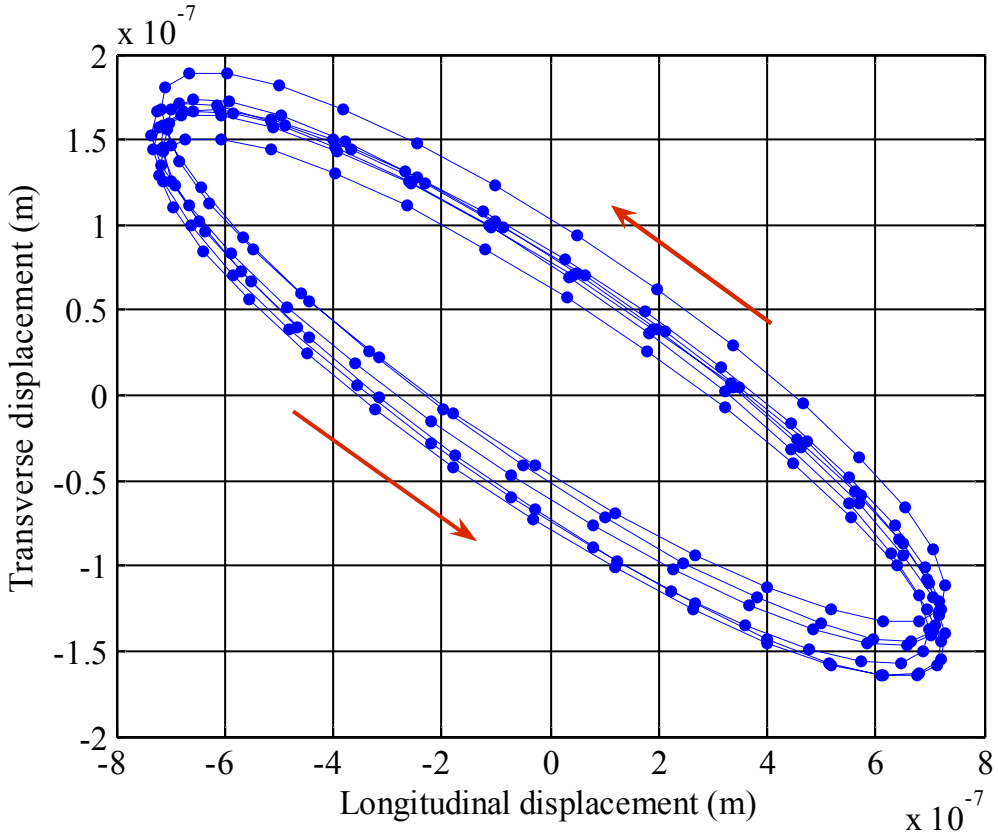

Figure 5.5 Elliptical trajectory of the middle tooth tip at the operating frequency.

5.5 Testing and Performance of the Ultrasonic Linear Motor with Dual Actuators

One objective of the ultrasonic motor design is to reduce the energy consumption, the number of actuators, the applied voltage and to simplify the motor structure for fabrication. Energy consumption of ultrasonic motors depends on the number of piezoelectric actuators used in the stator. Therefore, reducing the number of actuators directly affects the energy consumption of the motor. However, the amplitude of the generated wave must continuously remain. Conductive epoxy is used

for bonding the piezoelectric ceramic actuators with the stator, and the bonding between them is assumed to be perfect. Figure 5.6 illustrates the linear stator with the dual piezoelectric actuators. Three electrical wires are attached each onto the open surfaces of the two actuators and the stator. The two piezoelectric actuators are connected to the brass stator which functions as a common ground. Figure 5.7 shows full assembly of the ultrasonic linear motor with the dual actuators. The fixed support and the pre-load are integrated into the motor structure. In action, the stator faces down to contact the floor which acts as a stationary rotor. The motor moves itself relative to the floor in the direction opposite to the elliptical trajectory.

Figure 5.6 The linear stator with dual piezoelectric actuators.

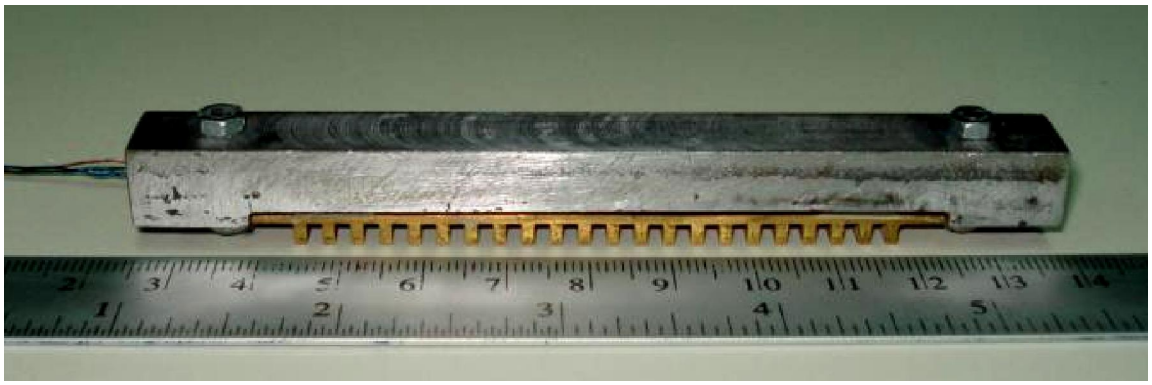

Figure 5.7 Full assembly linear motor with the fixed support and the pre-load.

Natural frequencies of the motor are measured by using an impedance analyzer machine (Hewlett Packard, model 4194A). Impedance response of the system is plotted over the frequency range of 20 to 34 kHz as shown in Figure 5.8. Noise occurs when the system is measured below 25 kHz. However, the natural frequency of the system can be indicated at the frequency that yields low impedance output. Result shows that natural frequencies of the motor occur at 20.85, 23.79, 26.88, 29.53 and 31.97 kHz. These respectively corresponding to the 12^{th} to the 16^{th} modes, as previously presented in Table 5.2. The experimental results are in positive agreements with the analytical and the finite element results.

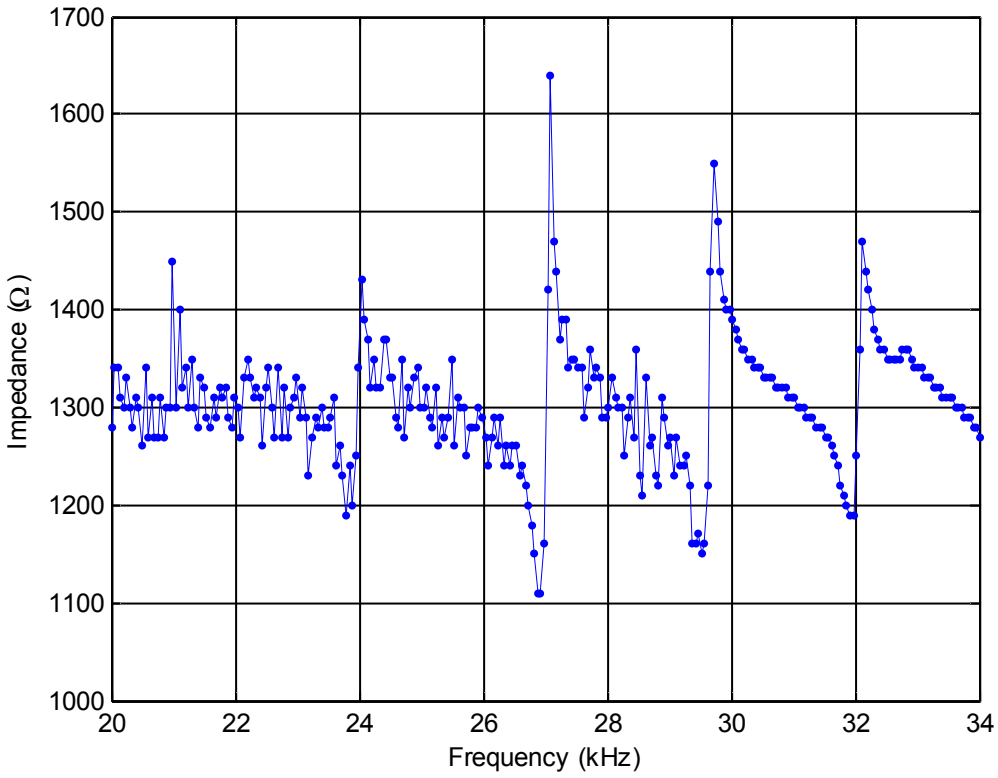

Figure 5.8 Impedance response of the linear motor with dual piezoelectric actuators.

Besides the above experiments, performance of the linear motor with the dual actuators is studied. The test setup is illustrated in Figure 5.9. The pre-load is a weight inclusive of the motor bodyweight which generates a compression force between the stator teeth and contact floor. The speed of the motor is measured by time-of-travel in a finite distance and calculated to be an average speed. The applied voltage is presented in terms of amplitude of the harmonic excitation signal. The driving force of the motor is measured by the capability of load pulling.

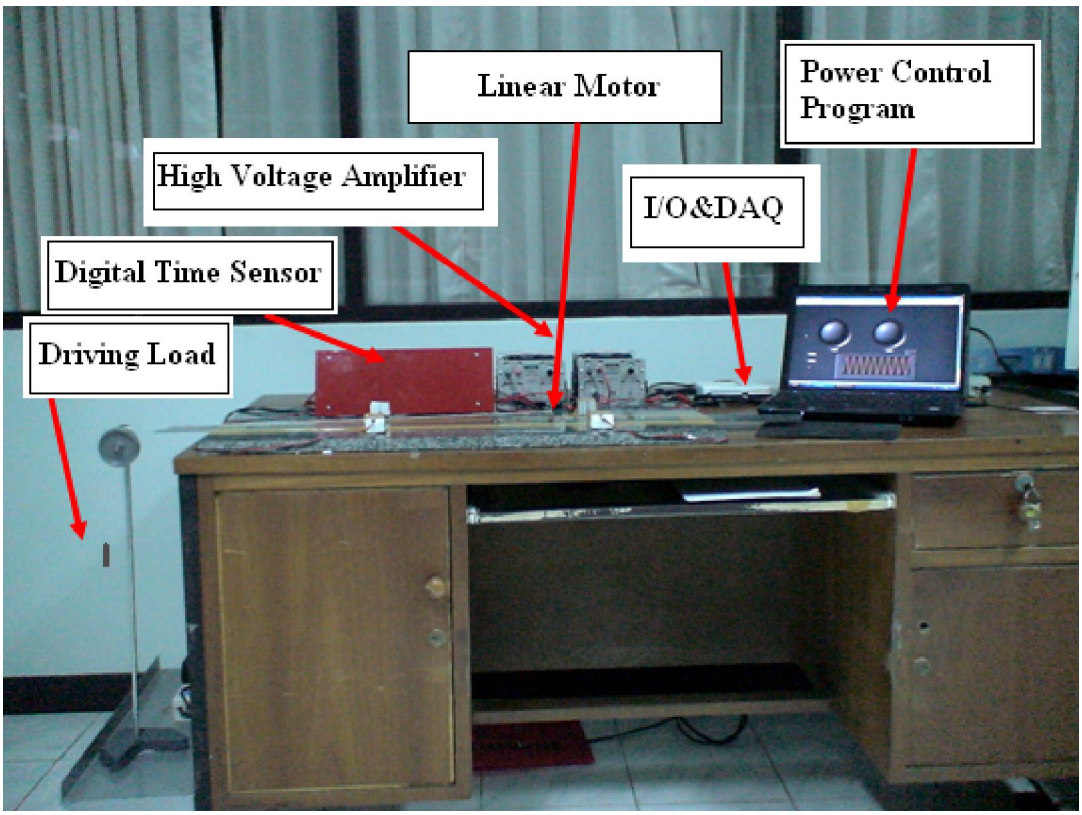

Figure 5.9 Test setup of the linear motor with dual piezoelectric actuators.

The linear motor performance is tested and reported. The relationship between velocity and the pre-load of the motor is shown in Figure 5.10. When amplitude of the applied voltage is constant, the motor velocity depends on the pre-load. The result reveals that velocity increases when pre-load increases for certain amount of the pre-load and after that the velocity decreases. Accordingly, the optimal pre-load of 101.5 g yields the maximum motor velocity of 11.43 cm/s at an applied voltage amplitude of 31 V. This optimal pre-load is subsequently used in the investigation of other performance parameters of the motor.

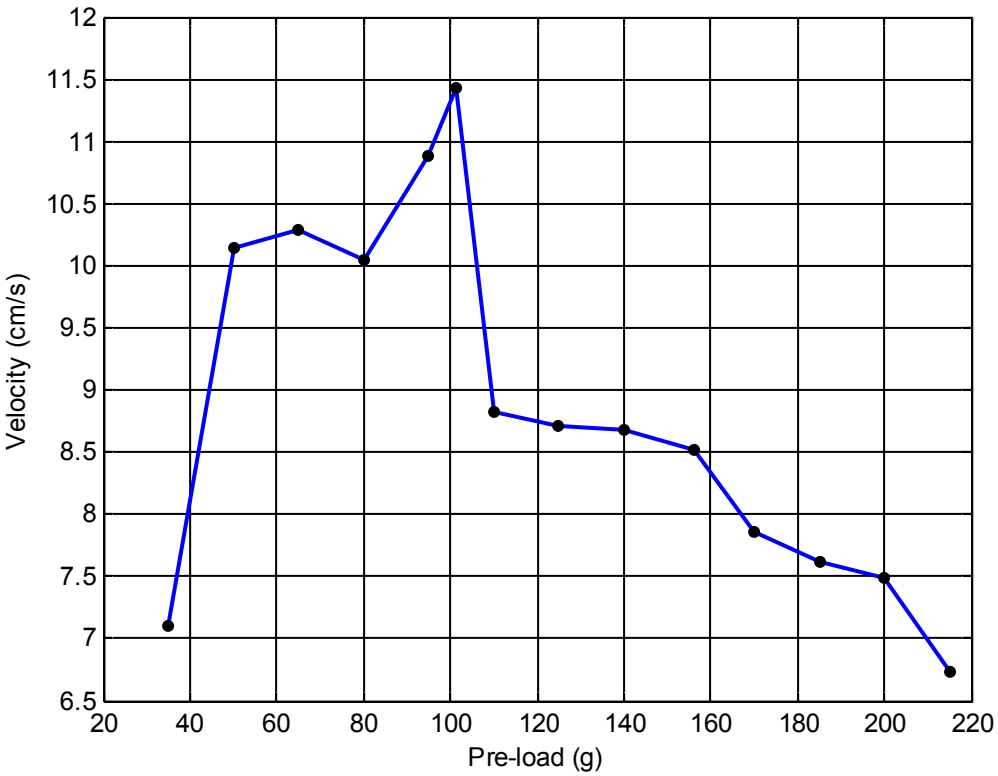

Figure 5.10 Relationship between motor velocity and pre-load.

Thereafter, relationships among performance parameters, such as velocity, driving force and applied voltage of the linear motor with the dual actuators are studied. Figure 5.11 illustrates relationship between velocity and applied voltage. The applied voltage on the piezoelectric actuators is varied from 25 V to 59 V, resulting in a linear increase of motor velocity. However, a too high electrical voltage could possibly cause depolarization of the piezoelectric actuators due to the rise of temperature during operation [13]. In the experiment, the operating frequency of the motor is 28.21 kHz which is a computer generated signal. The pre-load was set at 101.5 g. The result shows that a maximum velocity of 17.6 cm/s can be reached by applying an excitation voltage of 59 V. From determination of piezoelectric power consumption [64-65], the power consumption of the linear motor is 0.2 W.

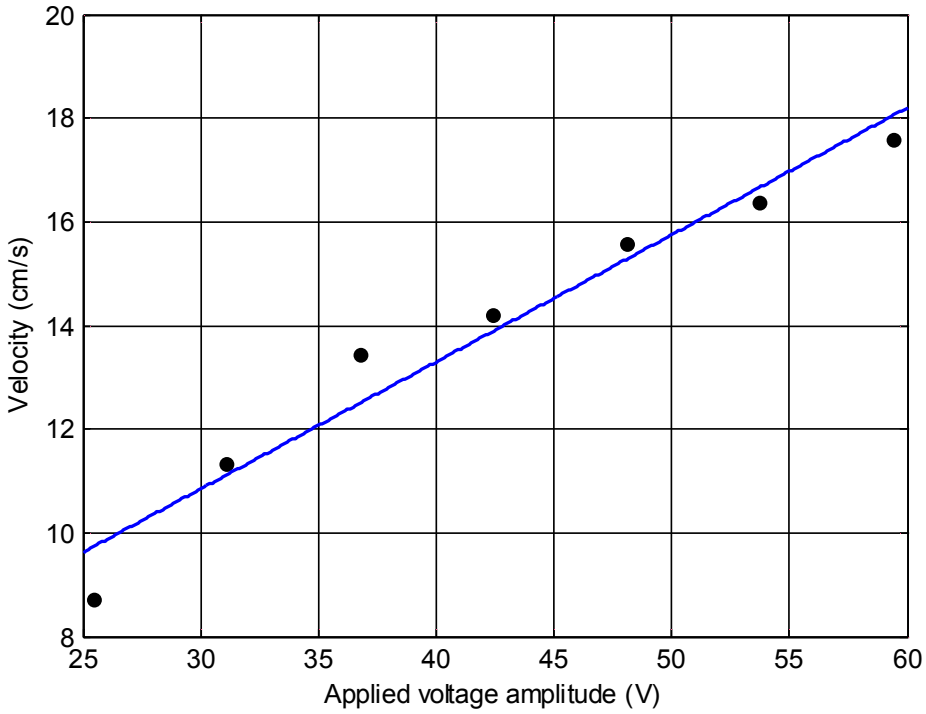

Figure 5.11 Relationship between motor velocity and applied voltage amplitude.

The relationship between driving force and the applied voltage is illustrated in Figure 5.12. Experimental result indicates that the driving force depends on the applied voltage on the piezoelectric actuators. The driving force linearly increases as applied voltage amplitude increases. In the test, the linear motor yields a maximum driving force of 0.343 N at an applied voltage amplitude of 60.8 V. Thus, the power consumption at maximum driving force is 0.22 W.

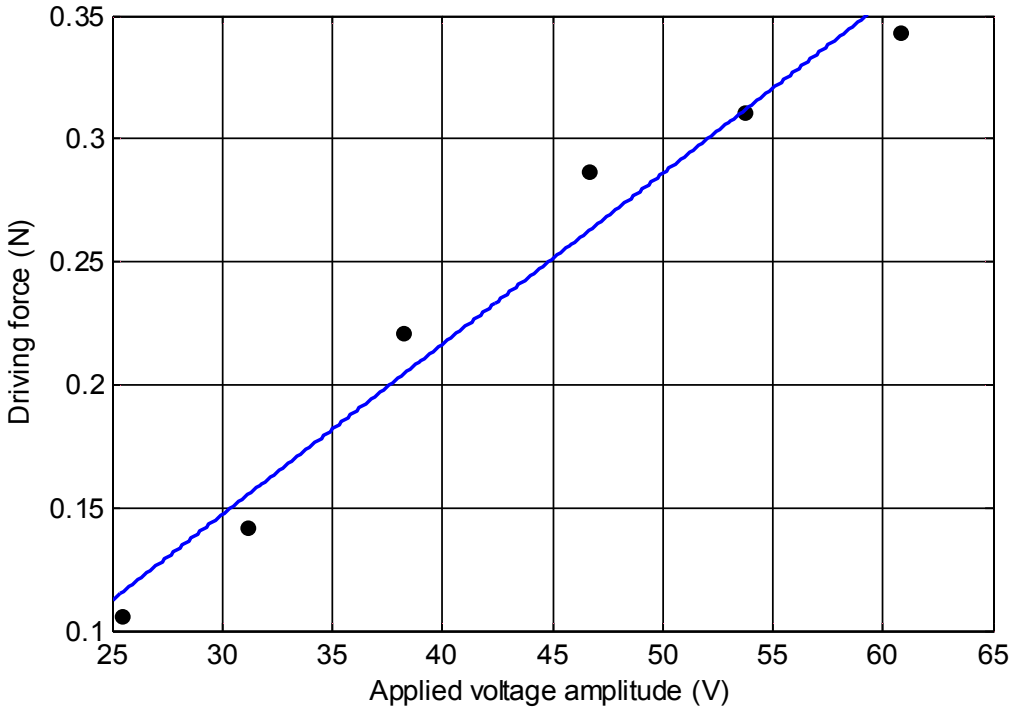

Figure 5.12 Relationship between driving force and applied voltage amplitude.

The relationship between the velocity and driving force of the motor is further determined as illustrated in Figure 5.13. The experimental results reveal that maximum motor velocity occurred at zero driving force as known as the no-load speed. On the other hand, maximum driving force is generated when the motor operates at the zero speed. For the test setup at the applied voltage of 54 V, the result shows that the maximum velocity is 16.41 cm/s and the maximum driving force is 0.31 N and the power consumption of the motor is 0.17 W.

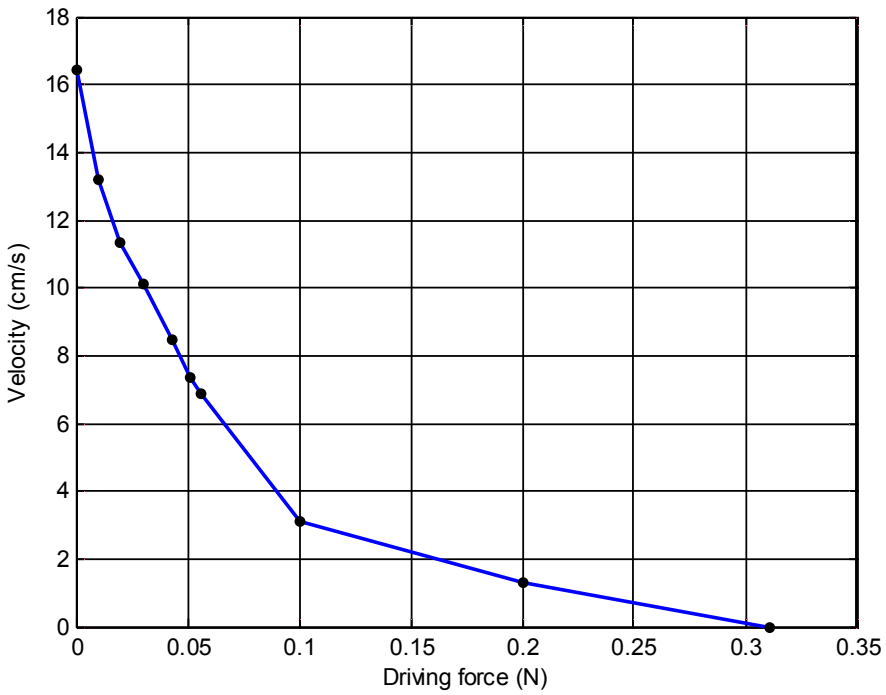

Figure 5.13 Relationship between motor velocity and driving force at applied voltage of 54 V.

Figure 5.14 shows the performance characteristic of the motor which is the relationship between the motor velocity and driving force. In addition, efficiency of

the motor operation calculated based on Equation (3.30) is depicted in Figure 5.14. It shows that, the efficiency increases when driving force increases for certain amount of the driving force and efficiency decreases afterwards. In this motor, the maximum efficiency is 2.23 % at the driving force of 0.06 N.

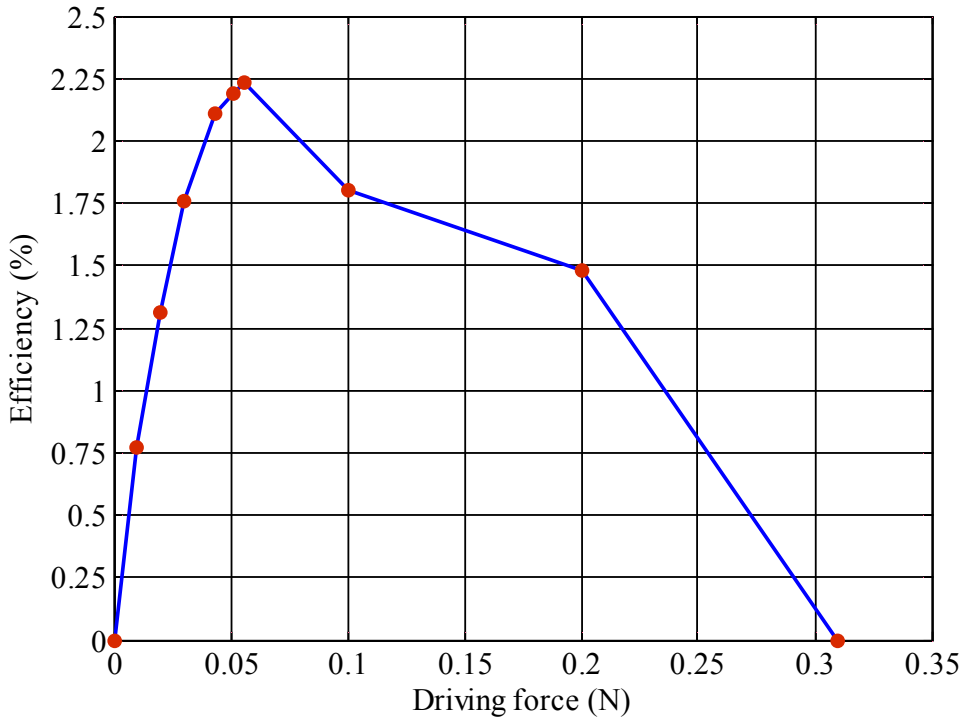

Figure 5.14 Relationship between driving force and efficiency at applied voltage of 54 V.

Performance of other ultrasonic linear motors are also reviewed and summarized in Table 5.3. Note that they cannot be compared to each other because their size and operating conditions are different. Key design factors and performances, such as volume of piezoelectric actuator, size of stator without teeth, pre-load, applied voltage, total power input, maximum driving force, no-load velocity and driving frequency are reported.

Table 5.3 shows that Lu et al.'s motor [15] employed the largest volume of piezoelectric actuator; while the presented motor used the least volume of that. Though, sizes of these stators are different, several performance indices such as applied voltage and no-load velocity are still in the comparable range. Moreover, amount of the input power consumption are in the range of 0.2 to 2.5 W. The presented motor yields almost double no-load speed compared with Lu et al.'s motor [15]. The power density of Rho et al.'s motor is higher than that of the presented linear motor. Meanwhile, the effort of the presented motor is close to the Rho et al.'s motor. Other design factors and performances are also reported in Table 5.3.

Table 5.3 Design factors and performances of ultrasonic linear motors

	Volume of actuator (mm^3)	Size of stator (mm)	Pre-load (g)	Applied voltage (V_{amp})	Total power input (W)	Maximum driving force (N)	No-load velocity (cm/s)	Driving frequency (kHz)	Power density (w/mm^3)	Effort (N/W)
Presented motor	60	85x6x1	101.5	60	0.22	0.343	17.6	28.2	3.7e-3	1.56
Lu et al. 2006 [15]	435.2	40.5x11 x2	N/A	92	N/A	N/A	9.45	38.6	N/A	N/A
Rho et al. 2005 [91]	280	53x10x3	N/A	99	2.45	3.99	36	35.4	8.7e-3	1.68
Roh and Kwon 2004 [13]	384	54x8x1	100	100	N/A	0.29	62	28.6	N/A	N/A
Roh et al. 2001 [25]	432	75x8x1	200	100	N/A	N/A	40	23.5	N/A	N/A
He et al. 1998 [27]	400	40x10x1	100	36	N/A	N/A	8	23.4	N/A	N/A

Note: maximum, minimum

5.6 Conclusion

An ultrasonic linear motor with dual piezoelectric actuators has been studied and tested in this work. The design deploys two piezoelectric actuators that are bonded with a linear stator, one actuator near each end of the support. Movement direction of the motor is controlled by alternating phase difference between two harmonic control signals. Analytical, finite element and experimental results of the natural frequency of the linear stator reveal positive agreement. The operating frequency resulted from the finite element analysis (29.2 kHz) is in good comparison to that of the experimental result (28.2 kHz). Based on the experimental testing, the suitable pre-load pressed on the motor is 101.5 g. The maximum velocity of the motor is 17.59 cm/s at the applied voltage of 59 V. The power consumption of the motor is 0.2 W. The power density of the linear motor is 3.7×10^3 W/mm^3. The effort of the motor is 1.56 N/W which is close to the Rho et al.'s motor [91].

The design of the ultrasonic linear motor with dual piezoelectric actuators exhibits a simpler structure with less number of actuators, thus yielding a low system structural stiffness and a lower electrical power consumption in comparison to conventional ultrasonic linear motors with fully laminated actuators. Moreover, the design of the linear motor is capable of being scaled down to size. This opens up an opportunity for many applications that require a tiny translation actuator together with low power consumption.

Chapter 6

Ultrasonic Linear Driver with Single Piezoelectric Actuator

6.1 Introduction

The ultrasonic linear driver with a piezoelectric actuator is studied in this chapter. The motor system consists of a brass beam and piezoelectric ceramic (PZT-4). Generally, an ultrasonic linear motor has piezoelectric actuator patches bonded on a stator more than one patch for generating the propagation wave [13, 15, 25, 92-93]. A great number of piezoelectric actuators bonded on a stator directly effect the energy consumption of the motor, because the energy consumption depends on a number of piezoelectric actuators. Hence, reducing number of piezoelectric actuators will be decreasing the energy consumption. Accordingly, the main objective of this chapter is to design an ultrasonic motor with the least number of the actuator and investigate the motor performance. For validating the results, the finite element method, mathematical model and experiment are used as presented next.

6.2 Operation Principle of Single Piezoelectric Actuator Linear Driver

The dimensions of the single actuator ultrasonic linear driver are shown in Figure 6.1. The system consists of a brass beam, a single piezoelectric actuator. The

stator tooth is designed for expanding the propagation wave amplitude and creating the elliptical locus at the top surface of the tooth [18, 20]. An electrical signal of Asin(ωt) excites the piezoelectric actuator. The actuator design is that the length of the actuator is equal to the wave length (λ). The stator generates the propagation wave when the piezoelectric actuator is subjected to the harmonic excitation.

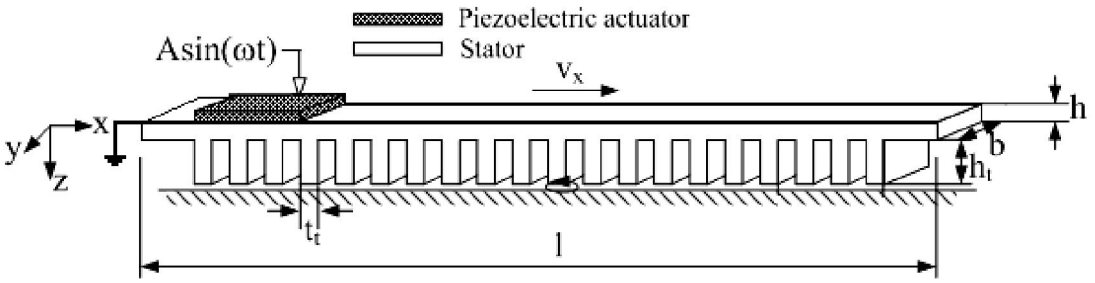

Figure 6.1 Dimensions of the single actuator ultrasonic linear driver.

6.3 Finite Element Modeling of the Linear Stator

Finite element software package, MSC.Marc, is also used for modeling the single actuator ultrasonic linear driver and to evaluate its operating frequency, mode shape and harmonic response. The finite element model is shown in Figure 6.2. The piezoelectric actuator is excited by the electrical voltage of 76sin(ωt). Dimensions of the stator are width b of 6 mm, length l of 85 mm and thickness h of 1 mm. The teeth dimensions are height h_t of 3 mm, width b_t of 6 mm and thickness t_t of 1.5 mm. The teeth of stator are used for amplifying the propagation wave amplitude at the stator-rotor contact areas. The piezoelectric actuator is made of Lead Zirconate Titanate

(PZT-4) with the length l_a of 10 mm, width b_a of 6 mm and thickness h_a of 0.5 mm. The length of the actuator is equal to a wave length on the stator. Note that all dimensions of the stator and actuator are the same with the dual actuators driver, except that the single actuator driver uses only one actuator patch.

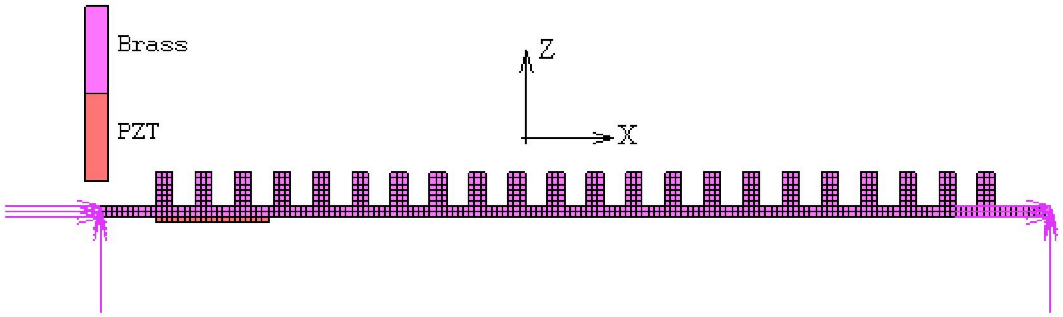

Figure 6.2 Finite element model of the single actuator ultrasonic linear motor.

The piezoelectric actuator is located on one side near the end of the stator. All material properties of the single actuator ultrasonic linear driver are piezoelectric ceramic and brass as described in Table 6.1.

Table 6.1 Material properties of the single piezoelectric actuator linear stator.

	PZT-4 actuator	Brass stator	Unit
Modulus of Elasticity	(Orthotropic)	(Isotropic)	
Y11	79	96	GPa
Y33	66	96	GPa
Density	7700	8400	kg/m3
Poisson's ratio	0.33	0.35	
Damping coefficient	0.0013	0.0005	
Piezoelectric constant			
e_{33}	17.56	-	C/m2
e_{31}	-4.38	-	C/m2
Permittivity	1.018x10-8	-	F/m
Capacitance	2096	-	pF

6.4 Fabrication of Single Actuator Ultrasonic Linear Driver

Objective of this study is to design the motor with the least number of the piezoelectric actuator. The ultrasonic linear driver system consists of two main parts. They are 1) a linear stator and 2) a piezoelectric actuator (Lead Zirconate Titanate: PZT-4). The stator is a brass beam. The PZT-4 actuator is manufactured by SPK Electronic Co. Ltd. The conductive epoxy is used for bonding of the piezoelectric actuator with the linear stator. The perfect bonding is assumed for interfacing between them. Figure 6.3 illustrates the linear stator with the piezoelectric actuator. Figure 6.4 shows the full assembly of the single piezoelectric actuator ultrasonic linear driver.

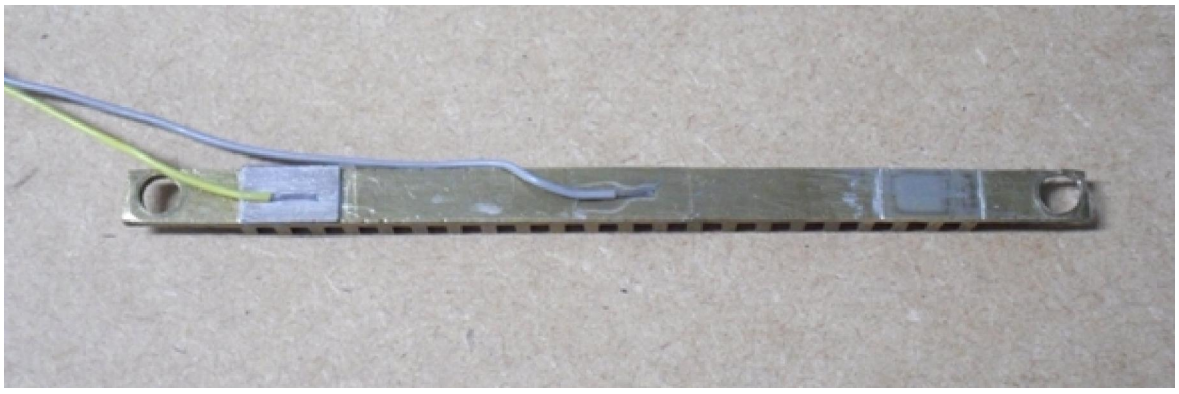

Figure 6.3 The linear driver with single actuator.

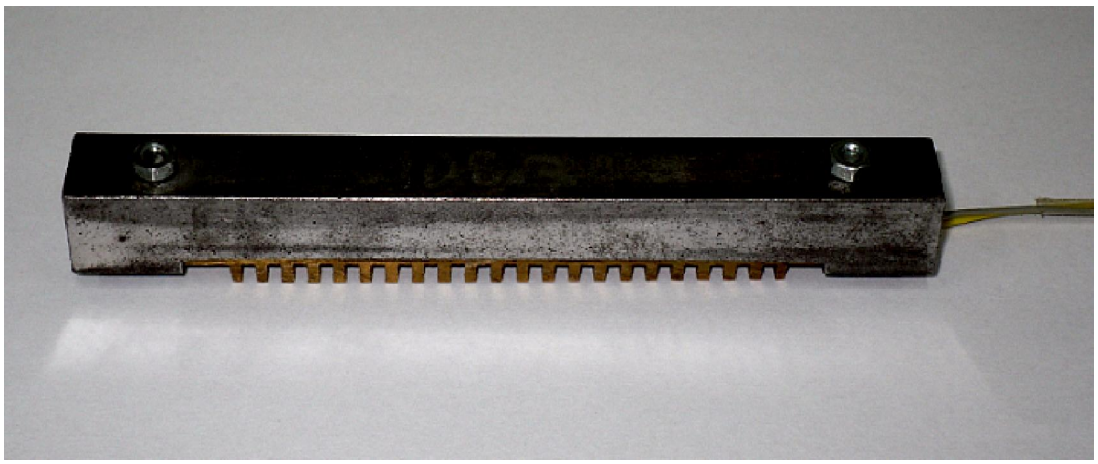

Figure 6.4 Assembly of the single actuator piezoelectric linear motor.

The experimental setup for testing the single actuator linear driver is shown in Figure 6.5. The instrument set consists of a high voltage amplifier, a digital time sensor, a function generator, and an ultrasonic linear driver. The high voltage amplifier is for amplify the electrical applied voltage driving the actuator. It is the same apparatus that used to test the dual actuators linear motor.

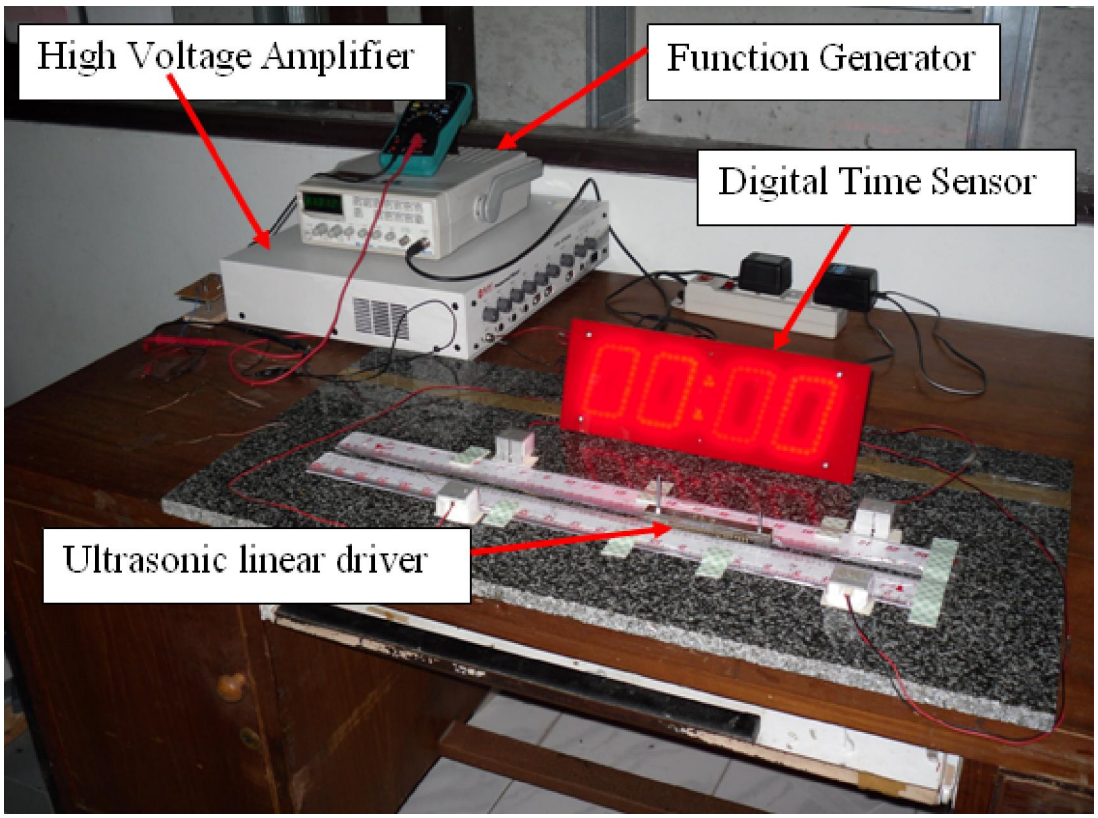

Figure 6.5 The experimental setup for the single actuator linear driver.

6.5 Finite Element and Experimental Results

6.5.1 Finite element results

Finite element method of modeling the single actuator ultrasonic linear driver and predicting the system response has been previously discussed. The propagation wave is generated by applying the electrical applied voltage on the piezoelectric actuator. The sinusoidal electrical excitation with amplitude of 76 V is applied. Both of vibration characteristics and harmonic responses of the ultrasonic linear driver are investigated in this section. The operating frequency, which generated propagation

wave, is 31.2 kHz. The deformation of the stator in the 16th mode at the 30.69 kHz is illustrated in Figure 6.6.

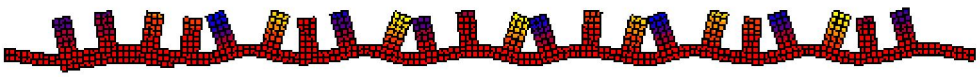

Figure 6.6 Deformation of the stator in the 16th mode at 30.69 kHz.

Frequency response, as known as harmonic response, of the single actuator ultrasonic linear driver is investigated. The piezoelectric actuator is excited by sinusoidal electrical applied voltage of 76sin(ωt). The excitation frequency is varied from 20 to 35 kHz. It is found that, the operating frequency to generate the propagation wave is at 31.2 kHz. The displacement response at natural frequency higher than that of the other frequencies [4, 15, 84, 91-92]. The relationship between the driving frequencies and longitudinal and transverse displacements is illustrated in Figure 6.7.

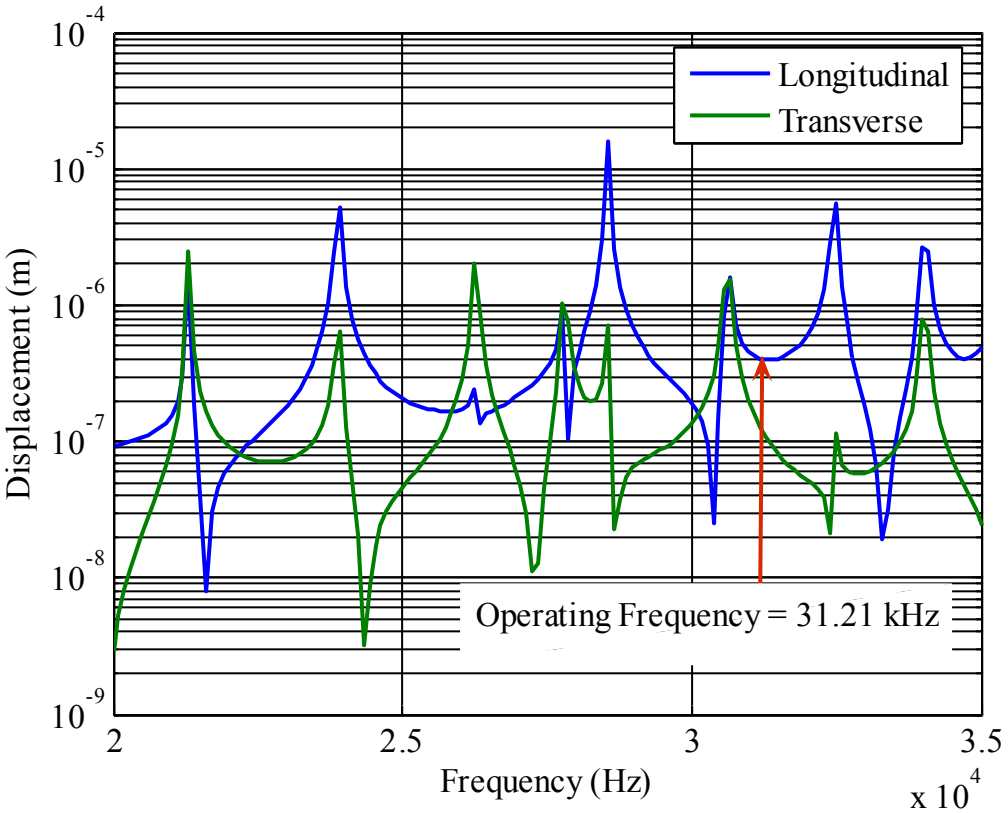

Figure 6.7 Harmonic responses with the applied voltage of 76 V.

The elliptical trajectory of the tooth tip is shown Figure 6.8. Generally, the elliptical trajectory is a coupled path between the longitudinal and transverse displacements. The trajectory of the elliptical locus is opposite to the propagation wave direction. In this study, the stator faces down to contact the floor which acts as a stationary rotor.

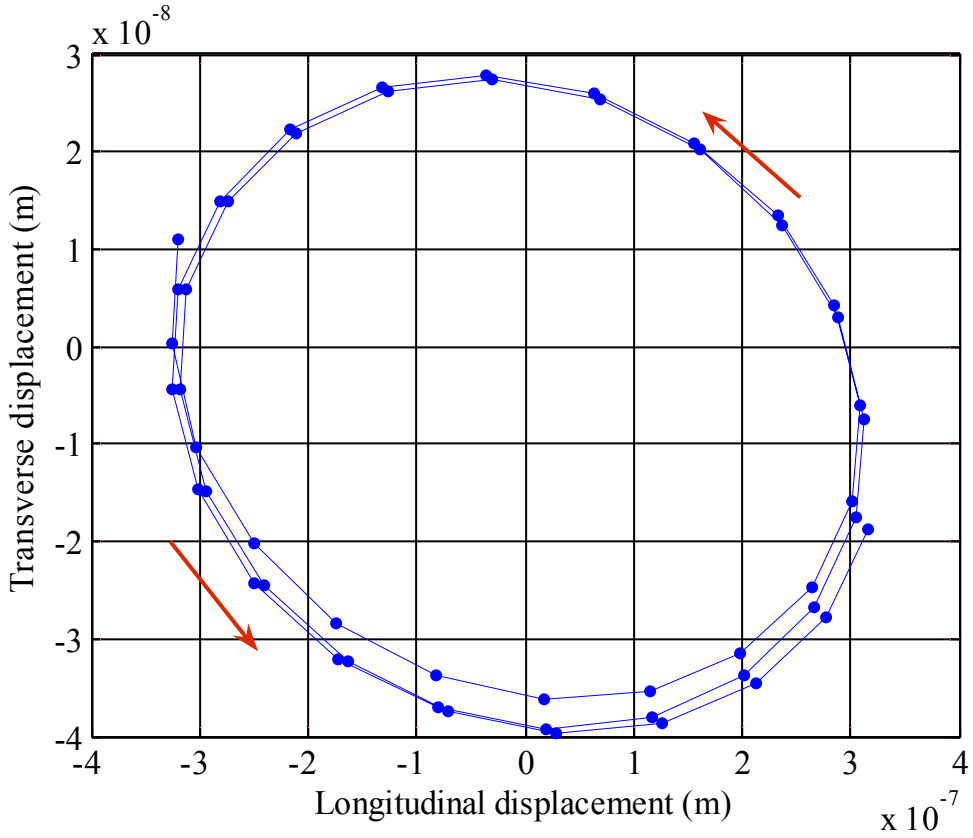

Figure 6.8 Elliptical trajectory of the middle tooth tip at the operating frequency of 76 V.

6.5.2 Experimental Results

Characteristics of the ultrasonic linear driver are also investigated in the experiments. They are relationships between the electrical applied voltage and velocity, maximum driving force and electrical applied voltage, and driving force and velocity. Furthermore, the natural frequency of the motor is measured by using the impedance analyzer machine (Hewlett Packard model 4194A). Afterwards, the result is compared with the finite element and analytical results.

Figure 6.9 illustrates the natural frequencies of the single actuator linear driver measured by the impedance analyzer. The result is in the frequency ranged above 22 kHz because the measured impedance below 22 kHz has noise.

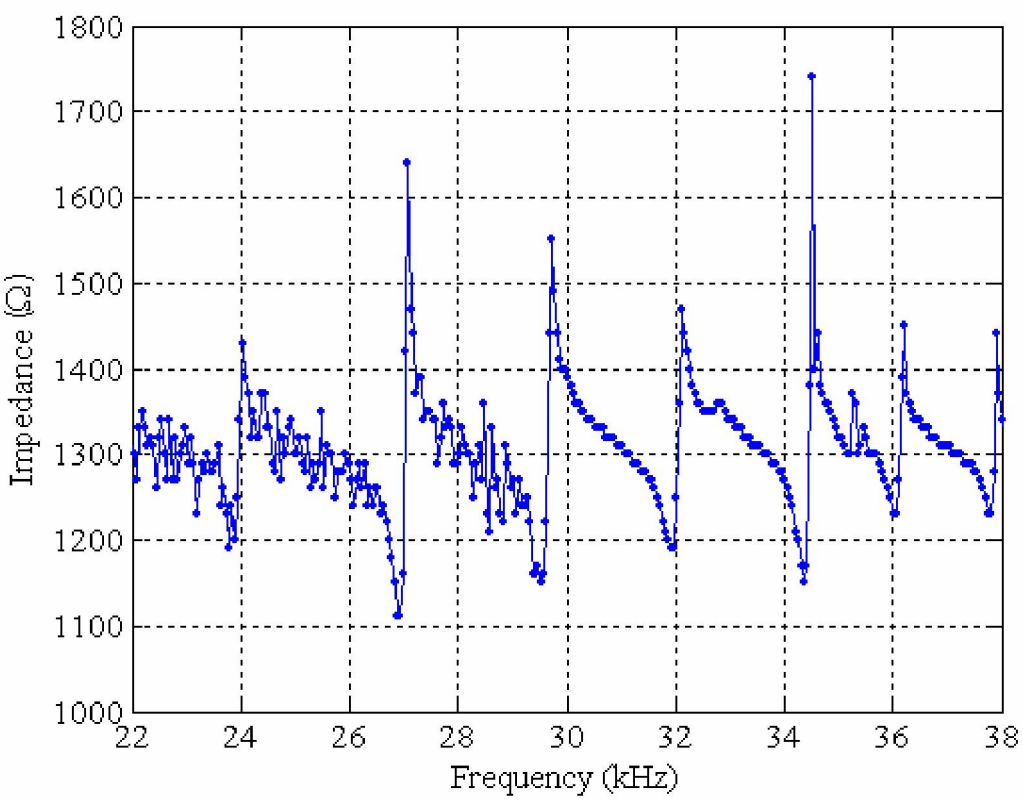

Figure 6.9 The natural frequency measured by the impedance analyzer.

Table 6.2 shows comparison of natural frequencies of the single actuator linear driver obtained by finite element, analytical and experiment methods. The finite element result is calculated by the MSC.Marc software, the experimental result is measured by the impedance analyzer, and the analytical result is calculated based on the Equation (3.1). Comparison of the natural frequencies obtained by these methods are in positive agreement.

Table 6.2 Natural frequencies of the single actuator ultrasonic linear driver.

Mode	**Natural frequency** (kHz)		
	Analytical	Finite Element	Experimental
12	23.41	21.37	21.05
13	27.30	23.95	23.89
14	31.50	26.33	26.88
15	35.99	28.61	29.58
16	40.79	30.69	31.92

The ultrasonic linear driver performance is tested and reported. The relationship between velocity and the pre-load of the motor is shown in Figure 6.10. When amplitude of the applied voltage is constant, the motor velocity depends on the pre-load. The result reveals that velocity increases when pre-load increases for a finite amount of the pre-load and after that the velocity decreases. Accordingly, the optimal pre-load of 101.5 g yields the maximum velocity of 10.85 cm/s at electrical applied voltage amplitude of 31 V. This optimal pre-load is consequently used in the investigation of other performance parameters of the motor.

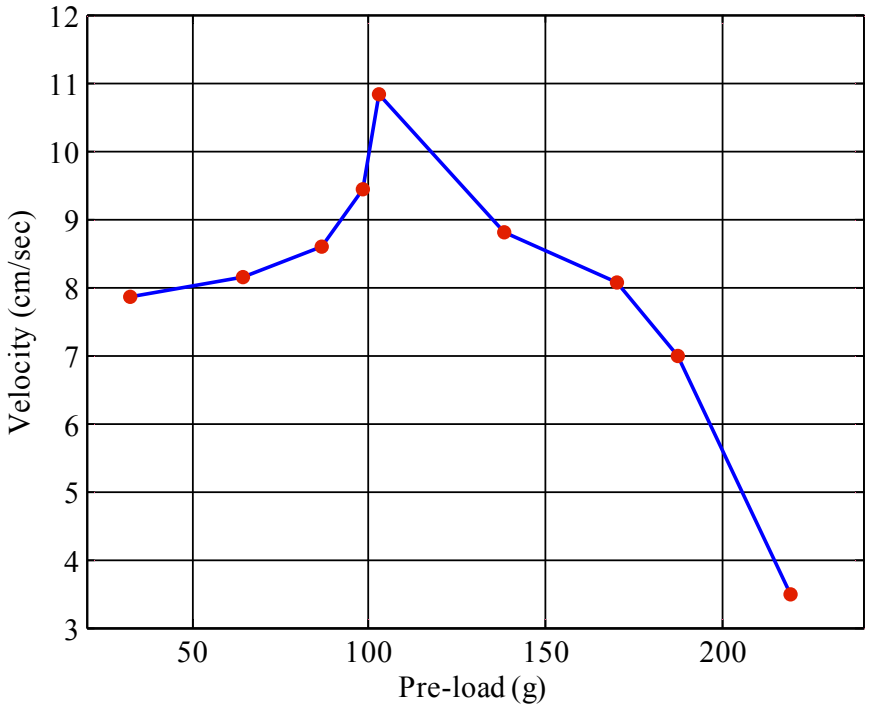

Figure 6.10 Relationship between motor velocity and pre-load.

Relationships among electrical applied voltage, velocity and driving force of the single actuator linear driver are studied. The relationship between the electrical applied voltage and motor velocity is illustrated in Figure 6.11. The electrical applied voltage excites on the piezoelectric actuator varies from 28 V to 86 V. It is found that the velocity depends on the voltage applied on the piezoelectric actuator. However, the high electrical applied voltage may cause de-polarization of piezoelectric material due to the temperature increases during operation [13]. In this experiment, the operating frequency is 31.32 kHz and the optimum pre-load is 101.5 g. The result shows that the maximum velocity is 14.48 cm/sec with the electrical applied voltage of 85.5 V. The electrical power consumption is 0.24 W.

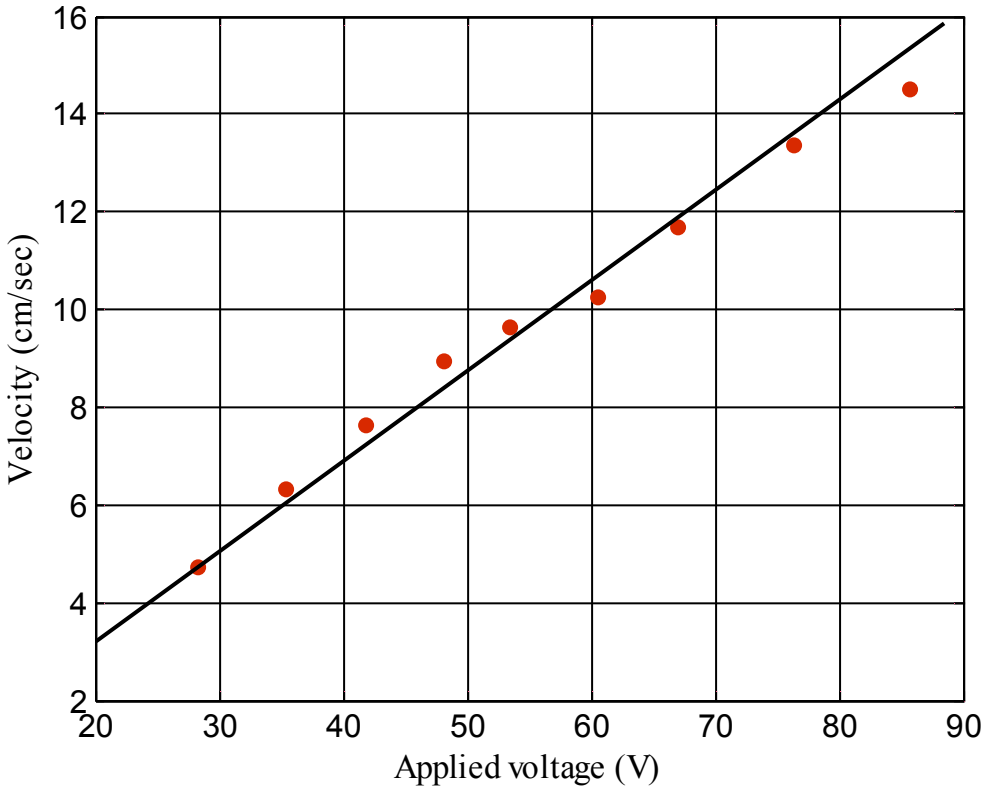

Figure 6.11 Relationship between the applied voltage and velocity of the linear driver with single actuator.

The electrical power consumption of the single actuator linear driver is proportional to the electrical applied voltage as presented in Equation (2.47). Figure 6.12 shows relationship between the applied voltage and electrical power consumption. In the test, the maximum power consumption is 0.24 W at the electrical applied voltage of 85.5 V.

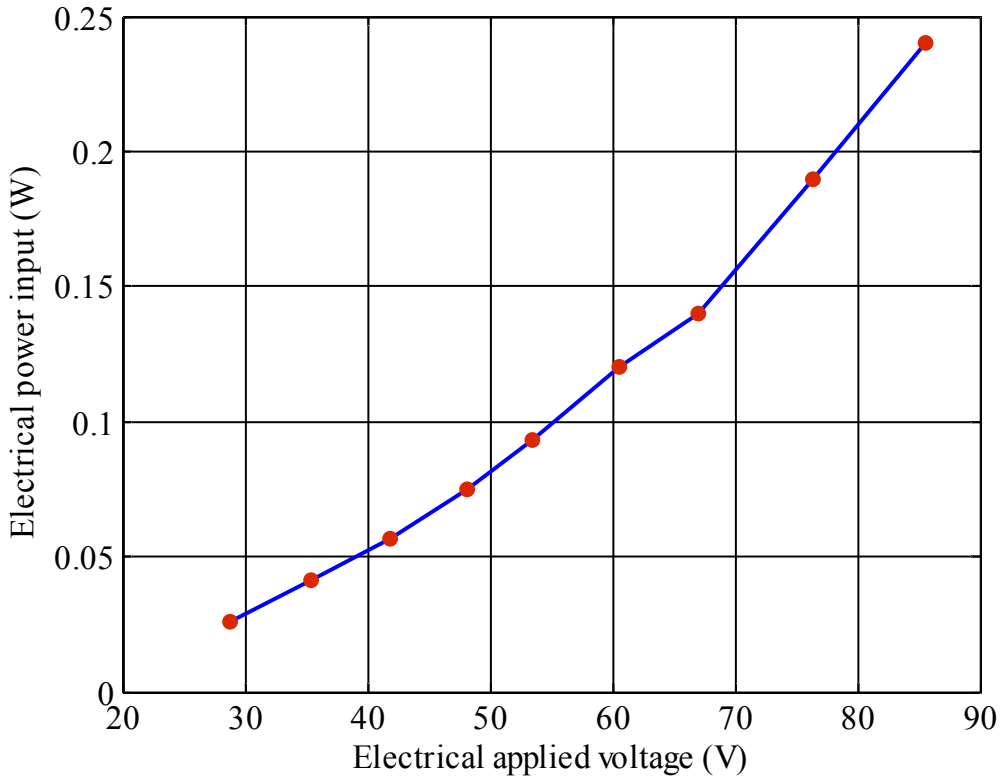

Figure 6.12 Relationship between the applied voltage and input power of the linear driver with single actuator.

Furthermore, the relationship between the maximum driving force and applied voltage is evaluated. The result is shown in Figure 6.13. It is found that the maximum driving force depends on the applied voltage. The maximum driving force is 0.22 N when the motor is subjected to the applied voltage of 85.5 V, and the power consumption at this state is 0.24 W.

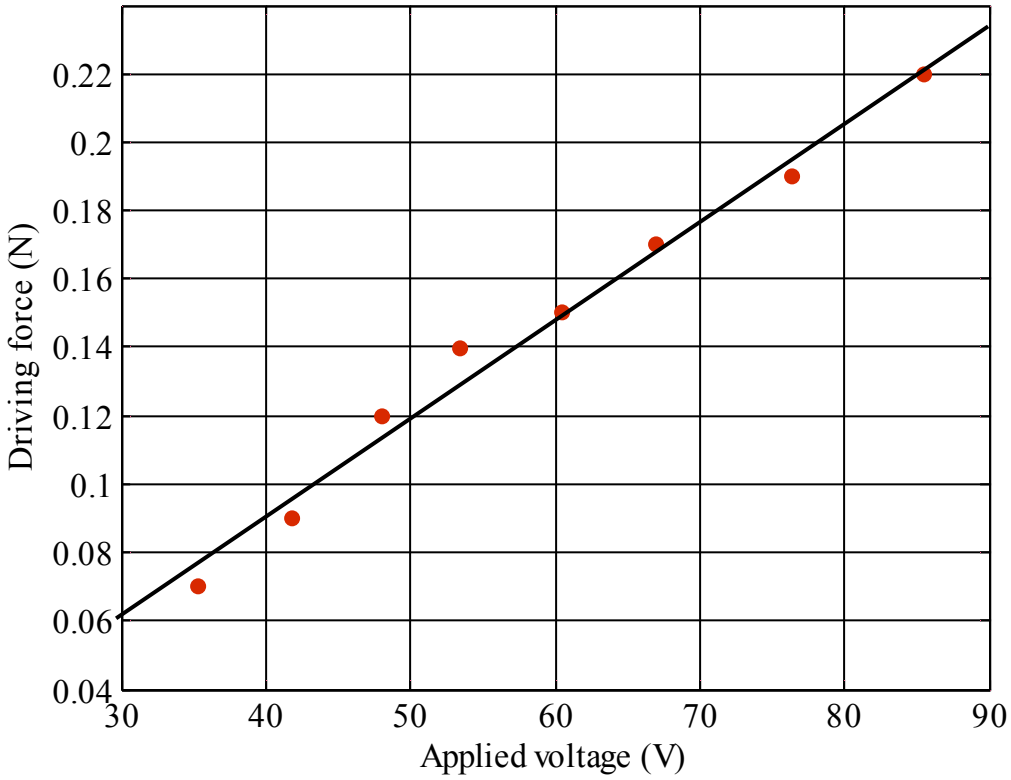

Figure 6.13 Relationship between the applied voltage and driving force of the linear driver with single actuator.

For the testing of motor performance, the applied voltage is 76.4 V, the pre-load is 101.5 g and the operating frequency is 31.32 kHz. The testing reveals that the maximum motor velocity occurred at zero driving force as known as the no-load speed. On the other hand, maximum driving force is generated when the motor operates at the zero speed. The result shows that the maximum velocity is 13.33 cm/sec at the zero driving force and the maximum driving force is 0.13 N at the zero velocity. The calculated power consumption is 0.19 W. Figure 6.14 shows the performance characteristic of the motor which is the relationship between the motor velocity and driving force. In addition, efficiency of the motor operation calculated

based on Equation (3.30) is depicted in Figure 6.15. It shows that the efficiency increases when driving force increases for certain amount of the driving force and efficiency decreases afterward.

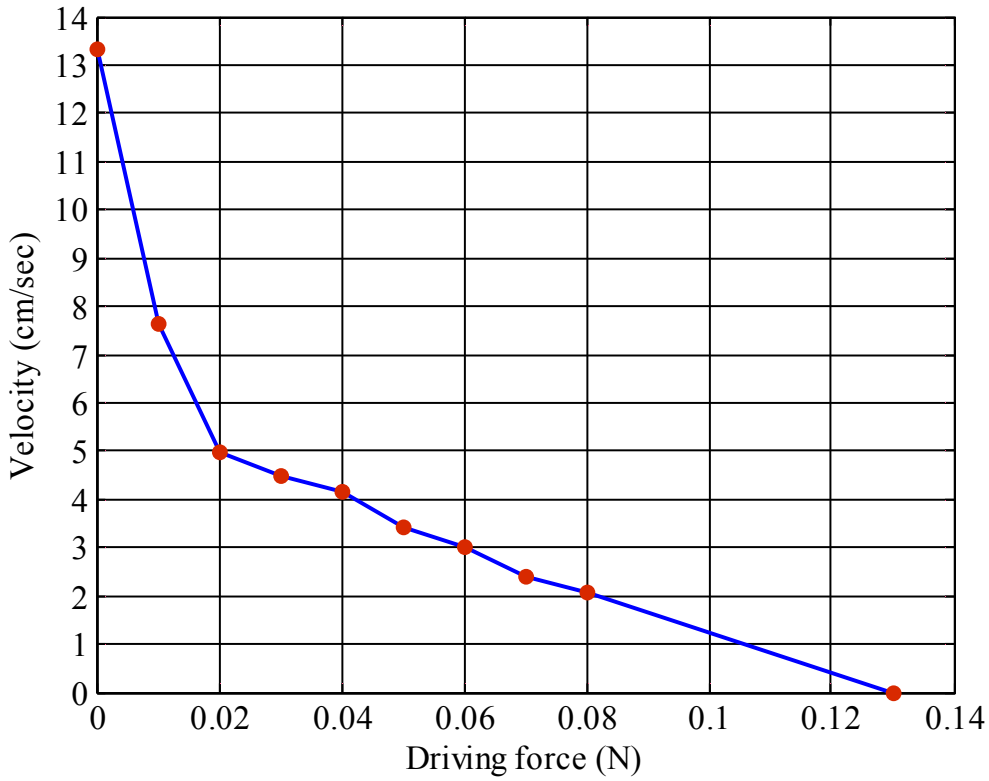

Figure 6.14 Experimental result between driving force and velocity of the motor.

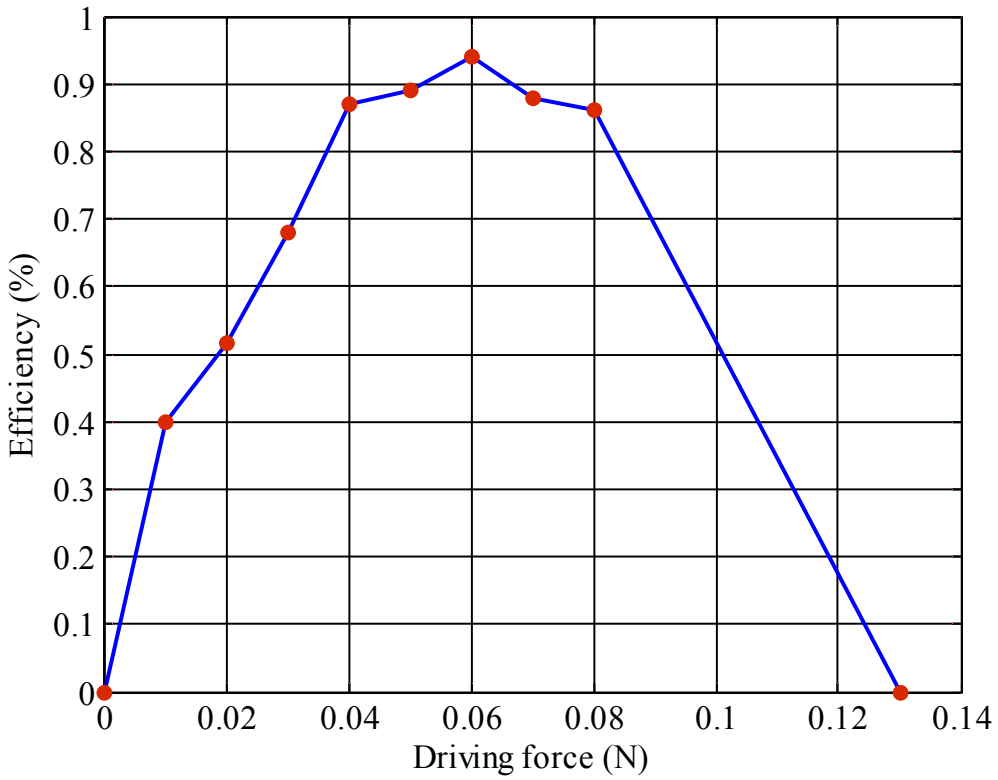

Figure 6.15 Efficiency and driving force of the linear driver with single actuator.

Performance comparison between the dual actuators, single actuator and Rho et al.'s motor is shown in Table 6.3. It is found that the input power consumption of the dual actuator motor is the least because it operates with electrical applied voltage and driving frequency lower than that of the other two motors. While, Rho et al.'s motor uses the highest volume of actuator and power input consumption. The power density of the single actuator ultrasonic linear driver is close to the Rho et al.'s motor. The volume of actuator of the single linear motor is nine times less than that of Rho et al.'s motor. Other design factors and performances are reported in Table 6.3.

Table 6.3 Comparison between dual actuator and single actuator drivers

	Volume of actuator (mm^3)	Size of stator (mm)	Pre-load (g)	Applied voltage (V_{amp})	Total power input (W)	Maximum driving force (N)	No-load velocity (cm/s)	Driving frequency (kHz)	Power density (w/mm^3)	Effort (N/W)
Dual actuator linear driver	60	85x6x1	101.5	60	0.22	0.343	17.62	28.2	3.7e-3	1.56
Single actuator linear driver	30	85x6x1	101.5	85.5	0.24	0.22	14.48	31.32	8e-3	0.92
Rho et al. 2005 [91]	280	53x10x3	N/A	99	2.45	3.99	36	35.4	8.7e-3	1.68

Note: maximum, minimum

6.6 Conclusion

In this chapter, the single actuator ultrasonic linear driver is investigated. The piezoelectric actuator is bonded with the linear stator near the support. The operating frequency of the ultrasonic linear driver shows agreement between the finite element (31.2 kHz) and experimental (31.32 kHz) results. For testing of the motor performance, it reveals that the maximum velocity is 14.48 cm/sec without driving load at the applied voltage of 85.5 V, the calculated power consumption is 0.24 W. The maximum driving force at the applied voltage of 76.4 V is 0.13 N and the power input consumption is 0.19 W. The maximum efficiency of 0.94 % is generated at the

driving force of 0.06 N. The effort of the motor is 0.92 N/W. The power density of the single actuator of $8x10^3$ W/mm^3 which is close to Rho et al.'s motor, but the volume of actuator is nine times less. In addition, the single actuator linear driver has power density two times larger than the dual actuator motor dose.

The advantages of the single actuator ultrasonic linear driver are that it is the simplest structure for fabrication with the least number of components, just only a brass beam and a piezoelectric actuator, it has the least amount of structural stiffness mostly depends on stiffness of the stator itself, and it has high power density. This is a break through design of the ultrasonic linear motor that never been published before [13, 25, 91, 94-95].

Chapter 7

Summary and Conclusions

7.1 Summary of Research

In this research, the ultrasonic linear motor is studied. Important topics investigated in the research include performance of the linear ultrasonic motor and reduction of the energy consumption. Decreasing of energy consumption can be done by reducing number of piezoelectric actuators used in the linear stator because the energy consumption of the motor depends on a number of the piezoelectric actuators. In this research, a design of ultrasonic linear motors with dual piezoelectric actuators and single piezoelectric actuator are proposed. The methodology of the research is described. This work is presented in seven chapters. Details of each chapter are described and summarized as follows.

In Chapter 1, the principle of the ultrasonic motors is studied and described. Fundamental working principle of the ultrasonic motor is based on two stages of energy conversions. The first stage, piezoelectric actuators converse the harmonic electrical energy input to high frequency mechanical oscillation. The second stage, the mechanical oscillatory vibration is rectified to macroscopic unidirectional rotary or linear motion, which is depended on the design. Generally, ultrasonic motors can be classified into two types which are rotary and linear ultrasonic motors. An ultrasonic motor system usually consists of a stator and a rotor. In addition, the ultrasonic linear

motor can be subdivided into several types. Through the literature review, they are stepping linear motor, impact motor, multi-mode type linear motor, traveling wave linear motor, surface acoustic wave motor and standing wave linear motor. To improve the motor performance, many techniques have been used such as using actuators that are made of multi-layer instead of single layer piezoelectric ceramics, replacing single driving foot with double driving feet to increase torque of the motor. However, the issue of energy consumption for the ultrasonic linear motor had not been completely reported. Consequently, objectives of this research is to reduce electrical energy consumption in the ultrasonic linear motor by decreasing a number of piezoelectric actuators used in the motor, and to study parameters that have a effect on the motor performance. An ultrasonic linear motor which is the traveling wave linear motor is investigated in this research. Besides, other objectives, scopes and expected results of this research are also mentioned.

In Chapter 2, both properties and mathematical model of the piezoelectric material which is used for actuation in the linear ultrasonic motor are described. The piezoelectric material has two effects: direct and inverse piezoelectric effects. The direct piezoelectric effect is that the material generates electrical charge in proportion of an external applied force. While, the inverse piezoelectric effect is that the material induces the mechanical displacement when the electrical voltage is applied. For the piezoelectric actuator application, the material must have high piezoelectric coefficient for generating high strain and vibration. Moreover, other parameters that should be considered are electromechanical coupling factor, k, working temperature and power consumption. Generally, the direct piezoelectric effect is a principle of transformer and igniter. Meanwhile, the inverse piezoelectric effect is a principle of

actuators and ultrasonic motors. This chapter describes the elastic compliance of the piezoelectric material which is defined based on relationship between stress and strain (Hook's law). Thermal property, mechanical property and electrical property of the piezoelectric material are analyzed through the thermodynamic principle. The reviewed literature reveals that piezoelectric ceramic devices can be categorized in four major applications: generator, sensor, actuator, and transducer. System characteristics of each application are briefly summarized. The mathematical models of the piezoelectric material, piezoelectric power consumption are also studied.

In Chapter 3, mathematical models of the contact interface between the stator and rotor of the ultrasonic motor are studied and discussed. Several published cases on characteristic and performance of the ultrasonic motor are reported [49,69,70- 71]. The relationship between the applied voltage and velocity, velocity and driving force (linear motor) or torque (rotary motor) is presented. Detail of the mathematical model consisted of the basic modeling assumption, natural frequencies, mode shapes and contact interface between the stator and rotor. Mathematical models of the contact mechanic have been reported by [72-76]. Also, equations for determination the motor efficiency is described.

In Chapter 4, the research methodology for studying characteristic and performance of the piezoelectric ultrasonic linear motor is described. The step of the research are 1) design of new linear ultrasonic motors with laminated piezoelectric actuator, the designs are dual actuators and single actuator ultrasonic linear motor, 2) the stator of the motor is modeled by using finite element method to study the vibration characteristics, 3) the prototype of the piezoelectric ultrasonic linear motor

is fabricated based on studied parameters and tested, 4) the finite element and experimental results are compared and discussed for validation, and 5) conclusion.

Three analyses are used to investigate the motor dynamics. They are modal, harmonic and transient analyses, respectively. Meanwhile, the experimental study is for investigating the motor performances. They are relationships between applied voltage and velocity, driving force and velocity, applied voltage and driving force, and the suitable preload. Other properties such as effective capacitance of the piezoelectric actuator and natural frequency of the ultrasonic piezoelectric linear motors are also measured. The test apparatus consists of power amplifiers, a data acquisition, a digital time sensor, function generators, a laptop computer, a Labview program, a motor preload and a driving load, a LCR meter and an impedance analyzer machine.

In Chapter 5, fabrication and investigation of an ultrasonic linear motor with dual actuator has been described. For this ultrasonic linear motor, the system consists of a brass beam which is a stator, piezoelectric materials which are polarized in the thickness direction, and damping material. The objectives of the study are to reduce the energy consumption, the number of actuators and the applied voltage, and to simplify the motor structure in fabrication. Energy consumption of ultrasonic linear motors depends on the number of piezoelectric actuators used in the stator. Therefore, reducing the number of actuators directly affects the energy consumption of the motor. Besides, teeth on the stator are designed to expand the wave amplitude and to create elliptical motions at the tips of the teeth. For investigating the motor performance, the finite element and experimental techniques are used. Finite element models of the stator with dual piezoelectric actuators are carried out and simulated to

determine the system response consists of modal, harmonic and transient analyses. For the experiment, the motor performance is evaluated. The LCR meter is for measuring of the capacitance of piezoelectric actuator. The natural frequencies of the motor are measured by using an impedance analyzer machine (Hewlett Packard, model 4194A). The experimental results show that the velocity of the linear motor increases when pre-load increases for a certain amount of the pre-load and decreases afterwards. The relationship between velocity and applied voltage reveals that the motor velocity proportionally increases as the applied voltage amplitude increases. The experimental results of the relationship between driving force and the applied voltage indicates that the driving force linearly increases as applied voltage amplitude increases and the relationship between the velocity and driving force reveals that maximum motor velocity occurred at zero driving force, while the maximum driving force is generated when the motor operates at zero speed.

In Chapter 6, the ultrasonic linear driver with single piezoelectric actuator is evaluated and reported. The motor system consists of a brass beam and a piezoelectric ceramic actuator so that the linear motor has the least number of actuator. Besides, the design of the linear ultrasonic motor has a lower system stiffness and electrical energy consumption compared with the fully laminated piezoelectric ultrasonic motors. To predict and validate the motor performances, the finite element method and experiments are carried out. Finite element models of the stator with single piezoelectric actuator are simulated to determine the system response. First, the modal analysis is used for studying free vibration characteristic of the motor. Second, the harmonic analysis is employed to calculate of displacement of the wave at the steady state response. Finally, the transient analysis is used for

studying the operating frequency that generated the propagating wave in the linear stator. The experiments have been done for investigating and evaluating the motor performance. They are relationships between electrical applied voltage and velocity, maximum driving force and electrical applied voltage, and driving force and velocity. The experimental results show that the motor velocity depended on the electrical applied voltage. Hence, when the electrical applied voltage excited on the piezoelectric actuator increases, the motor velocity also increases. In the same way, the maximum driving force increases when the electrical increases. Notice that a high electrical applied voltage can cause the piezoelectric actuator depolarization due to high temperature occurred during motor operation. The performance of the ultrasonic linear driver with single actuator can be obtained though the relationship between driving force and motor velocity. The result reveals that the motor velocity decreased when increasing the driving force. While, the maximum driving force is generated at the zero speed.

7.2 Conclusions

The design and investigation of the ultrasonic linear motors with dual actuators and single actuator have been thoroughly reported in this thesis. The key parameters such as characteristics and performance, pre-load, velocity, driving force, electrical applied voltage and power consumption of the motor are summarized. Based on the finite element analysis and experimental studies, it can be concluded that 1) the ultrasonic linear motors with dual actuators and single actuator are capable generating traveling wave, 2) the energy consumption of the ultrasonic motors

depends on the number of the actuator bonded with the stator, electrical applied voltage, operating frequency and the capacitance of the piezoelectric actuator, 3) for ultrasonic linear motor with dual actuators, the direction of the traveling waves can be controlled by alternating the phase difference between the two control signals, 4) the least number of the piezoelectric actuator used in the linear ultrasonic motor is a single piezoelectric actuator bonded with the stator. The designs of the linear ultrasonic motor suggested in this research are capable of scaling down. The motor have low structure stiffness and easy to fabricate. The energy consumption of both designs is less than 1 W, lower than other linear motors at the same size [90]. In summary, both designs of the ultrasonic linear motors in this research open an opportunity for many applications that require a tiny translational actuator with low electrical power consumption yet easy in fabrication.

7.3 Suggestions and Future Work

7.3.1 Suggestion of the linear motors

In this research, the piezoelectric materials used in both linear ultrasonic motors are based on the piezoelectric constant, d_{31}. Generally, it is well-known that the piezoelectric constant d_{31} has a low displacement conversion when it is excited with the electrical applied voltage compared with piezoelectric constant d_{33}. Thus, the actuation efficiency of the motor is low. The piezoelectric material which has high piezoelectric constant is recommended. On the other hand, the contact layer material is also important because it transforms the elliptical motion of the stator to the motor

driving force. Thus, the friction material with high friction coefficient is suggested for using as a contact interface of the ultrasonic motors.

7.3.2 Future Work

To improve the motor efficiency, the piezoelectric stack actuator which has a dominant piezoelectric constant d_{33} may be adopted to be the actuators. The piezoelectric stack actuator could generate higher displacement for the same amount of applied voltage. However, the draw back is that the piezoelectric stack actuator would have a bigger size. Hence, the ultrasonic linear motor that uses piezoelectric stack actuator should be carefully redesigned to overcome the size issue. Furthermore, the impedance matching for all components used in the linear ultrasonic motor system must be considered. If the motor system has good impedance matching, the traveling wave with higher wave amplitude can be generated. In the future work, the ultrasonic linear motor with the piezoelectric stack actuators and impedance matching of the motor system are the issues that worth to investigate.

References

[1] Y. Liu, J. Liu, W. Chen, and S. Shi, "Working principle and design of a linear ultrasonic motor with rectangular-type stator," in *Eighteenth IEEE International Symposium on Applications of Ferroelectrics, 2009. ISAF 200*9, pp. 1–4, 2009.

[2] Z. Fu, and H. Guo, "A study of linear ultrasonic motor," in *IEEE International Conference on Applied Superconductivity and Electromagnetic Device, 2009. ASEMD2009,* pp.104-107, 2009.

[3] T. Hemsel and J. Wallaschek, "Survey of the present state of the art of piezoelectric linear motors," *Ultrasonics*, vol. 38, no. 1, pp. 37–40, 2000.

[4] Y. Chen, Q. L. Liu, and T. Y. Zhou, "A traveling wave ultrasonic motor of high torque," *Ultrasonics*, vol. 44, pp. e581–e584, 2006.

[5] P. Smithmaitrie, J. G. DeHaven, K. Higuchi, and H. S. Tzou, "Vibration response and harmonic wave propagation of ultrasonic arc drivers," *Mechanical Systems and Signal Processing*, vol. 21, no. 2, pp. 1174–1187, 2007.

[6] P. Smithmaitrie, P. Suybangdum, S. Muensit, and H. S. Tzou, "Wave propagations of curvilinear motors driven by partially laminated piezoelectric actuators," *Smart Materials and Structures*, vol. 17, p. 065015, 2008.

[7] J. Yoo, S. Lee, J. Hong, H. Song, D. Park, and E. Hwang, "Design and Simulation of Ultrasonic Linear Motor using Multilayer Ceramic Actuator," in *Sixteenth IEEE International Symposium on Applications of Ferroelectrics, 2007. ISAF 2007*, pp. 792–794, 2007.

[8] K. J. Lim, J. S. Lee, S. H. Park, S. H. Kang, and H. H. Kim, "Fabrication and characteristics of impact type ultrasonic motor," *Journal of the European Ceramic*

Society, vol. 27, no. 13, pp. 4159–4162, 2007.

[9] D. S. Paik, K. H. Yoo, C. Y. Kang, B. H. Cho, S. Nam, and S. J. Yoon, "Multilayer piezoelectric linear ultrasonic motor for camera module," *Journal of electroceramics*, vol. 22, no. 1, pp. 346–351, 2009.

[10] H. P. Ko, S. Kim, S. N. Borodinas, P. E. Vasiljev, C. Y. Kang, and S. J. Yoon, "A novel tiny ultrasonic linear motor using the radial mode of a bimorph," *Sensors and Actuators A: Physical*, vol. 125, no. 2, pp. 477–481, 2006.

[11] J. Jin and C. Zhao, "A vibrators alternation stepping ultrasonic motor," *Ultrasonics*, vol. 44, pp. e565–e568, 2006.

[12] M. Mracek, and J. Wallaschek, "A system for powder transport based on piezoelectrically excited ultrasonic progressive waves," *Materials Chemistry and Physics*, vol. 90, no. 2, pp. 378–380, 2005.

[13] Y. Roh and J. Kwon, "Development of a new standing wave type ultrasonic linear motor," *Sensors and Actuators A: Physical*, vol. 112, no. 2, pp. 196–202, 2004.

[14] Y. Ming, Z. Meiling, R. C. Richardson, M. C. Levesley, P. G. Walker, and K. Watterson, "Design and evaluation of linear ultrasonic motors for a cardiac compression assist device," *Sensors and Actuators A: Physical*, vol. 119, no. 1, pp. 214–220, 2005.

[15] C. Lu, T. Xie, T. Zhou, and Y. Chen, "Study of a new type linear ultrasonic motor with double-driving feet," *Ultrasonics*, vol. 44, pp. e585–e589, 2006.

[16] B. Zhai, S. P. Lim, K. H. Lee, S. Dong, and P. Lu, "A modified ultrasonic linear motor," *Sensors and Actuators A: Physical*, vol. 86, no. 3, pp. 154–158, 2000.

[17] T. Hemsel, M. Mracek, J. Twiefel, and P. Vasiljev, "Piezoelectric linear motor concepts based on coupling of longitudinal vibrations," *Ultrasonics*, vol. 44, pp.

e591–e596, 2006.

[18] T. Sashida and T. Kenjo, *An introduction to ultrasonic motors*. Oxford University Press, USA, 1993.

[19] M. Kurosawa, M. Takahashi, and T. Higuchi, "Friction drive surface acoustic wave motor," *Ultrasonics*, vol. 34, no. 2, pp. 243–246, 1996.

[20] K. Uchino, "Piezoelectric ultrasonic motors: overview," *Smart materials and structures*, vol. 7, p. 273, 1998.

[21] M. K. Kurosawa, "State-of-the-art surface acoustic wave linear motor and its future applications," *Ultrasonics*, vol. 38, no. 1, pp. 15–19, 2000.

[22] M. Takasaki, M. Kuribayashi Kurosawa, and T. Higuchi, "Optimum contact conditions for miniaturized surface acoustic wave linear motor," *Ultrasonics*, vol. 38, no. 1, pp. 51–53, 2000.

[23] Y. Chen, T. Y. Zhou, Q. Zhang, X. Y. Chen, and S. H. Chen, "A study on the friction of a self-correction ultrasonic stepping motor," *Ultrasonics*, vol. 39, no. 9, pp. 667–671, 2002.

[24] E. Mujjalinvimut, M. Konghirun, and P. Laoratanakul, "A design study of ultrasonic motor drive," in *Sixteenth IEEE International Conference on Electrical Engineering/Electronics, Computer, Telecommunications and Information Technology, 2009. ECTI-CON 2009,* pp. 274-277, 2009.

[25] Y. Roh, S. Lee, and W. Han, "Design and fabrication of a new traveling wave-type ultrasonic linear motor," *Sensors and Actuators A: Physical*, vol. 94, no. 3, pp. 205–210, 2001.

[26] D. Sun, S. Wang, S. Hata, J. Sakurai, and A. Shimokohbe, "Driving mechanism and experimental realization of a cylindrical ultrasonic linear microactuator,"

Microelectronic Engineering, vol. 86, no. 4, pp. 1262–1266, 2009.

[27] S. He, W. Chen, X. Tao, and Z. Chen, "Standing wave bi-directional linearly moving ultrasonic motor," *IEEE Transactions on Ultrasonics, Ferroelectrics and Frequency Control*, vol. 45, no. 5, pp. 1133–1139, 1998.

[28] T. Hemsel, M. Mracek, J. Wallaschek, and P. Vasiljev, "A novel approach for high power ultrasonic linear motors," in *2004 IEEE International Ultrasonics,* vol. 2, pp. 1161-1164, 2004.

[29] F. Giraud, B. Semail, "Analysis and phase control of a piezoelectric traveling wave ultrasonic motor for haptic stick application," *IEEE Transaction on industry applications*, vol 40, no 6, 2004, pp. 1514-1549.

[30] D. Sun, J. Liu, and X. Ai, "Modeling and performance evaluation of traveling wave piezoelectric ultrasonic motors with analytical method," *Sensors and Actuators A: Physical*, vol. 100, no. 1, pp. 84–93, 2000.

[31] P. Smithmaitrie, and H. S. Tzou, "Electo-dynamics, micro-actuation and design of arc stators in an ultrasonic curvilinear motor," *Journal of Sound and Vibration*, vol. 284, no 3, pp 635-650, 2005.

[32] P. Smithmaitrie, and H. S. Tzou, "Micro-control of actuator patches laminated on hemispherical shells, *Journal of Sound and Vibration*, vol. 277, no 4, pp. 691-710, 2004.

[33] K. Uchino, *Piezoelectric actuator and ultrasonic motors*. Kluwer Academic Plublisher, Boston, 1996.

[34] S. S. Lih, Y. B. Cohen, and W. Grandia, "Rotary ultrasonic motors actuated by traveling flexural waves," presented at the SPIE International on Smart Structures and Integrated System (SPIE) International Conference, p. 6, 1997.

[35] H. Mojallali, R. Amini, R. I. Zamanabadi, and A. A. Jalali, "Systematic experimental based modeling of a rotary piezoelectric ultrasonic motor," *ISA Transactions*, vol. 46, no. 1, pp. 31-40, 2007.

[36] X. Chu, L. Ma, and L. Li, "A disk-pivot structure micro piezoelectric actuator using vibration mode B_{11}," *Ultrasonics*, vol. 44, pp. e561-e564, 2006.

[37] Y. Ming, and Q. Peiwen, "Performances estimation of a rotary traveling wave ultrasonic motor based on two-dimension analytical model," *Ultrasonics*, vol. 39, no. 2, pp. 115-120, 2001.

[38] C. Borda, D. Arsene, M. Marinescu, A. Moraru, L. Butu, and G. Arsene, "Study of the present state of ultrasonic linear motors," *The Annual Symposium of The Institute of Solid Mechanics and Session of the Commission of Acoustics*, *2008. SISOM 2008*, pp. 399-403, 2008.

[39] M. Kummel, S. Goldschmidt, and J. Wallaschek, "Theoretical and experimental studies of a piezoelectric ultrasonic linear motor with respect to damping and nonlinear material behaviour," *Ultrasonics*, vol. 36, no. 1, pp. 103-109, 1998.

[40] M. G. Bauer, *Design of a linear high precision ultrasonic piezoelectric motor*. Ph.D Thesis, North Carolina State University, USA, 2001.

[41] J. M. Fernandez, and Y. Perriard, "Characteristic, modeling and simulation of a traveling wave ultrasonic linear motor," in *IEEE Ultrasonics Symposium*, vol. 3, pp. 2247-2250, 2004.

[42] W. M. Kuo, S. F. Chuang, C. Y. Nian, and Y. S. Tarng, "Precision nano-alignment system using machine vision with motion controlled by piezoelectric motor," *Mechatronics*, vol. 18, no. 1, pp. 21-34, 2008.

[43] M. K. Kurosawa, H. Itoh, and K. Asai, "Elastic friction drive of surface acoustic wave motor," *Ultrasonics*, vol. 41, no. 4, pp. 271-275, 2003.

[44] M. Kurosawa, "Ultrasonic motor," *International Journal of Japanese Sociology Precision Engineering*, vol. 31, no. 2, pp. 87-91, 1997.

[45] J. M. Fernandez, and Y. Perriard, "Sensitivity analysis and optimization of a standing wave ultrasonic linear motor," *IEEE Transaction on Ultrasonics, Ferroelectrics, and Frequecy Control*, vol. 53, no. 7, pp. 1352-1361, 2006.

[46] Y. Yano, K. Iida, K. Yabugami, and Y. Nakata, "Approach to speed control using temperature characteristics of ultrasonic motor," in *47th IEEE International Midwest Symposium on Circuits and Systems*, pp. 155-158, 2004.

[47] S. Ueha, Y. Tomigawa, M. Kurosawa, and N. Nakamura, *Ultrasonic motors theory and application*. Clarendon Press, Oxford, UK, 1993.

[48] H. P. Ko, S. Kim, C. Y. Kang, H. J. Kim, and S. J. Yoon, "Optimization of a piezoelectric linear motor in terms of the contact parameters," *Materials Chemistry and Physics*, vol. 90, no. 2, pp. 322-326, 2005.

[49] J. Qu, F. Sun, and C. Zhao, "Performance evaluation of traveling wave ultrasonic motor based on a model with visco-elastic friction layer on stator," *Ultrasonics*, vol. 45, no. 1, pp. 22-31, 2006.

[50] H. Storck, W. Littmann, J. Wallaschek, and M. Mracek, "The effect of friction reduction in presence of ultrasonic vibrations and its relevance to traveling wave ultrasonic motors," *Ultrasonics*, vol. 40, no. 1, pp. 379-383, 2002.

[51] H. P. Ko, S. Kim, J. S. Kim, H. J. Kim, and S. J. Yoon, "Wear and dynamic properties of piezoelectric ultrasonic motor with frictional materials coated stator," *Materials Chemistry and Physics*, vol. 90, no. 2, pp. 391-395, 2005.

[52] J. Y. Liew, Y. Chen, and T. Y. Zhou, "The measurement on vibration friction coefficient of ultrasonic motor," in 2008 *IEEE Symposium on Ultrasonics,* pp. 154-156, 2008.

[53] W. Zheng, and C. Zhao, "A wear evaluation of friction materials used for rotary ultrasonic motors," *in IEEE Symposium on Ultrasonics,* pp. 1838-1841, 2008.

[54] M. Mracek, and T. Hemsel, "Synergetic driving concepts for bundle miniature ultrasonic linear motors," *Ultrasonics*, vol. 44, pp. e597-e602, 2006.

[55] L. Petit, and P. Gonnard, "A multilayer TWILA ultrasonic motor," *Sensors and Actuators A: Physics*, vol. 149, no. 1, pp. 113-1119, 2009.

[56] S. T. Ho, "Modelling of the linear ultrasonic motor using an elliptical shape stator," *IEEE International Conference,* in *2006 IEEE International Conferences on Mechatronics,* pp. 82-87, 2006.

[57] J. Friend, A. Umeshima, T. Ishii, K. Nakamura, and S. Ueha, "A piezoelectric linear actuator formed from a multitude of bimorphs," *Sensor and Actuators A: Physics*, vol. 109, no. 3, pp. 242-251, 2004.

[58] D. H. Wu, W. T. Cien, C. J. Yang, and Y. T. Yen, "Coupled-field analysis of piezoelectric beam actuator using FEM," *Sensor and Actuators A: Physics*, vol. 118, no. 1, pp. 171-176, 2005.

[59] P. Suybangdum, and P. Smithmaitrie, "Analysis of piezoelectric actuator locations for generating traveling wave on an ultrasonic curvilinear motor," in *Second Reginal Conference on Artificial Life and Robotics*, 2006. AROP 2006, pp 53-57, 2006.

[60] P. Sukwisut, *Transducer Elements Made from Piezoelectric Stacks*. Master Thesis, Prince of Songkla University, Thailand, 2009.

[61] Lang, S. B. and Das-Gupta, D. K. "Pyroelectricity: Fundamentals and Application" *Ferroelecrics Review*, vol 2, pp. 217-354, 2000.

[62] T. Ikeda, *Fundamental of piezoelectricity*. Oxford University Press, Oxford New York Tokyo, 1990.

[63] C. Liang, F. P. Sun, and C. A. Rogers, "Investigation of the energy transfer and consumption of adaptive structures," in *Proceeding of the thirtieth one IEEE Conference on Decision and Control*, vol. 2, pp. 1791-1796, 1992.

[64] C. Liang, F. P. Sun, and C. A. Rogers, "Coupled electro-mechanical analysis of adaptive material system-determination of the actuator power consumption and system energy transfer," *Journal of Intelligent Material System and Structure*, vol. 5, pp.12-20, 1994.

[65] M. C. Brennan and A. R. McGowan, "Piezoelectric power requirements for active vibration control," *presented at the Society of Photo-Optical Instrumentation Engineers (SPIE) Conference Series*, pp. 660-669, 1997.

[66] S. C. Stein, C. Liang, and C. A. Rogers, "Power consumption of piezoelectric actuators driving a simply supported beam considering fluid coupling," *Journal of Acoustic Society of America*, vol.96, no. 3, pp. 1598-1604, 1994.

[67] T. Jordan, Z. Ounaies, J. Tripp, and P. Tcheng, "Electrical properties and power considerations of a piezoelectric actuator," *ICASE Report no. 8*, p. 8, 2000.

[68] C. Liang, F. Sun, and C. A. Rogers, "Electro-mechanical impedance modeling of active material systems," *Smart Materials and Structures*, vol. 5, pp. 171-186, 1996.

[69] Knowledge center (2011). Piezoelectricity, APC International. http://www.americanpiezo.com/knowledge-center/piezo-theory/piezoelectricity.html. (accessed November 5, 2011).

[70] J. Walluschek, "Contact mechanics of piezoelectric ultrasonic motors," *Smart Matertials and Structures*, vol. 7, pp. 369-381, 1998.

[71] A. M. Flynn, *Piezoelectric ultrasonic micromotors*, Ph.D Thesis, Massachusetts Institute of Technology, USA, 1995.

[72] K. P. Yi, J. S. Rho, and H. K. Jung, "Analysis of a linear ultrasonic motor using numerical and analytic method," in *IEEE International Conference on Electrical Machines and System, 2008. ICEMS 2008,* pp. 3716-3719, 2008.

[73] J. P. Schmidt, P. Hagedorn, and M. Bingqi, "A note on the contact problem in an ultrasonic traveling wave motor," *International Journal of Non-Linear Mechanics*, vol. 31, no. 6, pp. 915-924, 1996.

[74] H. Storck, and J. Walluschek, "The effect of tangential elasticity of the contact layer between stator rotor in traveling wave ultrasonic motors," *International Journal Non-Linear Mechanics*, vol. 38, no. 2, pp. 143-159, 2003.

[75] Y. Ting, C. C. Li, L. C. Chen, and C. M. Yang, "Traveling-wave piezoelectric linear motor Part II: Experiment and performance evaluation," *IEEE Transaction on Ultrasonics, Ferroelectrics, and Frequency Control*, vol. 54, no. 4, pp. 854-860, 2007.

[76] Y. Ting, C. C. Li, L. C. Chen, and C. M. Yang, 2005. "A new type of piezoelectric linear motor: Carriage design and performance analysis," *Proceeding of the IEEE International Conference on Mechatronics & Automation*, pp 1267-1271, 2005.

[77] Y. Hojjat, and M. R. Karafi, "Introduction of roller interface ultrasonic motor (RIUSM)," *Sensors and Actuators A, Physical*, vol. 163, no. 1, pp. 304-310, 2010.

[78] Y Hojjat, M R Karafi and M D Tehrani, “A novel ultrasonic motor with roller interface (RUSM),” in *IEEE/ASME International Conference on Advance Intelligent Mechatronics*, 2009. AIM 2009, pp. 1406-1411, 2009.

[79] J. J. Qu, Y. L. Wang, and N. N. Zhou, “Numerical simulation of contact state of ultrasonic motor with gradient friction material,” *Joint Conference of the 2009 Symposium on Piezoelectricity, Acoustic Wave and Device Applications (SPAWDA) and China Symposium on Frequency Control Technology*, pp. 174-178, 2009.

[80] L. Huafeng, Z. Chunsheng, and G. Chenglin, “Study on the contact model of ultrasonic motor considering shearing deformation,” *Journal of Electrical Engineering*, vol. 55, no. 7, pp. 216-220, 2004.

[81] F. Z. Kebbab, Z. Boumous, and S. Belkhiat, “Traveling wave ultrasonic motor type Daimler-Benz AWM90-X: Modeling and simulation mechanical characteristics,” *Journal of Electrical System*, no. 1, pp. 24-29, 2009.

[82] M. T. E. Hagry, A. A. Mahfouz, and H. S. Ahmed, “Experimental investigation of a mathematical model for traveling wave ultrasonic motors," in *Fourth WSEAS International Conference on Applied Mathematics and Computer Sciene*, 2005. AMCOS 2005, p. 10, 2005.

[83] J. Maas, P. Ide, N. Frohleke, and H. Grotstollen, “Simulation model for ultrasonic motors powered by resonant converters,” *Conference Record of the 1995 IEEE on Industry Applications Conference, Thirtieth IAS Annual Meeting*, vol. 1, pp 111-120, 1995.

[84] M. Bullo, and Y. Perriard, “Performance analysis and optimization of the traveling wave ultrasonic motor,” *Conference of the Industry Applications Conference, 37th IAS Annual Meeting*, vol. 3, pp. 1907-1913, 2002.

[85] M. Zhu, "Contact analysis and mathematical modeling of traveling wave ultrasonic motor," *IEEE Transactions on Ultrasonics, Ferroelectrics, and Frequency* Control, vol. 51, no. 6, pp. 668-679, 2004.

[86] F. Lu, H. P. Lee, and S. P. Lim, "Contact modeling of viscoelastic friction layer of traveling wave ultrasonic motors," *Smart Materials and Structures*, vol. 10, pp. 314-320, 2001.

[87] Blevins, R.D, *Formulars for natural frequency and mode shape*. Hrieger Publisher Company, USA, 1995.

[88] J. M. Fernandez and Y. Perriard, "Comparative analysis and modeling of both standing and travelling wave ultrasonic linear motor," in *2003 IEEE Symposium on Ultrasonics*, vol. 2, pp. 1770-1773, 2003.

[89] K. Higuchi, "A piezoelectric linear motor driven by superposing standing waves with phase difference," in *36th AIAA/ASME/ASCE/AHS/ASC Structures, Structural Dynamics, and Materials Conference and AIAA/ASME Adaptive Structures Forum*, pp. 3296–3303, 1995.

[90] H. Zhang, S. Dong, S. Zhang, T. Wang, Z. Zhang, and L. Fan, "Ultrasonic micro-motor using miniature piezoelectric tube with diameter of 1.0 mm," *Ultrasonics*, vol. 44, pp. e603–e606, 2006.

[91] J. S. Rho, B. J. Kim, C. H. Lee, H. W. Joo, and H. K. Jung, "Design and characteristic analysis of L1B4 ultrasonic motor considering contact mechanism," *IEEE Transactions on Ultrasonics, Ferroelectrics and Frequency Control*, vol. 52, no. 11, pp. 2054–2064, 2005.

[92] C. H. Yun, B. Watson, J. Friend, and L. Yeo, "A piezoelectric ultrasonic linear micromotor using a slotted stator," *IEEE Transactions on Ultrasonics, Ferroelectrics,*

and Frequency Control, vol. 57, no. 8, pp. 1868-1874, 2010.

[93] S. Dembele and K. Rochdi, "A three DOF linear ultrasonic motor for transport and micropositioning," *Sensors and Actuators A: Physical*, vol. 125, no. 2, pp. 486–493, 2006.

[94] J. Jin, D. Wan, Y. Yang, Q. Li, and M. Zha, "A linear ultrasonic motor using ($K_{0.5}Na_{0.5}$) NbO3 based lead-free piezoelectric ceramics," *Sensors and Actuators A: Physical*, vol. 165, no. 2, pp. 410–414, 2011.

[95] W. H. Lee, C. Y. Kang, D. S. Paik, B. K. Ju, and S. J. Yoon, "Butterfly-shaped ultra slim piezoelectric ultrasonic linear motor," *Sensors and Actuators A: Physical*, vol. 168, no. 1, pp. 127-130, 2011.

APPENDIX

APPENDIX A:

Comparison of the dual actuators ultrasonic linear motors with different piezoelectric constants, d_{31}

These are several parameters that represent the performance of the linear ultrasonic motors, such as operating frequency, pre-load, driving force, and velocity. In case of the driving force and velocity, they depend on the amplitude of the traveling wave. For increasing the amplitude of the traveling wave, the electrical applied voltage has to be increased. However, the high electrical applied voltage can depolariz of the piezoelectric property of the actuators. Furthermore, the high electrical applied voltage also affect the power consumption of the ultrasonic linear motors. To solve this problem, the piezoelectric material with higher piezoelectric constant should be used.

The frequency responses of the stators with dual piezoelectric actuators that have different of piezoelectric constants are illustrated in Figure A-1. The dual actuators are subjected to two sinusoidal voltages with amplitudes of 54 V. These are $54\sin(\omega t)$ and $54\cos(\omega t)$ for the left and right actuators, respectively. The excitation frequency ω is varied from 20 to 35 kHz to investigate the system responses and determine the operating frequency. In the case study, the piezoelectric constant, $d_{31,}$ is varied to investigate amplitude of the traveling wave. The piezoelectric constants are -125 PC/N and -250 PC/N. The results show that the wave amplitude of traveling wave increases when the magnitude of piezoelectric constant increases.

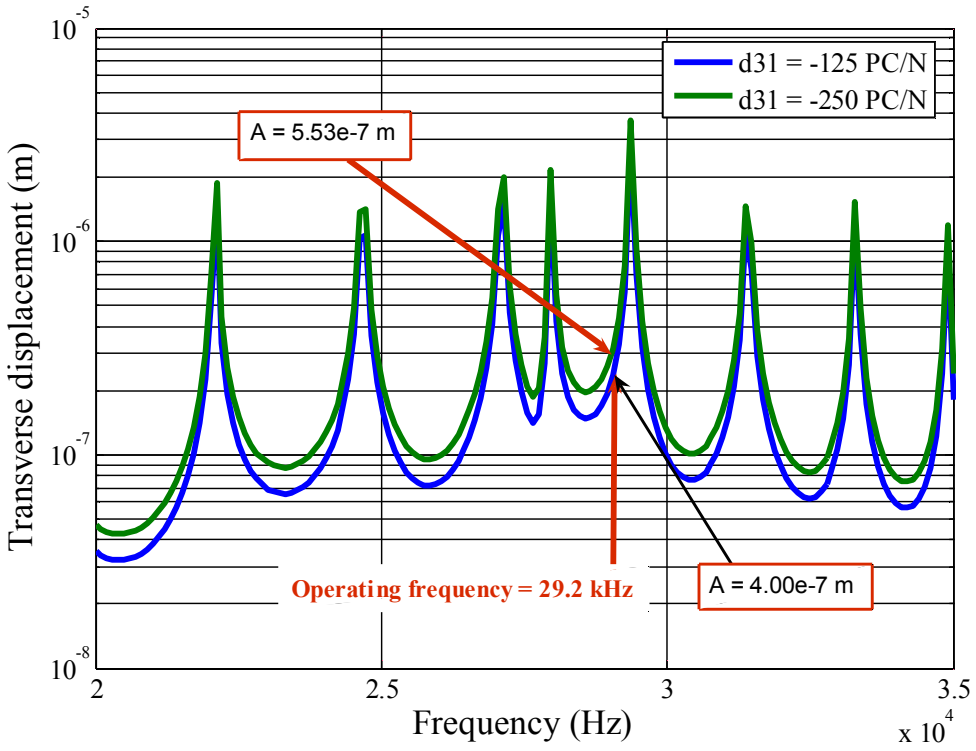

Figure A-1 Harmonic responses of the linear stators with different properties of dual piezoelectric actuators.

Amplitude of the traveling wave of a linear motor is changed when the piezoelectric constant varies as reported in Table A-1. The wave amplitude dependes on the piezoelectric constant. If the piezoelectric constant is increased, the wave amplitude of the traveling wave increases. Since, the motor velocity is proportional to the wave amplitude, then the motor velocity increases linearly. The velocity of an ultrasonic linear motor can be defined as Equation (A-1).

$$V_{S(x)} = -aA\left(\frac{2\pi}{\lambda}\right)^2 f\lambda \cos\left(\frac{2\lambda x}{\lambda}\right) \qquad \text{(A-1)}$$

where a = 3.5 mm is the distance from the beam neutral surface to the teeth contact surface. The wave amplitude of an ultrasonic linear motor is calculated by the finite element method. The results show that the wave amplitude of A = $4.00x10^{-7}$ m when using the piezoelectric constant of d_{31} = -125 PC/N and the wave amplitude of A = $5.53x10^{-7}$ m when using the piezoelectric constant of d_{31} = -250 PC/N. For the both cases, the operating frequencies are f = 29.2 kHz, and the wavelengths are λ = 11.5 mm. Equation (A-1) is adopted to calculate of the motor velocity. The calculated results show that the motor velocity is 14.03 cm/sec with the piezoelectric constant of -125 PC/N; meanwhile, the velocity of the motor is 19.4 cm/sec with the piezoelectric constant of -250 PC/N. The comparison of the dual actuators linear ultrasonic motors with different piezoelectric constants are summarized in Table A-1.

Table A-1 The performance of the dual actuators linear ultrasonic motors.

Piezoelectric constant	Unit (PC/N)	Wave amplitude (m)	Operating frequency (kHz)	Velocity (cm/sec)
d_{31}	-125	$4x10^{-7}$	29.2	14.03
d_{31}	-250	$5.53x10^{-7}$	29.2	19.4

According to the results described above, the value of the piezoelectric constant is very important to improve the motor performance because the wave amplitude relies the piezoelectric constant while the electrical applied voltage remains constant. Consequently, the piezoelectric material with high piezoelectric constant should be implemented on the ultrasonic linear motor in order to improve the motor performance.

VITAE

Name Mr. Panumas Suybangdum

Student ID 5010130015

Educational Attainment

Degree	Name of Institution	Year of Graduation
B.Eng.(Post-Harvest and Processing Engineering)	Rajamangala Institute of Technology	1998
M.Eng (Mechanical Engineering)	Prince of Songkla University	2007

Scholarship Awards during Enrolment

Thailand Graduate Institute of Science and Technology (TGIST), 2007-2010

List of Publication and Proceedings

Publication

1. P. Smithmaitrie, **P. Suybangdum**, S. Muensit, and H. S. Tzou, "Wave propagations of curvilinear motors driven by partially laminated piezoelectric actuators," *Smart Materials and Structures*, vol. 17, p. 065015, 2008.

2. Pruittikorn Smithmaitrie, Panumas Suybangdum, Pitak Laoratanakul, and Nantakan Muensit, "Design and performance testing of an ultrasonic linear motor with dual piezoelectric actuators," IEEE Transaction on Ultrasonics, Feroelectrics, and Frequency Control, vol. 59, no. 5, pp. 1033-1042, 2012.

Proceedings

1. **P. Suybangdum**, P. Smithmaitrie, and P. Laoratanakul, "Dual piezoelectric actuators for the traveling wave ultrasonic linear motor" Fourth International Conference on Experimental Mechanics (SPIE 2009), 18-20 November 2009, vol. 7552, Singapore.

2. **P. Suybangdum**, P. Smithmaitrie, and P. Laoratanakul, "Effect of stator stiffness for generating traveling wave on an ultrasonic curvilinear motor" The 22nd Conference of Mechanical Engineering Network of Thailand, 15-17 October 2008, Thammasat University, Thailand.